

STEER-BY-WIRE: IMPLICATIONS FOR VEHICLE HANDLING AND SAFETY

A DISSERTATION

SUBMITTED TO THE DEPARTMENT OF MECHANICAL ENGINEERING
AND THE COMMITTEE ON GRADUATE STUDIES
OF STANFORD UNIVERSITY
IN PARTIAL FULFILLMENT OF THE REQUIREMENTS
FOR THE DEGREE OF
DOCTOR OF PHILOSOPHY

Paul Yih

January 2005

© Copyright by Paul Yih 2005

All Rights Reserved

I certify that I have read this dissertation and that, in my opinion, it is fully adequate in scope and quality as a dissertation for the degree of Doctor of Philosophy.

J. Christian Gerdes
(Principal Adviser)

I certify that I have read this dissertation and that, in my opinion, it is fully adequate in scope and quality as a dissertation for the degree of Doctor of Philosophy.

Kenneth J. Waldron

I certify that I have read this dissertation and that, in my opinion, it is fully adequate in scope and quality as a dissertation for the degree of Doctor of Philosophy.

Stephen M. Rock
(Aeronautics and Astronautics)

Approved for the University Committee on Graduate Studies.

This thesis is dedicated to the memory of Dr. Donald Streit.

Abstract

Recent advances toward steer-by-wire technology have promised significant improvements in vehicle handling performance and safety. While the complete separation of the steering wheel from the road wheels provides exciting opportunities for vehicle dynamics control, it also presents practical problems for steering control. This thesis begins by addressing some of the issues associated with control of a steer-by-wire system. Of critical importance is understanding how the tire self-aligning moment acts as a disturbance on the steering system. A general steering control strategy has been developed to emphasize the advantages of feedforward when dealing with these known disturbances. The controller is implemented on a test vehicle that has been converted to steer-by-wire.

One of the most attractive benefits of steer-by-wire is active steering capability. When supplied with continuous knowledge of a vehicle's dynamic behavior, active steering can be used to modify the vehicle's handling dynamics. One example presented and demonstrated in the thesis is the application of full vehicle state feedback to augment the driver's steering input. The overall effect is equivalent to changing a vehicle's front tire cornering stiffness. In doing so, it allows the driver to adjust a vehicle's fundamental handling characteristics and therefore precisely shift the balance between responsiveness and safety.

Another benefit of steer-by-wire is the availability of steering torque information from the actuator current. Because part of the steering effort goes toward overcoming the tire self-aligning moment, which is related to the tire forces and, in turn, the vehicle motion, knowledge of steering torque indirectly leads to a determination of the vehicle states, the essential element of any vehicle dynamics control system. This

relationship forms the basis of two distinct observer structures for estimating vehicle states; both observers are implemented and evaluated on the test vehicle. The results compare favorably to a baseline sideslip estimation method using a combination of Global Positioning System (GPS) and inertial navigation system (INS) sensors.

Acknowledgements

Many people have influenced my life in the time it took to complete the work in these pages. First and foremost has been my advisor and mentor, Chris Gerdes. I was fortunate enough to find someone who shares the same passion for automobiles, how they shape our world, and our responsibility as engineers and researchers to make them better. Chris provided the imagination and guidance to turn mere notions into reality. That's how we ended up with our own Corvette with which to do vehicle research. Many of the ideas in this thesis were developed at his suggestion. I hope I have done them justice.

I would also like to thank my reading committee, Ken Waldron and Steve Rock, for taking the time to read and critique this thesis. Their input has been invaluable. Thanks also to Günter Niemeyer for serving on my defense committee.

I have had the pleasure of working in the Dynamic Design Lab with some great people. They made the lab a fun and enjoyable place to talk about research, or anything at all. Special thanks go to Eric Rossetter and Josh Switkes for the countless hours they spent helping me get the steer-by-wire Corvette up and running. Special thanks also to Jihan Ryu, my vehicle test copilot, who never once complained when I said, "just one more data set."

Finally, I want to thank my parents for their patient support throughout all my years in school and who would have been just as happy had I decided to do something else. There's no longer any need to ask how much time before I'm finished with my Ph.D. Yes, I really am done!



Contents

	iv
Abstract	v
Acknowledgements	vii
1 Introduction	1
1.1 Evolution of automotive steering systems	1
1.2 Technical advantages of steer-by-wire	2
1.3 An increasing need for sensing and estimation	8
1.4 Thesis contributions	9
1.5 Thesis overview	10
2 An experimental steer-by-wire vehicle	13
2.1 Steer-by-wire system	14
2.1.1 Conversion from conventional system	14
2.1.2 Steering actuation	15
2.1.3 Force feedback	18
2.1.4 Processing and communications	19
2.2 System identification	22
3 The role of vehicle dynamics in steering	28
3.1 Feedback control	29
3.1.1 Proportional derivative feedback	29

3.2	Feedforward control	29
3.2.1	Cancellation of steering system dynamics	29
3.2.2	Steering rate and acceleration	30
3.2.3	Friction compensation	31
3.2.4	Effect of tire self-aligning moment	33
3.2.5	Aligning moment compensation	36
3.3	Combined control	38
3.3.1	Error dynamics	39
4	A means to influence vehicle handling	40
4.1	Historical background: variable stability aircraft	41
4.2	Vehicle dynamics	43
4.2.1	Linear vehicle model	43
4.2.2	The fundamental handling characteristics: understeer, oversteer, and neutral steer	45
4.3	Handling modification	49
4.3.1	Full state feedback: a virtual tire change	49
4.3.2	GPS-based state estimation	51
4.3.3	Experimental handling results	54
4.4	Limitations of front wheel active steering	63
5	A vehicle dynamics state observer	66
5.1	Steering system model	67
5.2	Linear vehicle model	69
5.2.1	Observability	70
5.3	Vehicle state estimation using steering torque	71
5.3.1	Conventional observer	71
5.3.2	Disturbance observer	74
5.3.3	Vehicle state observer	76
5.3.4	Alternate formulation	77
5.3.5	Observer performance	79
5.4	Closed loop vehicle control	86

5.4.1	Handling modification	86
5.4.2	Experimental results	87
6	Conclusion and Future Work	95
6.1	Conclusion	95
6.2	Future work	97
6.2.1	Handling at the limits	97
6.2.2	Steering wheel force feedback	97
6.2.3	Diagnostics	99
A	The Pacejka Tire Model	101
A.1	Lateral force (F_y)	103
A.2	Aligning torque (M_z)	103
B	Hydraulic Power Assisted Steering	106
B.1	Power steering components	106
B.2	Hydraulic model	106
B.3	Mechanical model	108
B.4	Power steering nonlinearities	110
C	Extension to Four-Wheel Steering Vehicles	112
C.1	Linear vehicle model with four-wheel steering	112
C.2	Full state feedback vehicle control	114
C.3	Limitations of four-wheel active steering	115
	Bibliography	117

List of Tables

A.1 Tire formulae coefficients for typical passenger car tire with load influence.	102
--	-----

List of Figures

1.1	May 25, 1972 at the NASA Dryden Flight Research Center, Edwards, CA: the first test flight of a digital fly-by-wire aircraft, a modified Navy F-8C Crusader, shown here with test pilot Gary Krier. Credit: NASA	3
1.2	Automotive applications for by-wire technology. Credit: Motorola . . .	4
1.3	Yaw moment generated by differential braking (left) versus active steering (right).	6
2.1	Experimental steer-by-wire Corvette with a few of its developers (left to right): Paul Yih, Prof. Chris Gerdes, Josh Switkes, and Eric Rossetter. Photo credit: Mark Hundley	14
2.2	Conventional steering system.	15
2.3	Conventional steering system converted to steer-by-wire.	16
2.4	Universal joint.	16
2.5	View of left side of engine compartment showing steer-by-wire system servomotor actuator (encased in heat shielding).	17
2.6	Steering wheel force feedback system in test vehicle. Photo credit: Linda Cicero	19
2.7	View of trunk area with steer-by-wire electronics. Photo credit: Linda Cicero	20
2.8	Configuration of electronic components in the test vehicle. Thin dark line is electrical current at 13.8 V. Heavy dark line is current at 42 V. Medium line is motor current from the amplifier. Light lines are signals from the steering angle sensors.	21
2.9	Steering system dynamics with no tire-to-ground contact.	22

2.10	Block diagram for closed loop system identification.	23
2.11	Commanded and actual steering angle.	24
2.12	DFT of input and output signals.	24
2.13	ETFE with identified Bode plot. Discrepancy at lower frequencies is due to friction and power steering nonlinearities.	25
2.14	Comparison between actual and identified system response without friction model.	25
2.15	Comparison between actual and identified system response with friction model.	26
3.1	Feedback control only.	31
3.2	Feedback with feedforward compensation.	32
3.3	Feedback with feedforward and friction compensation.	32
3.4	Steering system dynamics with tire-to-ground contact.	33
3.5	Error due to aligning moment.	34
3.6	Tire operating at a slip angle.	35
3.7	Component of aligning moment due to mechanical trail.	35
3.8	Wheel camber and kingpin inclination angle.	36
3.9	Steering controller with aligning moment compensation.	37
3.10	Steering controller block diagram.	38
4.1	NASA's F6F-3 Hellcat variable stability airplane circa 1950 at the Ames Aeronautical Laboratory, Moffett Field, California with flight personnel. Note the vane on the wingtip for measuring aircraft sideslip angle. Credit: NASA	41
4.2	Front views of aircraft showing (a) positive dihedral, (b) sideslip due to bank angle, and (c) stabilizing roll moment. Credit: NASA	42
4.3	Bicycle model.	44
4.4	The fundamental handling characteristics as determined by the sign of the understeer gradient.	46
4.5	Steady state cornering.	47

4.6	Nonlinear vehicle simulation with and without handling modification: neutral steering case.	52
4.7	Nonlinear vehicle simulation with and without handling modification: oversteering case.	52
4.8	Sideslip and yaw rate estimation.	53
4.9	Steer-by-wire Corvette undergoing testing on the West Parallel of Moffett Federal Airfield at the NASA Ames Research Center. Moffett is an active airfield.	54
4.10	Comparison between yaw rate of bicycle model and experiment with normal cornering stiffness.	55
4.11	Comparison between sideslip angle of bicycle model and experiment with normal cornering stiffness.	56
4.12	Difference in road wheel angle with effectively reduced front cornering stiffness.	57
4.13	Comparison between yaw rate of normal and effectively reduced front cornering stiffness.	57
4.14	Comparison between lateral acceleration of normal and effectively re- duced front cornering stiffness.	58
4.15	Comparison between yaw rate of bicycle model and experiment with reduced front cornering stiffness.	58
4.16	Comparison between sideslip angle of bicycle model and experiment with reduced front cornering stiffness.	59
4.17	Difference in road wheel angle with effectively increased front cornering stiffness.	59
4.18	Comparison between yaw rate of normal and effectively increased front cornering stiffness.	60
4.19	Comparison between lateral acceleration of normal and effectively in- creased front cornering stiffness.	60
4.20	Comparison between yaw rate of bicycle model and experiment with increased front cornering stiffness.	61

4.21	Comparison between sideslip angle of bicycle model and experiment with increased front cornering stiffness.	61
4.22	Comparison between yaw rate of unloaded and loaded vehicle.	62
4.23	Comparison between yaw rate of unloaded vehicle and loaded vehicle with handling modification.	63
5.1	Steering system dynamics.	67
5.2	Conventional observer block diagram.	72
5.3	Cascaded observer block diagram.	74
5.4	Estimated steer angle from conventional observer.	80
5.5	Estimated steer rate from conventional observer.	80
5.6	Estimated sideslip from conventional observer.	81
5.7	Estimated yaw rate from conventional observer.	81
5.8	Estimated steer angle from disturbance observer.	82
5.9	Estimated steer rate from disturbance observer.	82
5.10	Estimated sideslip from disturbance observer.	83
5.11	Estimated yaw rate from disturbance observer.	83
5.12	Estimated disturbance torque.	84
5.13	Estimated disturbance torque versus slip angle.	85
5.14	Comparison between estimated yaw rate, INS measurement, and bicycle model simulation with normal cornering stiffness.	88
5.15	Comparison between estimated sideslip angle, GPS measurement, and bicycle model simulation with normal cornering stiffness.	88
5.16	Difference in road wheel angle with effectively reduced front cornering stiffness.	89
5.17	Comparison between lateral acceleration with normal and effectively reduced front cornering stiffness.	90
5.18	Comparison between estimated yaw rate, INS measurement, and bicycle model simulation with reduced front cornering stiffness.	90
5.19	Comparison between estimated sideslip angle, GPS measurement, and bicycle model simulation with reduced front cornering stiffness.	91

5.20	Difference in road wheel angle with effectively increased front cornering stiffness.	91
5.21	Comparison between lateral acceleration with normal and effectively increased front cornering stiffness.	92
5.22	Comparison between estimated yaw rate, INS measurement, and bicycle model simulation with increased front cornering stiffness.	92
5.23	Comparison between estimated sideslip angle, GPS measurement, and bicycle model simulation with increased front cornering stiffness.	93
6.1	Tire cornering stiffness in the nonlinear region represented by $C_{\alpha,NL}$	98
6.2	Next generation experimental drive-by-wire vehicle.	100
A.1	Tire operating at a slip angle.	101
A.2	Tire lateral force versus slip angle.	104
A.3	Slip angle versus component of aligning moment due to pneumatic trail.	104
B.1	Hydraulic power assist schematic.	107
B.2	Mechanical representation of steering system with hydraulic power assist.	109
B.3	Orifice area versus valve angle.	111
B.4	Typical power steering boost curve: assist pressure versus input torque with linear approximation.	111
C.1	Bicycle model with front and rear steering.	113

Chapter 1

Introduction

1.1 Evolution of automotive steering systems

The proliferation of electronic control systems is nowhere more apparent than in the modern automobile. During the last two decades, advances in electronics have revolutionized many aspects of automotive engineering, especially in the areas of engine combustion management and vehicle safety systems such as anti-lock brakes (ABS) and electronic stability control (ESC). The benefits of applying electronic technology are clear: improved performance, safety, and reliability with reduced manufacturing and operating costs. However, only recently has the electronic revolution begun to find its way into automotive steering systems in the form of electronically controlled variable assist and, within the past two years, fully electric power assist [5, 40].

The basic design of automotive steering systems has changed little since the invention of the steering wheel: the driver's steering input is transmitted by a shaft through some type of gear reduction mechanism (most commonly rack and pinion or recirculating ball bearings) to generate steering motion at the front wheels. One of the more prominent developments in the history of the automobile occurred in the 1950s when hydraulic power steering assist was first introduced. Since then, power assist has become a standard component in modern automotive steering systems. Using hydraulic pressure supplied by an engine-driven pump, power steering amplifies and supplements the driver-applied torque at the steering wheel so that steering effort

is reduced. In addition to improved comfort, reducing steering effort has important safety implications as well, such as allowing a driver to more easily swerve to avoid an accident.

The recent introduction of electric power steering in production vehicles eliminates the need for the hydraulic pump. Electric power steering is more efficient than conventional power steering, since the electric power steering motor only needs to provide assist when the steering wheel is turned, whereas the hydraulic pump must run constantly. The assist level is also easily tunable to the vehicle type, road speed, and even driver preference [32, 6]. An added benefit is the elimination of environmental hazard posed by leakage and disposal of hydraulic power steering fluid.

The next step in steering system evolution—to completely do away with the steering column and shaft—represents a dramatic departure from traditional automotive design practice. The substitution of electronic systems in place of mechanical or hydraulic controls is known as by-wire technology. This idea is certainly not new to airplane pilots [46]; many modern aircraft, both commercial and military, rely completely on fly-by-wire flight control systems (Figure 1.1). By-wire technology paved the way for high performance aircraft designed to have a degree of maneuverability never before possible. If not for the intervention of flight control computers, some of these planes—because they are inherently unstable—could not be flown by human pilots without crashing.

1.2 Technical advantages of steer-by-wire

A number of current production vehicles already employ by-wire technology for the throttle and brakes (Figure 1.2) [21]. A few supplement conventional front steering with rear steer-by-wire to improve low speed maneuverability and high speed stability [7, 53]. Completely replacing conventional steering systems with steer-by-wire, while a more daunting concept than throttle- or brake-by-wire for most drivers, holds several advantages. The absence of a steering column greatly simplifies the design of car interiors. The steering wheel can be assembled modularly into the dashboard and located easily for either left- or right-hand drive. The absence of a steering shaft



NASA Dryden Flight Research Center Photo Collection
<http://www.dfrc.nasa.gov/gallery/photo/index.html>
NASA Photo: ECN-3091 Date: 1971

F-8 DFBW with test pilot Gary E. Krier

Figure 1.1: May 25, 1972 at the NASA Dryden Flight Research Center, Edwards, CA: the first test flight of a digital fly-by-wire aircraft, a modified Navy F-8C Crusader, shown here with test pilot Gary Krier. Credit: NASA

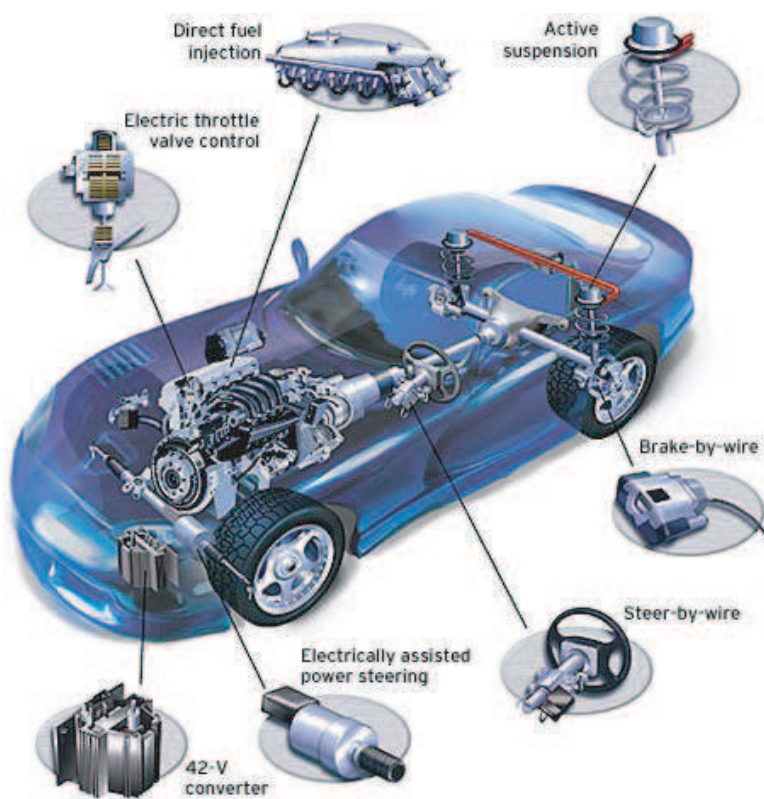


Figure 1.2: Automotive applications for by-wire technology. Credit: Motorola

allows much better space utilization in the engine compartment. Furthermore, the entire steering mechanism can be designed and installed as a modular unit. Without a direct mechanical connection between the steering wheel and the road wheels, noise, vibration, and harshness (NVH) from the road no longer have a path to the driver's hands and arms through the steering wheel. In addition, during a frontal crash, there is less likelihood that the impact will force the steering wheel to intrude into the driver's survival space. Finally, with steer-by-wire, previously fixed characteristics like steering ratio and steering effort are now infinitely adjustable to optimize steering response and feel.

Undoubtedly the most significant benefit of steer-by-wire technology to driving safety and performance is active steering capability: the ability to electronically augment the driver's steering input. As a part of fully integrated vehicle dynamics control, the first active steering system for a production vehicle was recently introduced in the 2004 BMW 5-Series. While not yet a by-wire system, this feature demonstrates the sort of handling improvements that can be made to a vehicle equipped with true steer-by-wire. Similar to electronic stability control (ESC) systems that have been available for several years, active steering is able to maintain vehicle stability and maneuverability by intervening on behalf of the driver when the vehicle approaches its handling limits, such as during an emergency maneuver, or when driving conditions call for a change in steering response.

Statistical and empirical studies have shown a substantial reduction in the accident rate for vehicles equipped with ESC [4, 10, 12, 25, 28, 38]. However, active steering and steer-by-wire technology take vehicle control one step further. In current ESC systems, a computer analyzes information from multiple vehicle sensors and intervenes on behalf of the driver to prevent potentially catastrophic maneuvers by either selectively braking individual wheels or reducing engine power. Because these types of systems are motivated by safety, their engagement sometimes interrupts the continuity of driving feel and therefore limits the vehicle's performance envelope. Steer-by-wire introduces the possibility that one can indeed have the best of both worlds: improved driving safety *and* handling performance. Instead of intruding suddenly, a steer-by-wire system smoothly integrates steering adjustments during

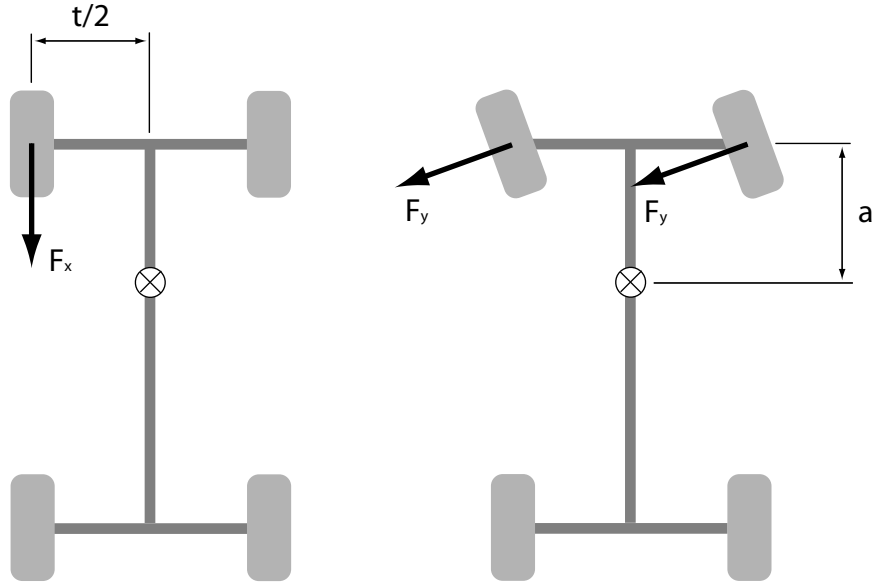


Figure 1.3: Yaw moment generated by differential braking (left) versus active steering (right).

an emergency maneuver to maintain stability [7]. The benefits go beyond stability control: for example, a large, heavy vehicle can be made to feel as responsive as a smaller, lighter vehicle during normal driving. The ability to actively steer the front wheels allows artificial tuning of a vehicle's handling characteristics to suit the driver's preference.

Furthermore, in some cases it is actually advantageous to utilize steering instead of differential braking to generate yaw moment, because steering requires less friction force between the tires and ground. Consider the case when the rear tires have reached their limits of adhesion during cornering, e.g. a rear wheel slide; the only means of control are the front wheels. This situation typically leads to a spinout or, with poorly timed steering inputs, a violent fishtailing that is nearly impossible to control. To generate a correcting yaw moment, one can either apply braking to the outside front wheel or counter steer the front wheels (Figure 1.3). The moment generated by differential braking is:

$$M = F_x \frac{t}{2} \quad (1.1)$$

The moment generated by front steering is approximately:

$$M = 2F_ya \quad (1.2)$$

for small steering angles. Considering that for most passenger vehicles the trackwidth, t , is approximately the distance, a , from the center of gravity (CG) to the front axle and equating Equations (1.1) and (1.2), we get:

$$F_y = \frac{F_x}{4} \quad (1.3)$$

The lateral force, F_x , at each tire is only one fourth of the longitudinal force, F_y , required to generate the same yaw moment, M . This result is especially useful when controlling a vehicle on low friction surfaces such as snow or ice where the limits of adhesion are easily reached. Of course, there are clearly limitations to the forces that can be generated by steering intervention alone. For example, when the front tires have already saturated in a turn, dialing in additional steering angle will not produce any more lateral force. In this situation, only differential braking of the rear wheels will have any influence on the dynamics of the vehicle. An ideal stability control system would have the choice of either steering or braking intervention or some combination of the two.

The potential benefits of active steering intervention to improve handling behavior during normal driving, not just emergencies, have likewise received considerable attention from both the automotive industry and research institutions. A number of ideas have been tested in experimental prototypes with specially designed active steering systems. As early as 1969, Kasselmann and Keranen [23] proposed an active steering system based on feedback from a yaw rate sensor. More recent work by Ackermann [3] combines active steering with yaw rate feedback to robustly decouple yaw and lateral motions. Experimental results demonstrate its effectiveness in cancelling out yaw generated while braking on a split friction surface. In [20], Huh and Kim devise an active steering controller that eliminates the difference in steering response between driving on slippery roads and dry roads. The controller is implemented in a driving simulator using feedback of vehicle roll to estimate lateral tire force. Most

recently, Segawa et al. [48] apply lateral acceleration and yaw rate feedback to an experimental steer-by-wire vehicle and demonstrate that active steering control can achieve greater driving stability than differential brake control.

1.3 An increasing need for sensing and estimation

While most of the previously implemented active steering systems rely on feedback of yaw rate or lateral acceleration or a combination of both, since these signals are readily measured with inexpensive sensors, significantly more comprehensive control can be achieved given information on vehicle sideslip angle. Sideslip is defined as the difference between the vehicle's forward orientation and its direction of velocity. The advantages of knowing sideslip are twofold: first, yaw rate and sideslip together completely describe a vehicle's motion in the road plane. Yaw rate alone is not always enough; for example, a vehicle could be undergoing an acceptable yaw rate, but it might be skidding sideways. The second reason for obtaining sideslip information is that the driver is particularly sensitive to sideslip motion of the vehicle and prefers the angle to be small [11]. This preference arises from the sensation of instability at larger angles which is perhaps rooted in the real potential for loss of control when sideslip angle and therefore tire slip angles are allowed to grow to large.

Although feedback of sideslip angle has been proposed theoretically [17, 34, 27, 35], the difficulty in estimating vehicle sideslip presents an obstacle to achieving sideslip control. Stability systems currently available on production cars typically derive slip rate from accelerometer integration, a physical vehicle model, or a combination of the two, but these estimation methods are prone to uncertainty [54]. For example, direct integration of lateral acceleration can accumulate sensor errors and unwanted measurements from road grade and bank angle. Because sideslip is extremely important to the driver's perception of handling behavior, quality of the driving experience depends strongly on quality of the feedback signal. This dependence is less critical for stability control systems, which tend to engage when the vehicle is already undergoing extreme maneuvers, but to improve handling behavior during normal driving requires cleaner and more accurate feedback.

An estimation scheme that overcomes some of these drawbacks supplements integration of inertial sensors with Global Positioning System (GPS) measurements [44]. Absolute GPS heading and velocity measurements eliminate the errors from inertial navigation system (INS) integration; conversely, INS sensors complement the GPS measurements by providing higher update rate estimates of the vehicle states. However, during periods of GPS signal loss, which frequently occur in urban driving environments, integration errors can still accumulate and lead to faulty estimates.

The growing presence of electric power steering systems in production vehicles introduces yet another absolute measurement—steering torque—from which vehicle sideslip angle may be estimated. Through the tire self-aligning moment, which comprises much of the resistance felt by the driver when turning the steering wheel, steering torque is directly related to the lateral front tire forces, which in turn relate to the tire slip angles and therefore the vehicle states. This approach is especially suited to vehicles equipped with steer-by-wire since the steering torque can easily be determined from the current applied to the steering motor. As such, steer-by-wire encompasses the entire scope of vehicle dynamics control: on the one hand, the steer-by-wire system is the actuator that provides control authority for the vehicle dynamics controller. On the other hand, it is the sensor from which the vehicle states are estimated.

1.4 Thesis contributions

The contributions of this dissertation are as follows:

- A general approach for steering control using a steer-by-wire system. The combined feedback and feedforward control strategy systematically cancels out the steering system dynamics, friction, and disturbance forces. In doing so, it establishes the need to compensate for the aligning moment effect on steering.
- The application of active steering and full vehicle state feedback to modify a vehicle’s handling characteristics. By augmenting the driver’s steering input,

the effect is equivalent to changing the front tire cornering stiffness and therefore the balance between handling responsiveness and stability.

- The development and implementation of a vehicle sideslip observer based on steering torque. The observer combines models of the steering system dynamics and vehicle dynamics in the way they are naturally linked through the tire forces.
- A springboard for critical research issues facing steer-by-wire technology, particularly by-wire diagnostics. A thorough understanding of steering system and vehicle dynamics and how to measure or estimate the key parameters form the elements of a comprehensive model-based diagnostic approach.

1.5 Thesis overview

The potential for improved driving safety and handling performance afforded by steer-by-wire capability deserves thorough study. There is no greater validation of a promising technology than to physically demonstrate its effectiveness in a real-world environment. Chapter 2 discusses the conversion of a conventional passenger car into a steer-by-wire prototype vehicle. It also describes a closed loop experimental method for identification of the steering system dynamics, since precise control of the steer-by-wire system depends on accurate knowledge of the steering system parameters.

The ability to precisely control the steering angle of the steer-by-wire system is crucial for both direct steering and active steering control. In other words, the steer angles at the road wheels must be as close as possible to the angles commanded by either the driver or the control system. Chapter 3 develops a proportional derivative controller with feedforward of steering rate and acceleration in order to cancel out the steering system dynamics. Particularly, this chapter emphasizes the importance of the vehicle dynamics forces as they are transmitted through the tire aligning moment to act on the steering system. Precise control cannot be achieved without accounting for these external forces.

There are certainly many ways in which active steering intervention can be applied to improve handling performance and safety. Chapter 4 presents a physically intuitive

application based on feedback of the vehicle states, yaw rate and sideslip angle. The effect is exactly equivalent to changing the cornering stiffness of the front tires. This “virtual tire change” results in a modification of the fundamental handling characteristics of the vehicle, i.e. from neutral steering to oversteering or understeering. Even though neutral steering is the ideal handling characteristic since it provides maximum steering response without instability, passenger vehicles are typically designed to be inherently understeering in order to avoid the possibility of unstable behavior when operating conditions—such as load distribution or disproportionate tire wear—cause an undesirable shift in handling characteristics. This design compromise necessarily reduces the responsiveness of the vehicle so that it is not as responsive as it could be in all situations. It is not possible to physically design a vehicle that handles optimally under every condition; however, with a combination of active steering and full state feedback control, optimal handling characteristics are achievable even though a vehicle’s physical parameters may be suboptimal. Thus, such a vehicle’s handling characteristics can be arbitrarily tuned to driver preference as well as to maintain consistent behavior when operating conditions vary. Active handling modification is demonstrated on the test vehicle using sideslip estimates from a GPS/INS system installed in the test vehicle.

The downside to relying on GPS for sideslip is that the GPS signal can be lost, particularly in urban environments. Fortunately, steer-by-wire provides a ready solution to the problem of sideslip estimation. Chapter 5 presents an alternative approach to estimating the vehicle sideslip using steering torque information. A complete knowledge of steering torque can be determined from the current applied to the system’s steering actuator. Through the tire self-aligning moment, steering torque can be directly related to the front tire lateral forces and therefore the wheel slip angles. Chapter 5 develops two observer structures based on linear models of the vehicle and tire behavior to estimate the vehicle states from measurements of steering angle and yaw rate. The first of the two structures combines the vehicle and steering system models into a single observer structure to estimate four states at once: sideslip angle, yaw rate, steering angle, and steering rate. The second structure incorporates an intermediate step. A disturbance observer based on the steering system model

estimates the tire aligning moment; this estimate becomes the measurement part of a vehicle state observer for sideslip and yaw rate. The handling modification experiments are repeated using this method of sideslip estimation in place of GPS/INS. For the tests performed, the sideslip estimation results are comparable to those obtained from the GPS/INS method. However, the results also suggest that in order to more effectively use the aligning moment for lateral force measurement, some changes to the original steer-by-wire system design are necessary. The future work section (Chapter 6) discusses some of the changes that are being implemented in the next generation of experimental by-wire vehicles.

Chapter 2

An experimental steer-by-wire vehicle

Although a number of automotive companies have developed their own steer-by-wire prototypes, very few examples of such vehicles exist at academic institutions. Most academic studies related to steer-by-wire have been theoretical and validated only in simulation [31, 59, 60, 18, 52] mainly due to the cost and complexity of acquiring a vehicle and converting it to steer-by-wire. The author's interest in steer-by-wire began as an effort to help experimentally verify promising research in lane-keeping assistance systems [43]. The desire for a relatively simple and robust system dictated the process of transforming a stock 1997 Chevrolet Corvette into a rolling testbed with steer-by-wire capability. Out of this endeavor emerged several new research directions, some of which are developed in the succeeding chapters.

The test vehicle, generously donated by General Motors Corporation, is a regular production model two-door coupe with a four-speed overdrive automatic transmission. Three factors make this vehicle ideal for experimental testing. First, the layout of the vehicle— front-engine, longitudinally mounted V-8, and open trunk area— facilitates the locating of test equipment and routing of electrical wiring. Second, the vehicle is designed and engineered with serviceability in mind, which means critical components are reasonably accessible and installation of experimental apparatus can be completed in a timely manner with minimal modification to the existing structure.



Figure 2.1: Experimental steer-by-wire Corvette with a few of its developers (left to right): Paul Yih, Prof. Chris Gerdes, Josh Switkes, and Eric Rossetter. Photo credit: Mark Hundley

Third, the Corvette is an extremely stable, well-balanced car with a deep well of performance, which allows the driver to execute high speed maneuvers with confidence. The following sections describe the process of converting the test vehicle to steer-by-wire as well as identification of the steering system's characteristics as installed in the vehicle.

2.1 Steer-by-wire system

2.1.1 Conversion from conventional system

Transforming a conventional steering system to steer-by-wire places limitations on the design of the steer-by-wire system. For example, to allow the left and right wheels to steer independently of each other would require extensive modification of the existing steering linkages, rack, and suspension components. The goal of this endeavor, however, is not to push the state-of-the-art in by-wire design, but to rapidly develop a steer-by-wire system that meets given performance requirements and is sufficiently robust for use as an experimental test vehicle. Thus, the aim of the design

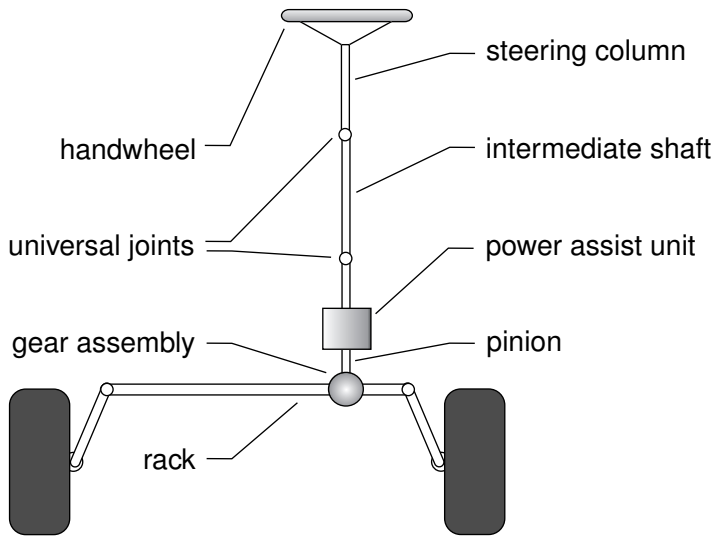


Figure 2.2: Conventional steering system.

presented here is to achieve full steer-by-wire capability with as little modification to the existing steering system as possible. A conventional steering system (Figure 2.2) typically consists of the handwheel (steering wheel), the steering column, intermediate shaft, rotary spool valve (an integral part of the hydraulic power assist system), the rack and pinion, and steering linkages. Since the steering column and pinion are almost never collinear, they are joined to the intermediate shaft via two universal joints matched to minimize torque and speed variations between steering column and pinion.

2.1.2 Steering actuation

The steer-by-wire implementation (Figure 2.3) makes use of all the conventional steering system components except for the intermediate steering shaft, which is cut in half with the upper end completely removed. Since this means that only one of the two universal joints remains, an effort is made to minimize the joint angle in the orientation of the connecting shafts. If necessary, any fluctuations in torque and speed

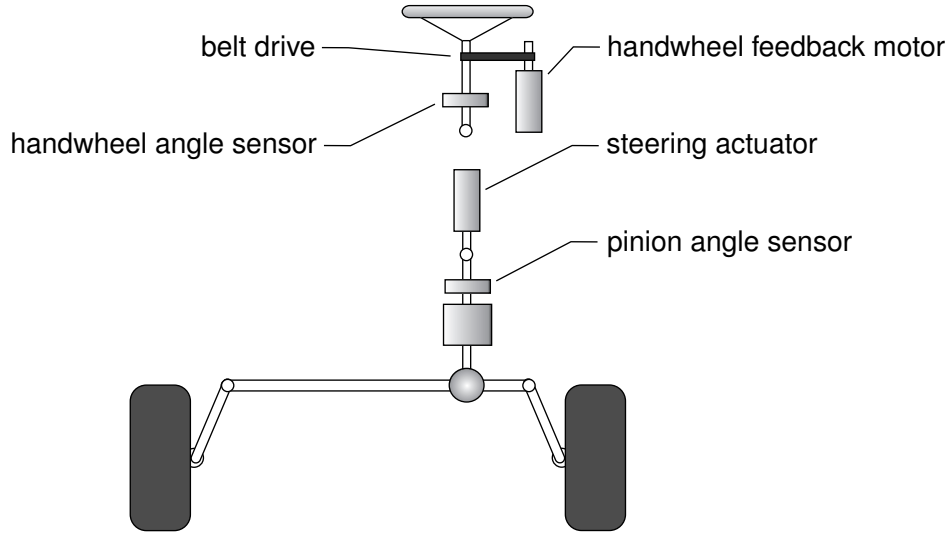


Figure 2.3: Conventional steering system converted to steer-by-wire.

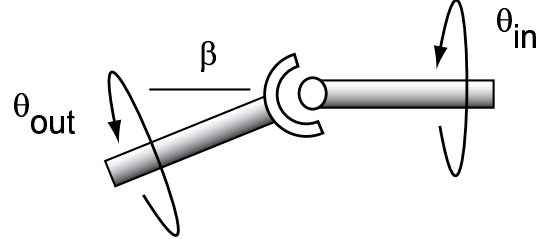


Figure 2.4: Universal joint.

transmission caused by the joint can be modelled analytically:

$$\begin{aligned}\theta_{out} &= \tan^{-1} \left(\frac{\tan \theta_{in}}{\cos \beta} \right) \\ \dot{\theta}_{out} &= \left(\frac{\cos \beta}{1 - \sin^2 \beta \cos^2 \theta_{in}} \right) \dot{\theta}_{in} \\ \tau_{out} &= \left(\frac{\cos \beta}{1 - \sin^2 \beta \cos^2 \theta_{in}} \right) \tau_{in}\end{aligned}\tag{2.1}$$

where β is the angle between the input and output shafts (Figure 2.4).

To provide steering actuation in place of the handwheel, a brushless DC servomotor is attached to the remainder of the intermediate shaft via a flexible coupling, rigid in torsion but compliant in bending, that accommodates any axial misalignment

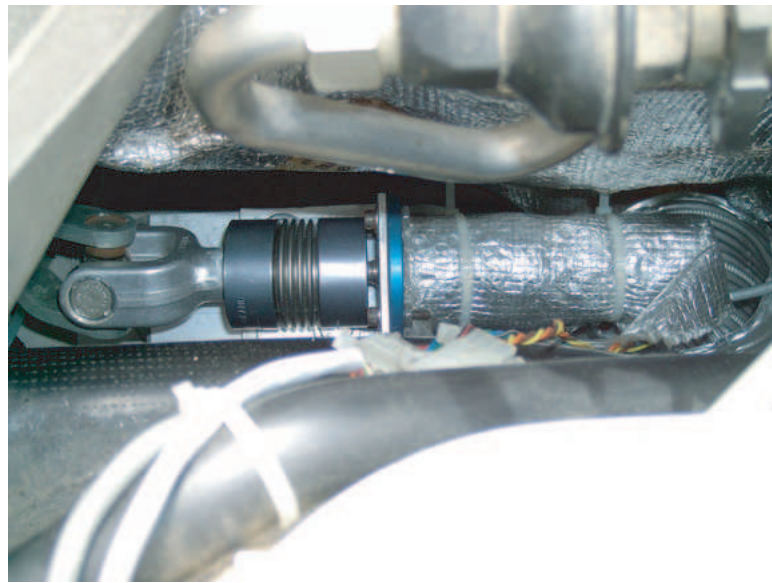


Figure 2.5: View of left side of engine compartment showing steer-by-wire system servomotor actuator (encased in heat shielding).

between the connecting shafts. The servomotor casing is fixed to the frame of the vehicle. Two thick-film variable resistance rotary position sensors are installed—one on the steering column and the other on the pinion—to provide an absolute reference for both angles. They are each supplemented by measurements from high resolution non-absolute encoders.

The original hydraulic power assist unit in the test vehicle was retained as part of the steer-by-wire system (see Appendix A for a full description of the hydraulic power assist system). The incorporation of the stock power assist unit eliminates the need for extensive modifications to the existing steering system and allows the use of a much smaller actuator since the assist unit provides a majority of the steering effort. The only drawback is that the hydraulic system has its own dynamics and in addition, the assist torque is a nonlinear function of the applied steering torque. However, for our test vehicle, the nonlinear effects did not present a major obstacle to achieving good steering control (see Chapter 3).

The servomotor (Figure 2.5), which consists of a motor and gearhead, was selected based on the maximum torque and speed necessary to steer the vehicle under typical

driving conditions including moderate emergency maneuvers. Studies in steering effort for a typical automobile have suggested that required steering torque at the handwheel during normal driving ranges from 0 to 2 Nm, while emergency maneuvers can demand up to 15 Nm of torque [49, 29]. The steering rate target is two full turns of the steering wheel per second, or a road wheel slew rate of approximately 45 deg/s. From these target values, the maximum current and voltage necessary to run the motor were calculated using the DC motor equations:

$$\begin{aligned} i_M &= k_I \tau_M \\ V_M &= i_M R + k_E \omega_M \end{aligned} \quad (2.2)$$

where i_M is the motor current, k_I is the current constant, V_M is the operating voltage, R is the terminal resistance, and k_E is the back-EMF constant. The motor torque, τ_M , and speed, ω_M , are related to torque and speed at the output shaft, τ_s and ω_s , respectively, by the gear reduction ratio, r_g , and gearhead efficiency, η :

$$\begin{aligned} \tau_M &= \frac{1}{\eta} \frac{\tau_s}{r_g} \\ \omega_M &= \omega_s r_g \end{aligned} \quad (2.3)$$

Since the only source of DC power is the vehicle's own charging system, which supplies approximately 13.8 V when the engine is running, a DC to DC step-up power converter is used to boost the voltage level. It was determined from the servomotor specifications and performance criteria that a supply voltage of 48 V from an off-the-shelf unit would be sufficient.

2.1.3 Force feedback

The purpose of the handwheel feedback motor (Figure 2.6) is to communicate to the driver via tactile means the direction and level of forces acting between the front tires and the road. A byproduct of these forces is the self-centering effect that occurs when the driver releases the steering wheel while exiting a turn (see Appendix A). Both the self-centering effect and the torque feedback are important characteristics that a driver



Figure 2.6: Steering wheel force feedback system in test vehicle. Photo credit: Linda Cicero

expects to feel when steering a car equipped with a conventional steering system. The force feedback system consists of a brushed DC servomotor with a timing belt drive that attaches the output shaft to a pulley on the steering column. The belt drive system is chosen due to space constraints around the steering column and its resistance to slip. Similar to the actuator, the servomotor and pulley ratio are selected based on typical feedback levels provided by conventional steering systems. Steering wheel force feedback, while not considered further in this thesis, is nonetheless critical for consumer acceptance of a commercial steer-by-wire system and is an area of ongoing study [51].

2.1.4 Processing and communications

The electronic control unit for both the steering actuator and force feedback motor consists of a single board computer running real-time code generated by MATLAB from Simulink block diagram models. Real-time code includes the steering control algorithms and device drivers for analog-to-digital and digital-to-analog converters in the single board computer (Figure 2.7). Multiple analog input channels receive signals from the steering position sensors; the steering controller, discussed in the next chapter, processes the sensor information and commands an analog voltage level



Figure 2.7: View of trunk area with steer-by-wire electronics. Photo credit: Linda Cicero

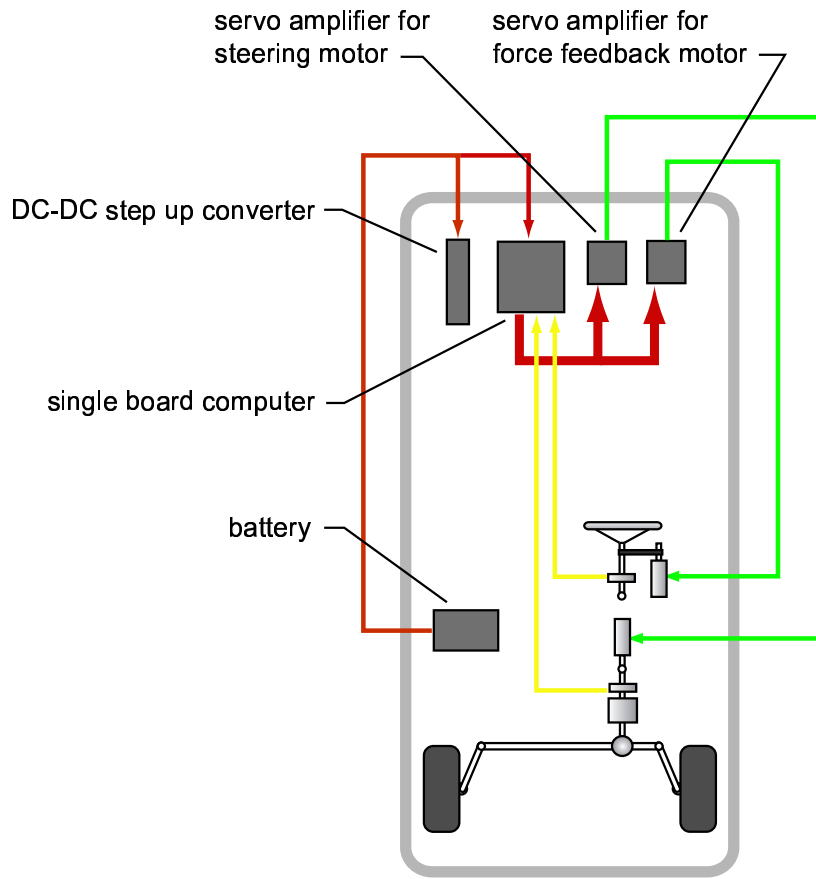


Figure 2.8: Configuration of electronic components in the test vehicle. Thin dark line is electrical current at 13.8 V. Heavy dark line is current at 42 V. Medium line is motor current from the amplifier. Light lines are signals from the steering angle sensors.

proportional to the required steering torque. Based on this signal, the servomotor amplifier supplies the appropriate motor current. The steer-by-wire system requires two analog output channels, one for the servomotor actuator command signal and the other for the feedback motor, and three analog input channels each for the two rotary position sensor signals (three signals are necessary to determine absolute position). Figure 2.8 illustrates the flow of power and signals through the system. A laptop computer communicating via Ethernet connection serves as the user interface to the single board computer.

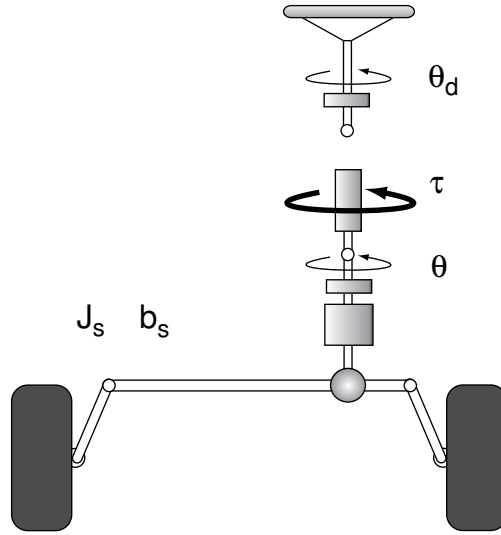


Figure 2.9: Steering system dynamics with no tire-to-ground contact.

2.2 System identification

Many detailed mathematical models have been developed for both rack and pinion steering systems and hydraulic power assist systems [2, 9, 33, 36, 41, 55]. Experimental identification of the test vehicle’s steer-by-wire system, however, suggests that its dynamics are well represented by a simpler second order model. The results also indicate that the dynamics of the individual components, such as the hydraulic power assist unit, are negligible compared to the overall steering system dynamics in the normal range of steering inputs. Note that these results may not hold true for all steering systems or operating conditions due to rate and torque limits; more complicated models may indeed be necessary in those cases (see Appendix B).

If tire forces are ignored, the transfer function describing the steering system dynamics (Figure 2.9) takes the following form:

$$G(s) = \frac{\Theta(s)}{T(s)} = \frac{1}{J_s s^2 + b_s s} \quad (2.4)$$

where θ is the pinion angle, τ is the actuator torque, J_s is the total moment of inertia of the steering system, and b_s is the effective viscous damping coefficient. A closed

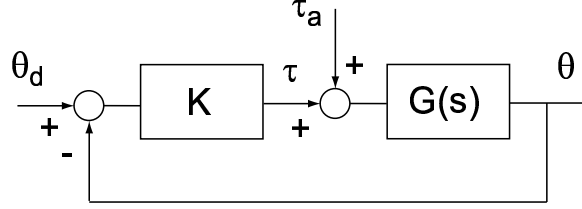


Figure 2.10: Block diagram for closed loop system identification.

loop system identification method is used to determine the parameters J_s and b_s of the real steering system (Figure 2.10). The front wheels are raised off the ground to temporarily eliminate the effect of the tire forces, represented by τ_a in the block diagram. With no tire forces, the closed loop transfer function is given by:

$$\frac{\Theta(s)}{\Theta_d(s)} = \frac{KG(s)}{1 + KG(s)} = \frac{K}{J_s s^2 + b_s s + K} \quad (2.5)$$

where θ_d is the commanded steering angle and K is the feedback gain. The input signal to the closed loop system is a sinusoidal waveform that sweeps through frequencies between 0 and 5 Hz over a 100 second time period. The feedback gain is chosen to be as large as possible without causing the amplifier current to saturate. Figure 2.11 shows the input signal, or commanded angle, θ_d , with the output, or actual steering angle, θ . The frequency response of the system can be approximated by the empirical transfer function estimate (ETFE), the ratio between the output and input Discrete Fourier Transform (DFT). The ETFE, shown in Figure 2.13, confirms that the steering system is second order, and the closed loop transfer can be written as:

$$\frac{\Theta(s)}{\Theta_d(s)} = \frac{\omega_n^2}{s^2 + 2\xi\omega_n s + \omega_n^2} = \frac{K}{J_s s^2 + b_s s + K} \quad (2.6)$$

where ω_n is the natural frequency and ξ is the damping ratio of the system as determined from the ETFE. From Equation (2.6), the system parameters J_s and b_s are easily calculated. In Figure 2.13, the Bode plot of the identified system is plotted over the ETFE for the system. The difference in response at lower frequencies between the actual and identified systems arises partly from the effect of Coulomb friction

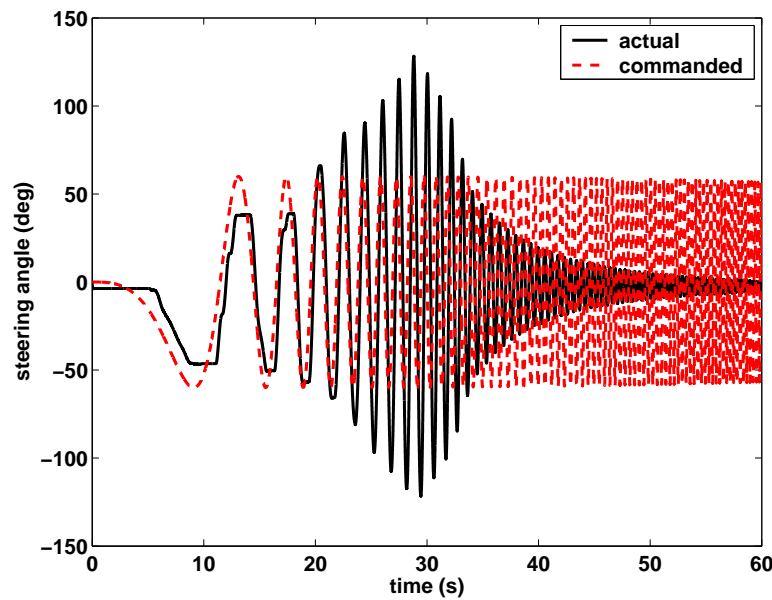


Figure 2.11: Commanded and actual steering angle.

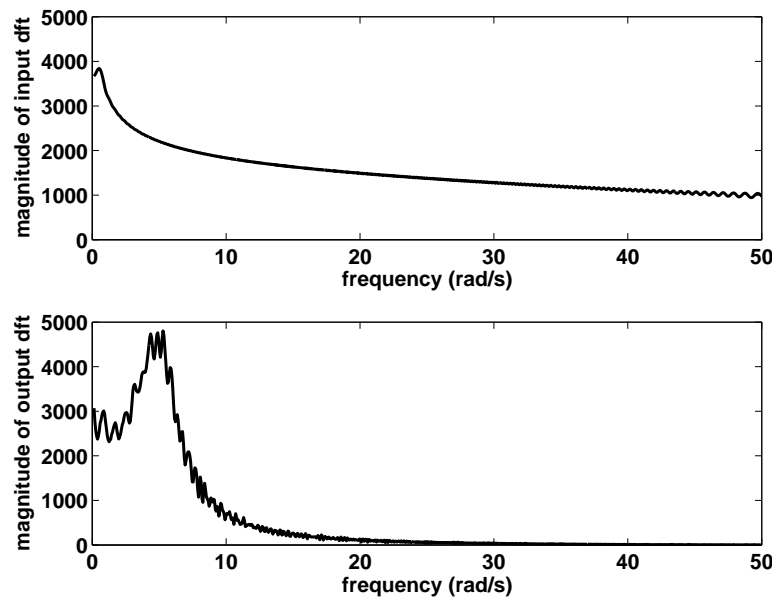


Figure 2.12: DFT of input and output signals.

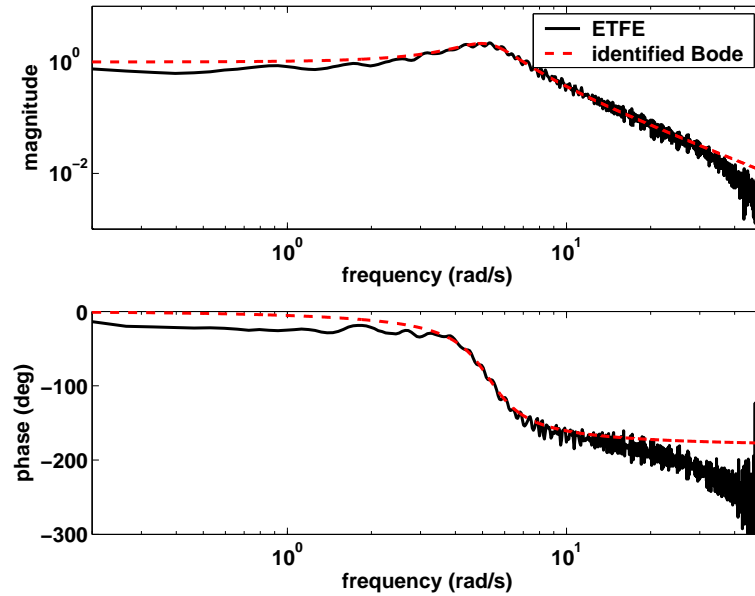


Figure 2.13: ETFE with identified Bode plot. Discrepancy at lower frequencies is due to friction and power steering nonlinearities.

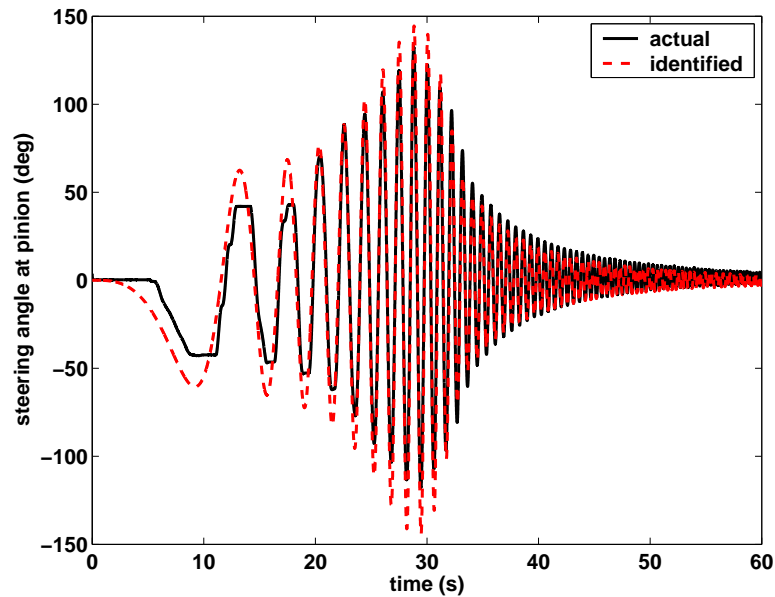


Figure 2.14: Comparison between actual and identified system response without friction model.

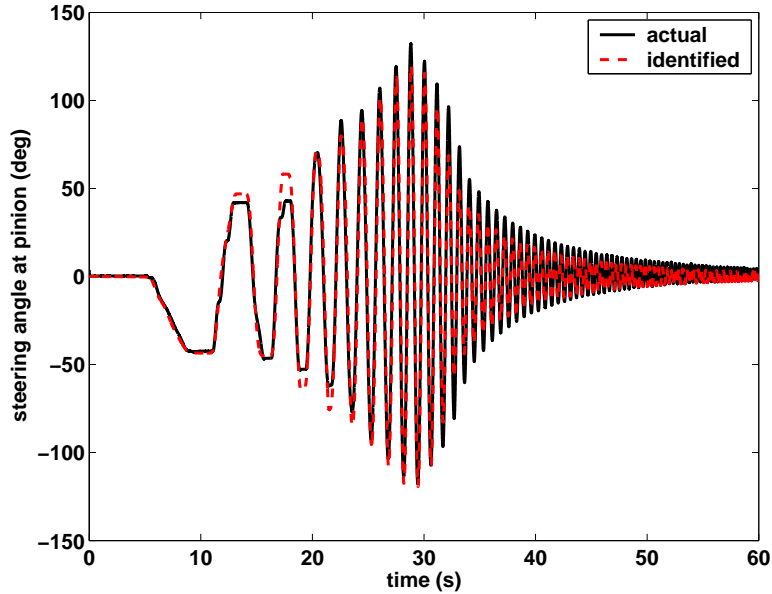


Figure 2.15: Comparison between actual and identified system response with friction model.

present in the real system. Thus, a more realistic model is described by

$$\tau = J_s \ddot{\theta} + b_s \dot{\theta} + F_s \text{sgn}(\dot{\theta}) \quad (2.7)$$

where F_s is the Coulomb friction constant. When Coulomb friction effects are included in the identified system, the response corresponds much more closely with the real system at low frequencies (Figure 2.15). The remaining difference can be attributed to the nonlinear power steering dynamics.

A good understanding of the steering system's dynamic characteristics is essential for accurate steering control. Identification of the system's physical parameters, particularly the moment of inertia, damping constant, and Coulomb friction constant provides a starting point for controller design. While the steering system parameters have so far been obtained without considering tire-to-ground contact, the influence of tire forces on the steering system cannot be ignored when driving the vehicle over the road. The next chapter addresses this critical link between the vehicle dynamics as

they are communicated through the tire forces and the steering control system which must take these forces into account.

Chapter 3

The role of vehicle dynamics in steering

The performance criteria for a steering controller are as follows: fast response, absence of overshoot or oscillatory behavior, and good accuracy with minimal steady-state error. According to automated highway researchers, an acceptable steering error for safe operation of a fully automated vehicle is a maximum of two percent of the road wheel angle [47]. At highway speeds, even a fraction of a degree change in steering angle can cause significant deviation from the vehicle's intended path. Although not directly related to steer-by-wire systems, this requirement serves as a useful guideline for evaluating steering controller performance.

Considering that the steering system has been identified as a second order system with some friction effects, these goals should be easily achievable. However, as with most controlled systems, the steering system is subject to a significant disturbance, here in the form of forces generated at the tire-road interface. Without some knowledge of the disturbance forces, designing an adequate controller would be impossible. Understanding the vehicle dynamics and how they influence the tire forces is the key to designing a controller that is robust to these disturbances.

3.1 Feedback control

3.1.1 Proportional derivative feedback

The target performance for the steer-by-wire system is, in the subjective sense, to duplicate steering commands that can be created by a driver. Normal steering inputs tend to be smooth and continuous but can vary widely in rate, so an important criterion for the steering controller is that it must follow fast inputs with minimal lag. In order to simplify the design of the controller, the case of no tire-to-ground contact (front wheels raised off the ground) is initially considered so that the influence of J_s , b_s , and F_s can be isolated from the tire disturbance forces. The control effort for this case consists of three components:

$$\tau = \tau_{feedback} + \tau_{feedforward} + \tau_{friction} \quad (3.1)$$

The proportional derivative (PD) feedback component is given by

$$\tau_{feedback} = K_p(\theta_d - \theta) + K_d(\dot{\theta}_d - \dot{\theta}) \quad (3.2)$$

where θ_d is the desired steer angle, K_p is the proportional feedback constant, and K_d is the derivative feedback constant. The feedback gains, K_p and K_d , are selected to give a fast closed loop system response without oscillatory behavior.

3.2 Feedforward control

3.2.1 Cancellation of steering system dynamics

When the real system is subject to the steering command input shown in Figure 3.1, PD control alone results in significant tracking errors (steering angle is given at the front wheels). The addition of feedforward compensation,

$$\tau_{feedforward} = J_s \ddot{\theta}_d + b_s \dot{\theta}_d \quad (3.3)$$

to the PD controller significantly improves the tracking error (Figure 3.2) by cancelling the effects of the steering system dynamics. Including the feedforward term, however, places additional demands on sensing strategy: steering rate and acceleration must be obtained from the derivatives of the position signal. Ideally, this signal should be fairly clean since high frequency noise tends to worsen with differentiation, and heavy filtering might induce lag in the signal. The test vehicle uses a combination of an automotive grade potentiometer and a high resolution encoder for both steering wheel angle and pinion angle. The potentiometer, which measures absolute angle but is subject to electrical noise, initializes the encoder, whose digital signal is immune to electrical noise but can only give relative position. An added benefit to the combined approach is physical redundancy in case of sensor failure [22].

3.2.2 Steering rate and acceleration

The solution for obtaining $\dot{\theta}_d$ and $\ddot{\theta}_d$ is to pass the measured steering wheel angle, $\theta_{d,sensor}$, through a first and second order filter, respectively. The first order filter is given by:

$$\frac{\Theta_d(s)}{\Theta_{d,sensor}(s)} = \frac{\omega_c}{s + \omega_c} \quad (3.4)$$

where ω_c is the filter cutoff frequency, chosen to be 5 Hz, low enough to filter out sensor noise and high enough to avoid disturbing the steering system dynamics. Taking the inverse Laplace transform yields an expression for desired steer rate:

$$\dot{\theta}_d = \omega_c(\theta_{d,sensor} - \theta_d) \quad (3.5)$$

Note that this filter is also applied to the feedback portion of the control signal. The second order filter is given by:

$$\frac{\Theta_d(s)}{\Theta_{d,sensor}(s)} = \frac{\omega_c^2}{s^2 + 2\omega_c s + \omega_c^2} \quad (3.6)$$

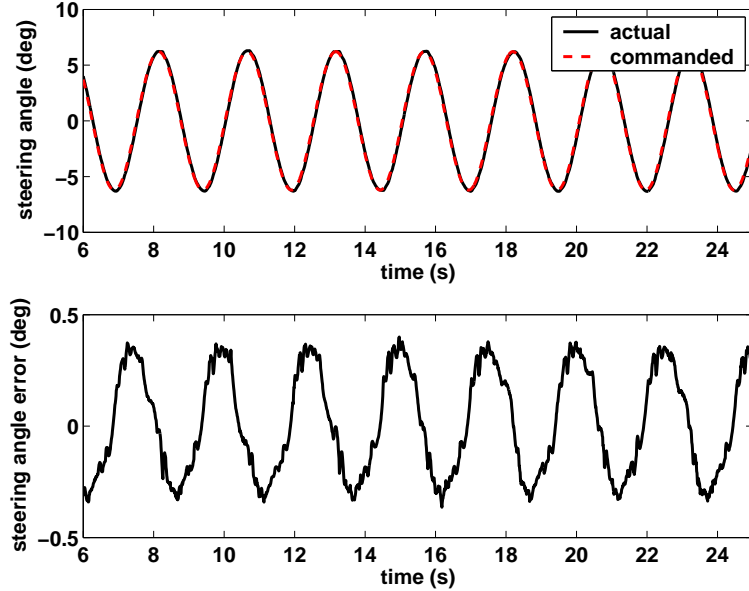


Figure 3.1: Feedback control only.

Again, taking the inverse Laplace transform leads to a system of equations from which $\ddot{\theta}_d$ can be calculated:

$$\ddot{\theta}_d = \omega_c^2(\theta_{d,sensor} - \theta_d) - 2\omega_c\dot{\theta}_d \quad (3.7)$$

3.2.3 Friction compensation

The remaining error in Figure 3.2 is associated with the internal friction of the steering system and requires an additional control term:

$$\tau_{friction} = F_s sgn(\dot{\theta}_d) \quad (3.8)$$

where F_s is the Coulomb friction constant obtained in Chapter 2. As shown in Figure 3.3, with control torque given by Equation (3.1), the tracking error can be reduced to between one and two percent of the commanded steering angle.

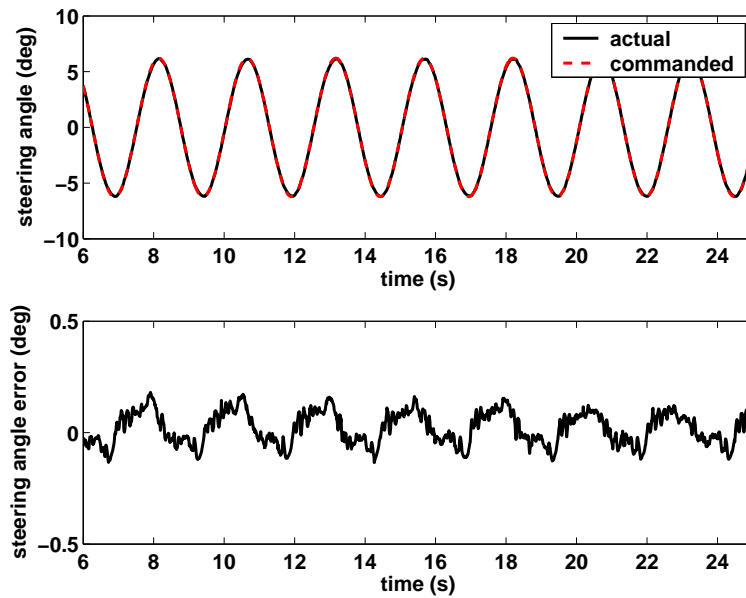


Figure 3.2: Feedback with feedforward compensation.

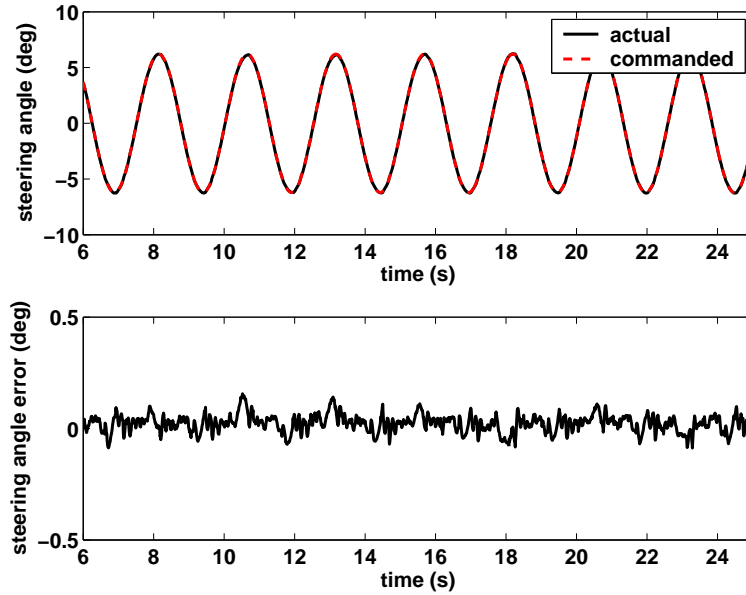


Figure 3.3: Feedback with feedforward and friction compensation.

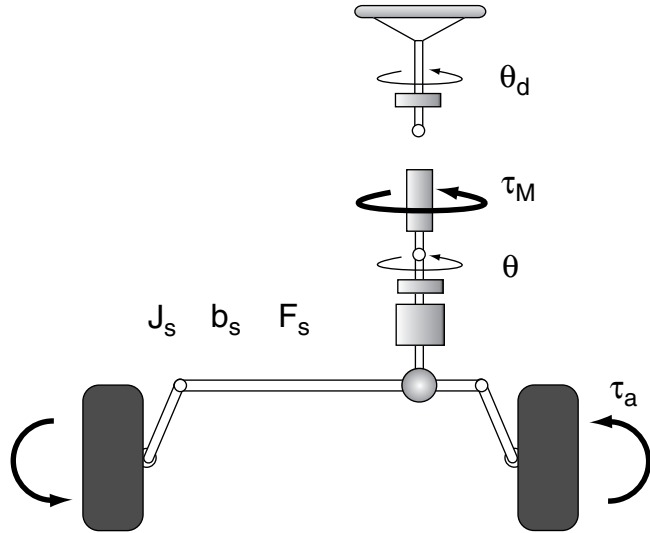


Figure 3.4: Steering system dynamics with tire-to-ground contact.

3.2.4 Effect of tire self-aligning moment

Now reintroducing tire-to-ground contact and with the vehicle moving at approximately 11.2 m/s (25 mi/hr), additional tracking error is evident in the steering system (Figure 3.5) even when the controller given by Equation (3.1) is applied. When a vehicle undergoes a turn, tire forces acting on the steering system tend to resist steering motion away from the straight-ahead position. These forces can be treated as a disturbance on the steering system and are directly attributable to tire self-aligning moment, which is a function of the steering geometry, particularly caster and kingpin angles, and the manner in which the tire deforms to generate lateral forces. In Figure 3.6, $F_{y,f}$ is the lateral force acting on the tire, α_f is the tire slip angle, t_p is the pneumatic trail, the distance between the application of lateral force and the center of the tire, t_m is the mechanical trail, the distance between the tire center and the point on the ground about which the tire pivots as a result of the wheel caster angle (Figure 3.7), and U is the velocity of the tire at its center. The total aligning moment is given by:

$$\tau_a = (t_p + t_m)F_{y,f}(\alpha_f) \quad (3.9)$$

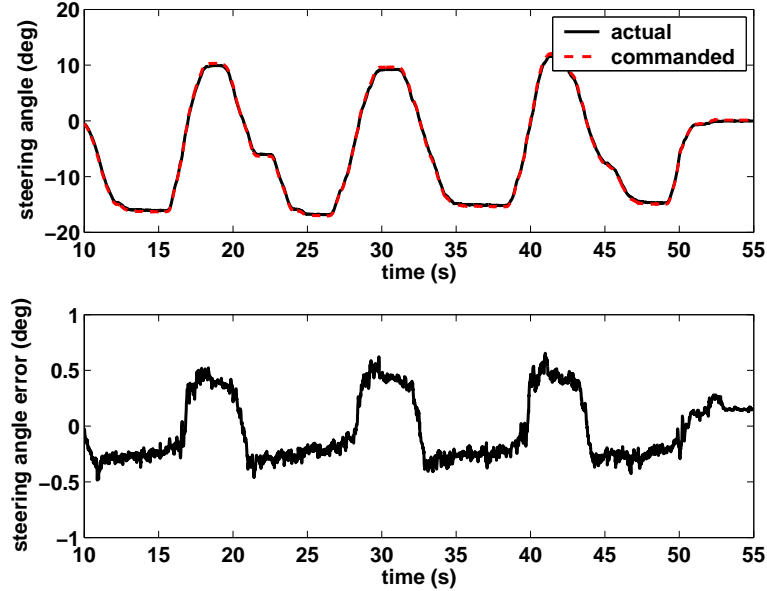


Figure 3.5: Error due to aligning moment.

The portion of aligning moment due to the tire pneumatic trail may be directly approximated as an empirical function of tire slip angle (see Appendix A). Although pneumatic trail is also a function of slip angle, it is linear for small angles. The steering geometry, particularly the kingpin inclination angle and camber angle, will cause the mechanical trail to vary with steering position (Figure 3.8). Here we assume a constant mechanical trail. Furthermore, the steering geometry often causes a slight vertical motion of the wheels—effectively raising and lowering the front of the vehicle as it is being steered—so that the steering effort must overcome the force of gravity on the vehicle sprung mass [49]. If the geometry is known, however, most of these effects can be modelled and accounted for by the controller. When the aligning moment disturbance, τ_a , is included, the steering system model given by Equation (2.7) becomes:

$$J_s \ddot{\theta} + b_s \dot{\theta} + F_s \text{sgn}(\dot{\theta}) = \tau - k_a \tau_a \quad (3.10)$$

where k_a is a scale factor to account for torque reduction by the steering gear.

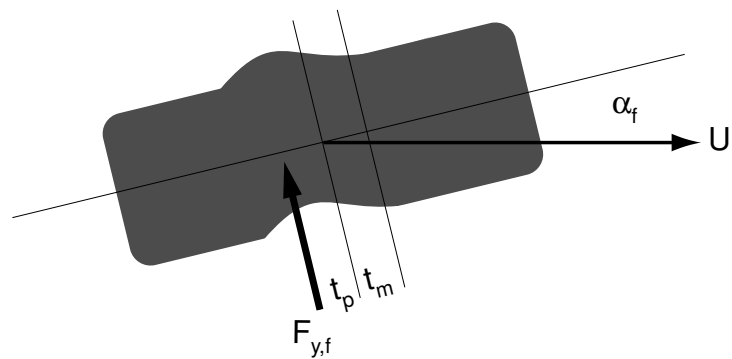


Figure 3.6: Tire operating at a slip angle.

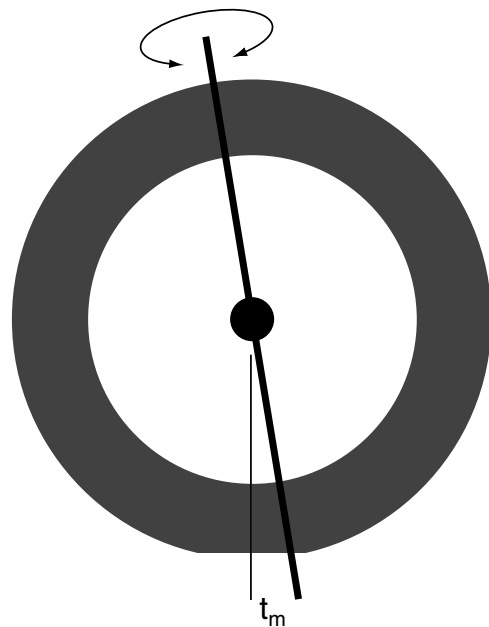


Figure 3.7: Component of aligning moment due to mechanical trail.

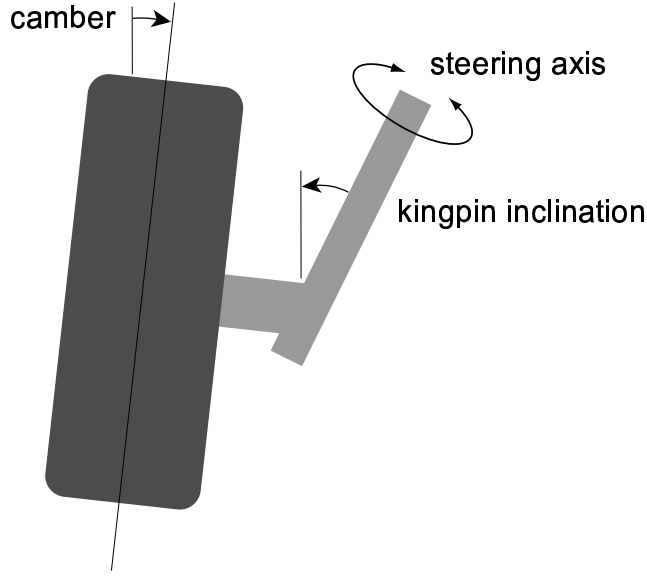


Figure 3.8: Wheel camber and kingpin inclination angle.

3.2.5 Aligning moment compensation

To cancel the effects of the tire disturbance forces, the approximation of aligning moment, $\hat{\tau}_a$, from tire slip angle measurements is added to the feedback, feedforward, and friction components of the control effort:

$$\tau = \tau_{feedback} + \tau_{feedforward} + \tau_{friction} + \tau_{aligning} \quad (3.11)$$

The aligning moment approximation is given by:

$$\tau_{aligning} = k_a \hat{\tau}_a(\alpha_f) \quad (3.12)$$

As shown in Figure 3.9, although this simple approximation may not be exact, its addition to the actuation torque effectively reduces the steering error to an acceptable range of less than two percent of the road wheel angle.

There are several reasons for considering the aligning moment separately in the steering controller. One reason is that the aligning moment disturbance makes up a

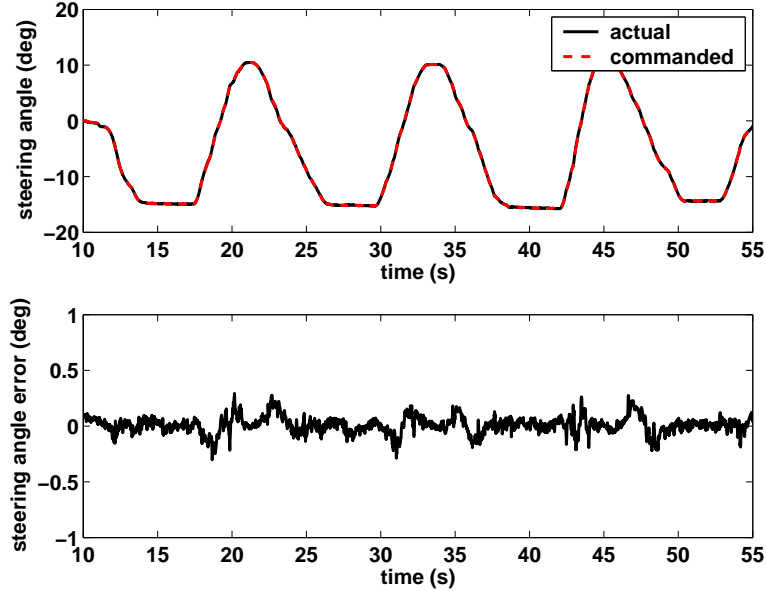


Figure 3.9: Steering controller with aligning moment compensation.

significant portion of the torque that the steering system needs to overcome. For example, during steady state cornering the actuation effort required to hold the steered wheels in place primarily serves to resist this moment. While the magnitude alone is significant, the fact that aligning moment depends on tire slip angle and therefore the vehicle dynamics means that it is a predictable physical effect that can be determined from a combination of typical vehicle sensors (see Chapter 5). This predictability makes feedforward control particularly suitable. Another reason for applying feedforward control has to do with closed loop stability. The principle behind proportional derivative feedback is to react to errors. To reduce tracking error, one can either increase the feedback gains, which leads to system instability, or add integral control, which could introduce integrator windup particularly in steering situations when there is a rapid change of direction. Neither of these outcomes is desirable.

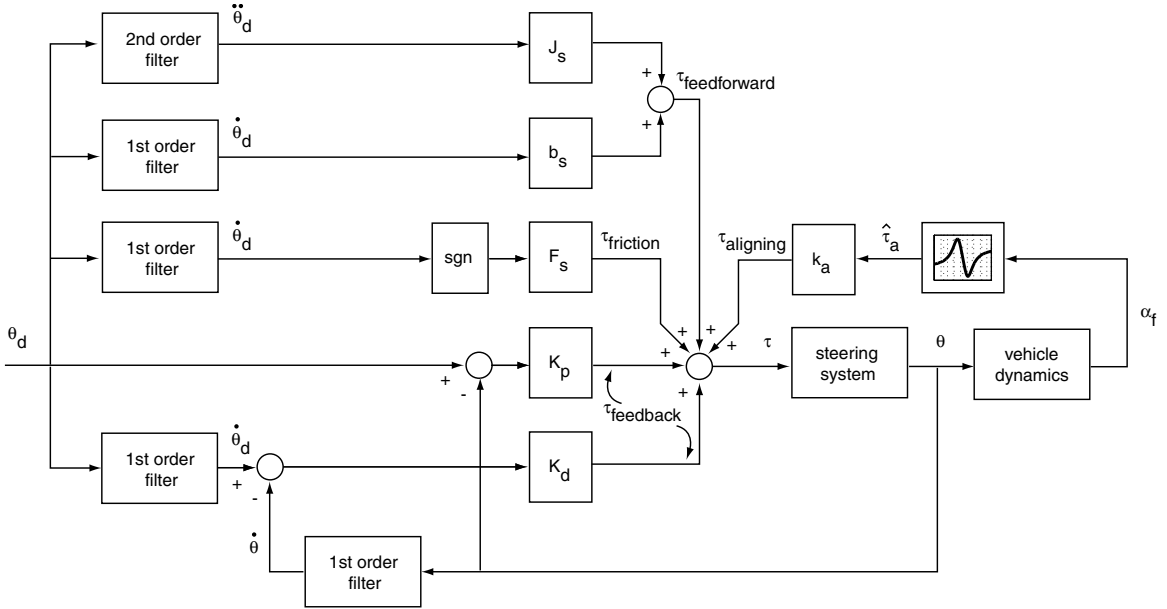


Figure 3.10: Steering controller block diagram.

3.3 Combined control

The solution to this problem is to feedforward a reasonable estimate of the effort needed to overcome the inertia, damping, friction, and tire forces. Since inertia, damping, and friction remain fairly constant in time and can be identified accurately, the feedback portion of the controller only needs to correct for errors caused by uncertainties in the disturbance approximation. By relying primarily on feedforward control, the tracking errors that feedback control must deal with are substantially reduced. Thus, the feedforward terms not only do not contribute to system instability, but they also eliminate the need for aggressive feedback. Practically speaking, such explicit cancellation of these terms is absolutely necessary to maintain stability while reducing tracking error during dynamic maneuvers. In addition, feedforward also tends to minimize control effort which is important for conserving limited electrical capacity on the vehicle. The full steering controller is summarized by the block diagram shown in Figure 3.10.

3.3.1 Error dynamics

The effectiveness of this control form can be easily seen in the error dynamics, which are determined by combining Equations (3.10) and (3.11),

$$\begin{aligned}\ddot{e} &= \frac{1}{J_s}(K_p e + K_d \dot{e}) + [F_s \text{sgn}(\dot{\theta}_d) - F_s \text{sgn}(\dot{\theta}) + k_a \hat{\tau}_a - k_a \tau_a] \\ &= \frac{1}{J_s}(K_p e + K_d \dot{e}) + \delta e\end{aligned}\quad (3.13)$$

where the error, e , is given by:

$$e = \theta_d - \theta \quad (3.14)$$

Aside from some uncertainties, δe , in compensating for the friction and tire aligning moment, the error dynamics are stable and approach zero quickly if K_p and K_d are chosen appropriately. Even with approximate values of the Coulomb friction constant, F_s , and aligning moment, $\hat{\tau}_a$, the controller can produce good tracking results, which suggests that it is robust to disturbances and variations in the steering system parameters.

Chapter 4

A means to influence vehicle handling

A vehicle's handling characteristics are dictated by its physical parameters: wheelbase, track width, center of gravity location, mass, moment of inertia, suspension design, and tire properties. Without active control, the only way to change how a vehicle handles is to alter one or more of these physical parameters. Such changes may involve significant design considerations and typically cannot be done "on the fly." The theme of this chapter offers exactly this possibility: with a combination of active steering capability and feedback control, a vehicle's response to the driver's inputs can be modified though the physical parameters of the vehicle remain unchanged. In other words, the application of dynamic feedback can modify the vehicle states so that, from the driver's perspective, the vehicle has a fundamentally different handling characteristic. This idea is compelling from a design viewpoint, since a near infinite number of physical design variations can be evaluated on a single platform [42, 27]. More practically, a vehicle with such a system could automatically compensate for unforeseen changes in physical parameters (i.e. mass and weight distribution due to loading) as well as changes in operating conditions (i.e. road friction) that might otherwise have a deleterious effect on handling behavior [20]. This chapter presents one way in which feedback of vehicle sideslip angle and yaw rate combined with active steering capability may be used to modify a vehicle's handling characteristics.



Figure 4.1: NASA's F6F-3 Hellcat variable stability airplane circa 1950 at the Ames Aeronautical Laboratory, Moffett Field, California with flight personnel. Note the vane on the wingtip for measuring aircraft sideslip angle. Credit: NASA

4.1 Historical background: variable stability aircraft

One of the earliest examples of applying feedback to achieve different dynamic characteristics is NASA's variable stability aircraft developed in the 1940s (Figure 4.1). An airplane's wing dihedral angle (Figure 4.2(a)) plays an important role in its lateral stability. When an aircraft experiences roll motion, the resulting bank angle produces an imbalance in forces that causes the plane to sideslip, or move sideways (Figure 4.2(b)). A positive dihedral (wing tips higher than base) subject to these side forces in turn produces forces and moments that tend to reduce the bank angle and restore the plane to equilibrium (Figure 4.2(c)). Other physical characteristics, such as the height of the wing base on the fuselage and degree of wing sweep, also influence lateral stability and contribute to the "effective" dihedral.

Thus, some effective dihedral is good for stability; a plane with too much dihedral, however, is "too stable" and therefore has limited maneuverability. The initial

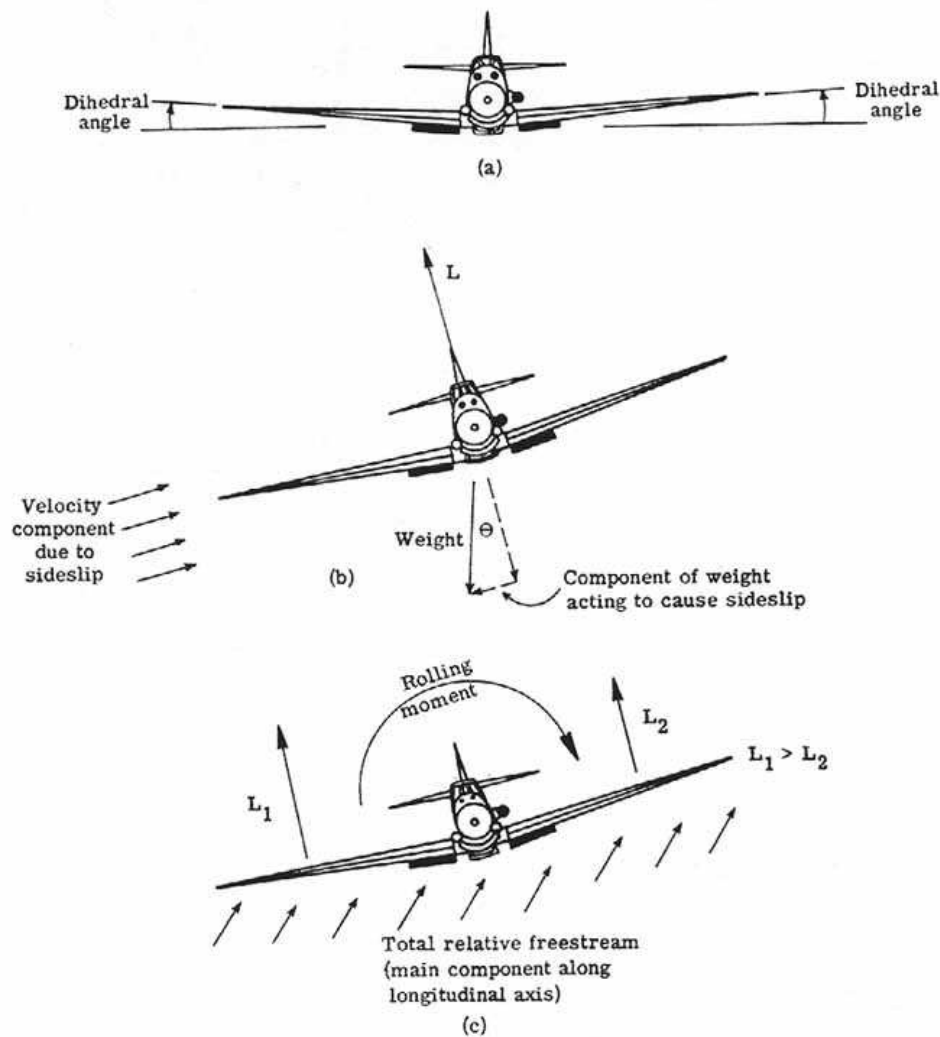


Figure 4.2: Front views of aircraft showing (a) positive dihedral, (b) sideslip due to bank angle, and (c) stabilizing roll moment. Credit: NASA

purpose for designing the variable stability aircraft was to find an acceptable range of dihedral without having to construct and test numerous planes, each with a different wing angle. To exactly duplicate a given effective dihedral, NASA designed a servomechanism that deflects the ailerons in response to the plane's sideslip angle [24]. The mechanism allowed the deflection to remain transparent to the pilot through the control stick except for the apparent change in flight stability characteristics.

4.2 Vehicle dynamics

By a similar concept, the stability characteristics of a steer-by-wire vehicle may be altered by virtually changing the front tires via feedback of the vehicle states, yaw rate and sideslip angle. To explain how changing front tire characteristics affects vehicle handling behavior, it is first necessary to develop a model that describes the fundamental handling characteristics in terms of the vehicle parameters.

4.2.1 Linear vehicle model

A vehicle's handling dynamics in the horizontal plane are represented here by the single track, or bicycle model with states of sideslip angle, β , at the center of gravity (CG) and yaw rate, r . In Figure 4.3, δ is the steering angle, $u_{x,CG}$ and $u_{y,CG}$ are the longitudinal and lateral components of the CG velocity, $F_{y,f}$ and $F_{y,r}$ are the lateral tire forces front and rear, respectively, and α_f and α_r are the tire slip angles. Derivation of the equations of motion for the bicycle model follows from the force and moment balance:

$$\begin{aligned} ma_{y,CG} &= F_{y,f} \cos \delta + F_{y,r} \\ I_z \dot{r} &= aF_{y,f} \cos \delta - bF_{y,r} \end{aligned} \quad (4.1)$$

I_z is the moment of inertia of the vehicle about its yaw axis, m is the vehicle mass, a and b are distances of the front and rear axles to the CG, and $a_{y,CG}$ is lateral acceleration at the CG. In the linear region of tire operation—typically slip angles of four degrees or less—lateral force at the front and rear is related to slip angle by

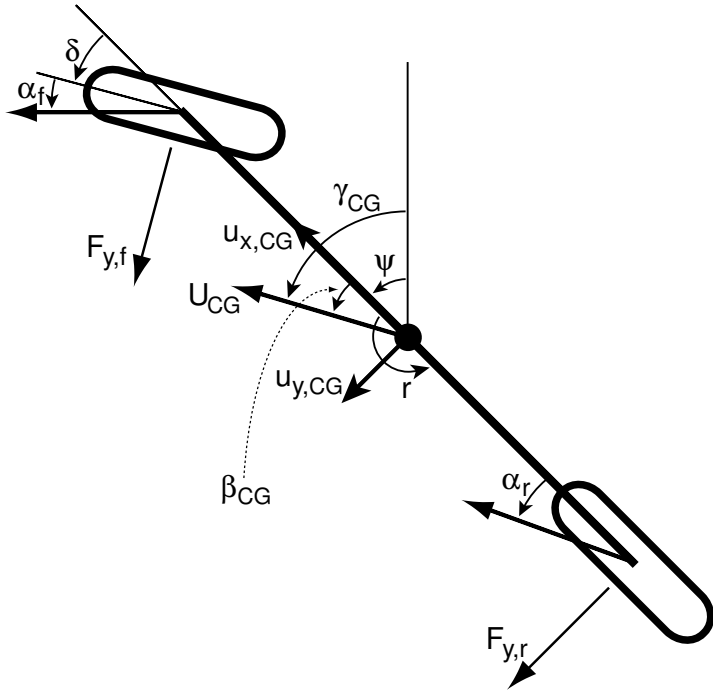


Figure 4.3: Bicycle model.

the total cornering stiffness of the front and rear tires:

$$F_{y,f} = -C_{\alpha,f}\alpha_f \quad (4.2)$$

$$F_{y,r} = -C_{\alpha,r}\alpha_r$$

At larger slip angles, the relation between force and slip angle becomes nonlinear (see Appendix A). Taking small angle approximations, slip angle can be written in terms of $u_{x,CG}$, $u_{y,CG}$, and r :

$$\begin{aligned} \alpha_f &= \frac{u_{y,CG} + ar}{u_{x,CG}} - \delta & (4.3) \\ \alpha_r &= \frac{u_{y,CG} - br}{u_{x,CG}} \end{aligned}$$

Assuming constant longitudinal velocity $u_{x,CG} = V$, the state equation for the bicycle model can be written as:

$$\begin{bmatrix} \dot{u}_{y,CG} \\ \dot{r} \end{bmatrix} = \begin{bmatrix} \frac{-C_{\alpha,f}-C_{\alpha,r}}{mV} & -V + \frac{C_{\alpha,r}b-C_{\alpha,f}a}{mV^2} \\ \frac{C_{\alpha,r}b-C_{\alpha,f}a}{I_zV} & \frac{-C_{\alpha,f}a^2-C_{\alpha,r}b^2}{I_zV} \end{bmatrix} \begin{bmatrix} u_{y,CG} \\ r \end{bmatrix} + \begin{bmatrix} \frac{C_{\alpha,f}}{m} \\ \frac{C_{\alpha,f}a}{I_z} \end{bmatrix} \delta \quad (4.4)$$

Given longitudinal and lateral velocity, u_x and u_y , at any point on the vehicle body, the sideslip angle at the point is defined by:

$$\beta = \arctan \left(\frac{u_y}{u_x} \right) \quad (4.5)$$

Sideslip angle can also be defined by the difference between the vehicle's forward orientation, ψ , and the direction of the velocity, γ , at any point on the body.

$$\beta = \gamma - \psi \quad (4.6)$$

Rewriting Equation (4.4) in terms of sideslip angle at the CG, β_{CG} , yields the state equation,

$$\begin{bmatrix} \dot{\beta}_{CG} \\ \dot{r} \end{bmatrix} = \begin{bmatrix} \frac{-C_{\alpha,f}-C_{\alpha,r}}{mV} & -1 + \frac{C_{\alpha,r}b-C_{\alpha,f}a}{mV^2} \\ \frac{C_{\alpha,r}b-C_{\alpha,f}a}{I_z} & \frac{-C_{\alpha,f}a^2-C_{\alpha,r}b^2}{I_zV} \end{bmatrix} \begin{bmatrix} \beta_{CG} \\ r \end{bmatrix} + \begin{bmatrix} \frac{C_{\alpha,f}}{mV} \\ \frac{C_{\alpha,f}a}{I_z} \end{bmatrix} \delta \quad (4.7)$$

with states of the bicycle model now defined by slip angle at the CG and yaw rate.

4.2.2 The fundamental handling characteristics: understeer, oversteer, and neutral steer

The bicycle model serves as a useful tool for describing a vehicle's fundamental handling characteristics. One way to approach an explanation of handling characteristics using the bicycle model is to define a term known as the understeer gradient:

$$K_{us} = \left(\frac{W_f}{C_{\alpha,f}} - \frac{W_r}{C_{\alpha,r}} \right) \frac{1}{g} \quad (4.8)$$

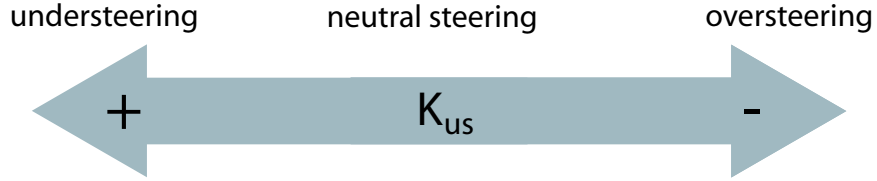


Figure 4.4: The fundamental handling characteristics as determined by the sign of the understeer gradient.

where W_f is the weight over the front axle of the vehicle, W_r is the weight over the rear axle, and g is the gravitational acceleration constant. The understeer gradient may also be written as:

$$K_{us} = -\frac{m}{L} \frac{C_1}{C_{\alpha,f} C_{\alpha,r}} \quad (4.9)$$

As expressed by Equation (4.8), the understeer gradient includes the vehicle parameters that most heavily influence handling stability: weight distribution and tire cornering stiffness. A positive understeer gradient results in a vehicle that is said to have understeering characteristics. This would be the case if the front and rear tires have similar properties and the weight is biased toward the front of the vehicle. If the weight is biased toward the rear of a vehicle, the result is a negative understeer gradient and an oversteering vehicle. If the weight is balanced equally front to rear, the vehicle has neutral steering characteristics and the understeer gradient is zero.

One of the key differences between the three types of handling characteristics can be observed during steady state cornering. For the same steering angle and vehicle speed, an oversteering vehicle will tend to turn in a tighter circle than a neutral steering vehicle (Figure 4.5). Just the opposite, an understeering vehicle will tend to follow a wider path around the turn. Note that weight transfer during acceleration or braking temporarily produces the same effect. While transient handling characteristics are quite a bit more complicated, the overall effect during normal driving is that an oversteering car tends to be more responsive to steering inputs, while an understeering car is less responsive.

From the perspective of vehicle stability, however, the oversteering vehicle, though more responsive, is not necessarily more desirable. To examine the stability characteristics of each of the three handling cases, one can take the Laplace transform of

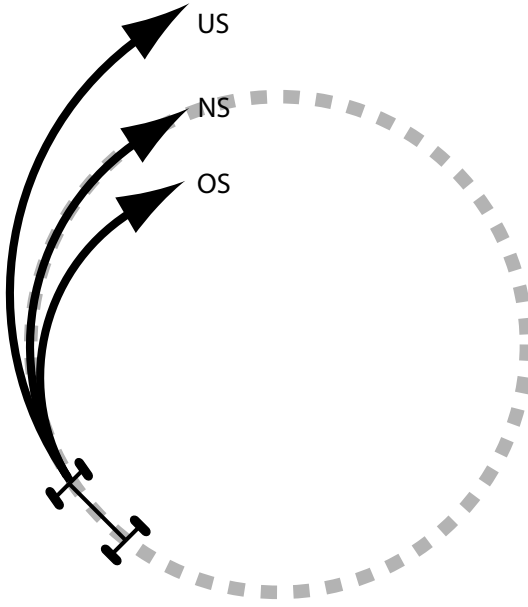


Figure 4.5: Steady state cornering.

the bicycle model equation to obtain the transfer function between either yaw rate and steering angle or sideslip and steering angle. The transfer function denominator, or characteristic equation of the system, contains all the information necessary to determine stability.

$$\frac{R(s)}{\Delta(s)} = \frac{aC_{\alpha,f}s + \left(\frac{aC_{\alpha,f}C_{\alpha,0} - C_{\alpha,1}C_{\alpha,f}}{mV}\right)}{I_z s^2 + \left(\frac{C_{\alpha,0}I_z + mC_{\alpha,2}}{mV}\right)s + \left(\frac{C_{\alpha,0}C_{\alpha,2}}{mV^2} - C_{\alpha,1} - \frac{C_{\alpha,1}^2}{mV^2}\right)} \quad (4.10)$$

To consolidate notation, $C_{\alpha,0}$, $C_{\alpha,1}$, and $C_{\alpha,2}$ are used to represent:

$$\begin{aligned} C_{\alpha,0} &= C_{\alpha,f} + C_{\alpha,r} \\ C_{\alpha,1} &= C_{\alpha,r}b - C_{\alpha,f}a \\ C_{\alpha,2} &= C_{\alpha,f}a^2 + C_{\alpha,r}b^2 \end{aligned}$$

The system is unstable if the roots of the characteristic equation are positive, or when

the third term in the denominator is less than zero:

$$\frac{C_{\alpha,0}C_{\alpha,2}}{mV^2} - C_{\alpha,1} - \frac{C_{\alpha,1}^2}{mV^2} < 0 \quad (4.11)$$

Since vehicle speed, V , is always positive, this also means that:

$$C_{\alpha,0}C_{\alpha,2} - C_{\alpha,1}^2 - C_{\alpha,1}mV^2 < 0 \quad (4.12)$$

Substituting for $C_{\alpha,0}$, $C_{\alpha,1}$, and $C_{\alpha,2}$ yields:

$$L^2C_{\alpha,f}C_{\alpha,r} - C_{\alpha,1}mV^2 < 0 \quad (4.13)$$

where $L = a+b$ is the wheelbase length. This can be simplified further by rearranging Equation (4.9) and substituting for the remaining $C_{\alpha,1}$ term:

$$L^2 + K_{us}V^2 < 0 \quad (4.14)$$

The inequality is only valid if the understeer gradient, K_{us} , is negative (the vehicle is oversteering) and the speed is above the critical speed, defined by:

$$V_{cr} = \sqrt{\frac{-L}{K_{us}}} \quad (4.15)$$

Therefore, the unstable condition does not exist for a vehicle with understeering or neutral steering characteristics. According to the linear vehicle model, instability occurs when an oversteering vehicle is travelling faster than its critical speed.

Passenger vehicles are never designed to have oversteering characteristics for this reason. In fact, most vehicles are designed with characteristics solidly in the understeering range of the handling scale: this is to provide a margin of safety in case, for example, passengers or cargo move the weight distribution rearward and therefore shift the handling behavior toward the oversteering end of the scale. Some types of vehicles, such as 15-passenger vans, are particularly susceptible to this problem [50]. To a lesser extent, differences in tire cornering stiffness between the front and rear due

to wear or tread characteristics can have a similar effect. Since a vehicle's handling characteristics are inherent to its physical design, there will always be a design trade-off between the stability and predictability of heavily understeering behavior and the responsiveness and potential instability of marginally understeering, neutral steering, or oversteering characteristics.

An important distinction should be made between oversteering as a handling characteristic and the term "limit oversteer," which describes the situation during cornering when the rear tires lose their grip on the pavement before the front tires. This behavior occurs outside of the linear handling region described by the linear tire force model ($F_y = C_{\alpha,f}\alpha_f$). If not corrected quickly enough, a vehicle undergoing limit oversteer will fishtail or spin out. Similarly, the term "limit understeer" refers to the opposite condition: the front tires reach the limits of adhesion before the rear tires, and the vehicle no longer responds to increasing steering angles. Any vehicle, whether understeering, neutral steering, or oversteering, can potentially experience either of these situations given the right (or wrong) driving conditions. During normal street driving, a vehicle almost never ventures into nonlinear handling territory. Limit oversteer and understeer are mainly of concern during emergency maneuvers, high performance driving, or on very slippery surfaces such as snow or ice. These situations involving transition to nonlinear tire characteristics will be addressed later in the thesis, as they are exactly analogous to the linear case.

4.3 Handling modification

4.3.1 Full state feedback: a virtual tire change

The full state feedback control law for an active steering vehicle is given by:

$$\delta = K_r r + K_\beta \beta + K_d \delta_d \quad (4.16)$$

where δ_d is the driver's steering angle measured at the handwheel and δ is the actual steering angle commanded by the controller. A physically intuitive way to modify a

vehicle's handling characteristics is to define a target front cornering stiffness as:

$$\hat{C}_{\alpha,f} = C_{\alpha,f}(1 + \eta) \quad (4.17)$$

and the state feedback gains as:

$$K_\beta = -\eta \quad K_r = -\frac{a}{V}\eta \quad K_d = (1 + \eta) \quad (4.18)$$

where η is the desired fractional change in the original front cornering stiffness, $C_{\alpha,f}$. Substituting the feedback law, Equation (4.16), into Equation (4.7) yields a state space equation of the same form as Equation (4.7) but with the new cornering stiffness, $\hat{C}_{\alpha,f}$:

$$\begin{bmatrix} \dot{\beta}_{CG} \\ \dot{r} \end{bmatrix} = \begin{bmatrix} \frac{-\hat{C}_{\alpha,f} - C_{\alpha,r}}{mV} & -1 + \frac{C_{\alpha,r}b - \hat{C}_{\alpha,f}a}{mV^2} \\ \frac{C_{\alpha,r}b - \hat{C}_{\alpha,f}a}{I_z} & \frac{-\hat{C}_{\alpha,f}a^2 - C_{\alpha,r}b^2}{I_z V} \end{bmatrix} \begin{bmatrix} \beta_{CG} \\ r \end{bmatrix} + \begin{bmatrix} \frac{\hat{C}_{\alpha,f}}{mV} \\ \frac{\hat{C}_{\alpha,f}a}{I_z} \end{bmatrix} \delta \quad (4.19)$$

Since a vehicle's handling characteristics are directly influenced by tire cornering stiffness, the effect of this modification is to make the vehicle either more oversteering or understeering depending on the sign of η . Of course, there are many other ways to apply full state feedback, but the physical motivation behind cornering stiffness adjustment makes clear through the bicycle model exactly how the handling characteristics have been modified. In fact, the effect of this modification is analogous to a common practice in automotive racing: changing tires during a pit stop to adjust a race car's handling dynamics.

A question that naturally arises from this form of vehicle dynamics control is whether similar handling changes can be achieved given only yaw rate feedback. Although yaw rate feedback is frequently proposed [23] [3] [48] as a way to control gross vehicle motion, yaw rate feedback alone leaves sideslip uncontrolled. It then becomes possible to change the vehicle transfer function to something that is neither physically realizable nor intuitive to the driver, and the effects of this are unclear. Furthermore, in extreme cases there may be good yaw tracking but excessive sideslip [1]. As mentioned before, this type of situation falls outside the realm of safe handling

behavior and is undesirable for most drivers.

Note that in the full state feedback formulation presented here, it is not necessary to know the real cornering stiffness of the front tire—only vehicle speed and weight distribution, which are relatively easy to measure—to achieve the desired handling modification. In addition, while the control law has a simple structure, there is a nonlinear relation between the vehicle speed, CG location, and cornering stiffness adjustment parameter in the yaw rate feedback gain, which is essentially a nonlinear gain scheduling approach to vehicle control. Finally, because the control law is additive—the control input is added on top of the command input—the modified handling behavior is rather insensitive to nonlinear vehicle characteristics such as tire saturation.

Figure 4.6 shows a nonlinear simulation of a neutral steering vehicle compared to an inherently oversteering vehicle made effectively neutral steering by handling modification. Figure 4.7 illustrates the same maneuver on an inherently oversteering vehicle compared to a neutral steering vehicle made equivalently oversteering by handling modification. Since handling modification is based on a linear vehicle model, it is expected that the results will not be exactly the same once the vehicle leaves the linear handling region. However, the outcomes are very similar and in the oversteering case, the modified handling actually maintains consistent stable behavior even as the oversteering vehicle begins to experience instability.

4.3.2 GPS-based state estimation

To implement the full state feedback control scheme described above requires accurate information on both vehicle states—yaw rate and sideslip angle. Although yaw rate data is available on many production cars from rate gyroscopes, sideslip cannot be directly measured and must be estimated instead. Two common techniques for estimating this value are to integrate inertial sensors directly and to use a physical vehicle model. Some methods use a combination or switch between these two methods appropriately based on vehicle states [13]. Direct integration methods can accumulate errors from sensor bias and unwanted measurements from road grade and

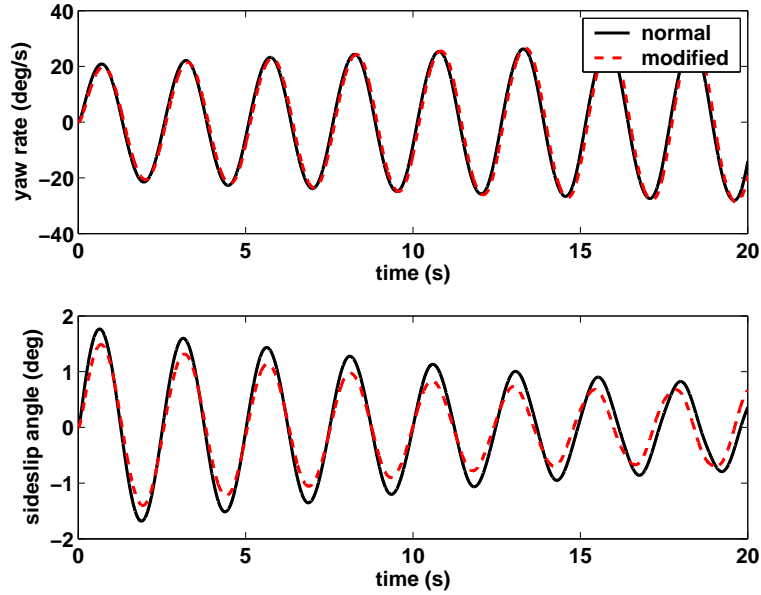


Figure 4.6: Nonlinear vehicle simulation with and without handling modification: neutral steering case.

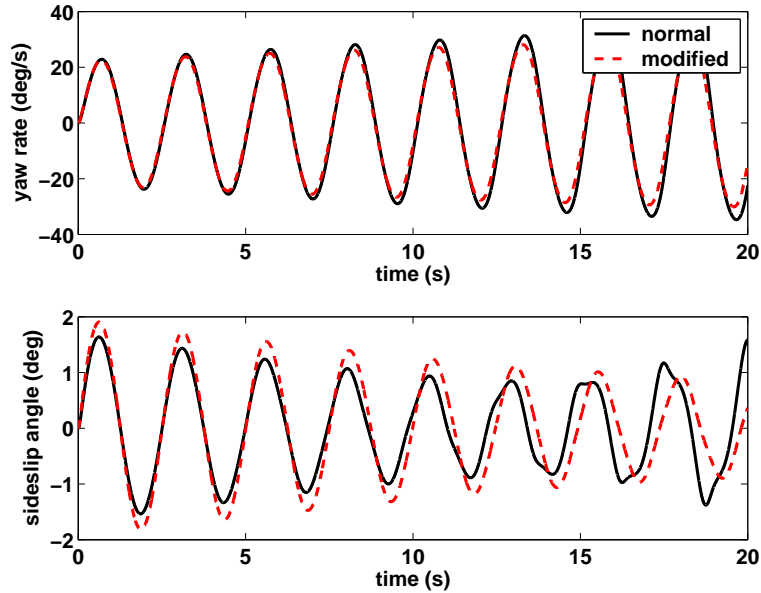


Figure 4.7: Nonlinear vehicle simulation with and without handling modification: oversteering case.

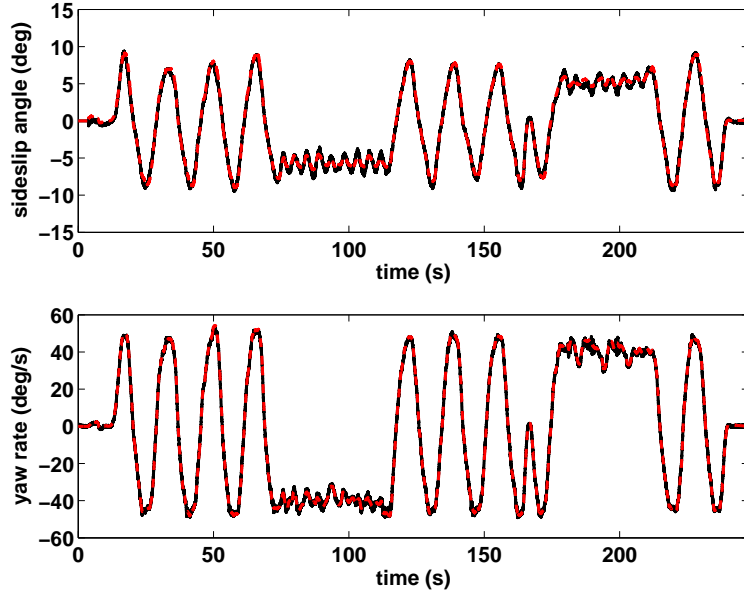


Figure 4.8: Sideslip and yaw rate estimation.

bank angle. In addition, methods based on a physical vehicle model can be sensitive to changes in the vehicle parameters and are only reliable in the linear region.

To overcome these drawbacks, a new method for estimating vehicle sideslip angle using GPS and INS sensor measurements is presented in [44]. In this scheme, GPS measurements from a two-antenna system are combined with INS sensor measurements to eliminate errors due to direct integration. Since both the vehicle heading and the direction of velocity are directly measured from a two-antenna GPS receiver, the sideslip angle can be calculated using Equation (4.6). INS sensors are integrated with GPS measurements to provide higher update rate estimates of the vehicle states and to handle periods of GPS signal loss. This method is also independent of any parameter uncertainties and changes because it is based on purely kinematic relationships. A Kalman filtering approach is used to combine the GPS and INS signals as a measurement update and time update to the estimator. Further details on this approach can be found in [44].

Experimental results from the GPS/INS integration are plotted in Figure 4.8 on



Figure 4.9: Steer-by-wire Corvette undergoing testing on the West Parallel of Moffett Federal Airfield at the NASA Ames Research Center. Moffett is an active airfield.

top of simulation results from the bicycle model for both yaw rate and sideslip angle. The similarity between estimated and simulated yaw rates indicates that the bicycle model used in the comparison is valid and calibrated correctly. The fact that the sideslip measurement is clean and correlates with the model makes it suitable for use as a feedback signal.

4.3.3 Experimental handling results

The handling modifications are implemented on the steer-by-wire test vehicle, which is further equipped with multiple-antenna GPS configured to provide absolute velocity and heading information. INS sensors measure lateral and longitudinal acceleration, yaw rate, and roll rate. The experimental setup for vehicle state estimation is the same as described in [45]. To conduct high speed evaluations, the author returned to the airfield at Moffett Field, California, where NASA’s variable dynamics aircraft was first developed and tested (Figure 4.9). All results presented here are based on the following test procedure: the vehicle accelerates from standstill in a straight line; once it reaches a steady speed of 13.4 m/s (30 mi/hr), the onboard computer begins to generate a sinusoidal steering command of constant amplitude and frequency

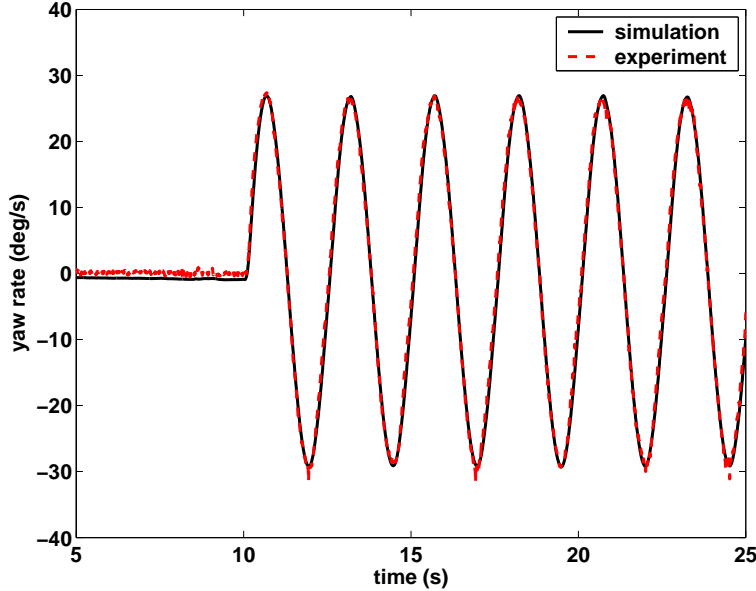


Figure 4.10: Comparison between yaw rate of bicycle model and experiment with normal cornering stiffness.

(equivalent to a driver's input at the steering wheel). For the first test, the vehicle is driven in the unmodified mode (no state feedback) such that the road wheel angle corresponds directly to command angle scaled by the steering ratio. In Figure 4.10, the measured yaw rate for this test compares well to simulation results from the bicycle model. Figure 4.11 shows the sideslip comparison for the same test data. Convergence of the state estimator causes some deviation from the simulation in the first few cycles. The sideslip data is also somewhat noisy due to unevenness in the pavement used for testing. However, given that the sideslip angle being measured is around one degree or less, the results match extremely well.

Changes in handling behavior under full state feedback control are evaluated by comparing measured vehicle response to the nominal case shown in Figures 4.10 and 4.11. In Figure 4.12, the effective front cornering stiffness is reduced 50% by setting the parameter η to -0.5, and the steering input has been modified by the control law to achieve exactly this characteristic. The experimental results exhibit lower peak yaw rate and lateral acceleration values than the nominal case (Figures 4.13 and 4.14).

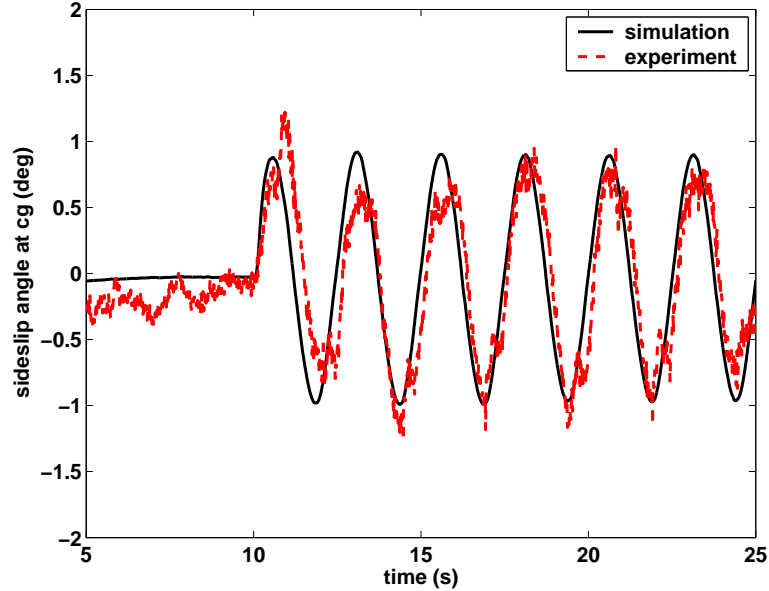


Figure 4.11: Comparison between sideslip angle of bicycle model and experiment with normal cornering stiffness.

These results are expected since reducing the front cornering stiffness causes more pronounced understeering behavior. Figures 4.15 and 4.16 confirm that test results for the reduced case match bicycle model simulation.

Experimental data show a corresponding but opposite change in handling behavior when the nominal steering input is modified to duplicate the condition of increased front cornering stiffness (Figure 4.17) such that there are more pronounced oversteering characteristics. For the same nominal steering input, the vehicle generates higher peak yaw rate and lateral acceleration than in the normal handling case (Figures 4.18, 4.19, and 4.20). The fact that peak lateral accelerations for this test approach 9.8 m/s^2 (1 g) (Figure 4.19) and experimental sideslip deviates from the sideslip predicted by the model in some places (Figure 4.21) indicates that the vehicle has entered the nonlinear handling region. Even though the linear model on which the controller is based is less valid in this case, it still produces reasonable and predictable handling behavior.

For the final series of tests, 182 kg (400 lb) of weight are added to the rear of the

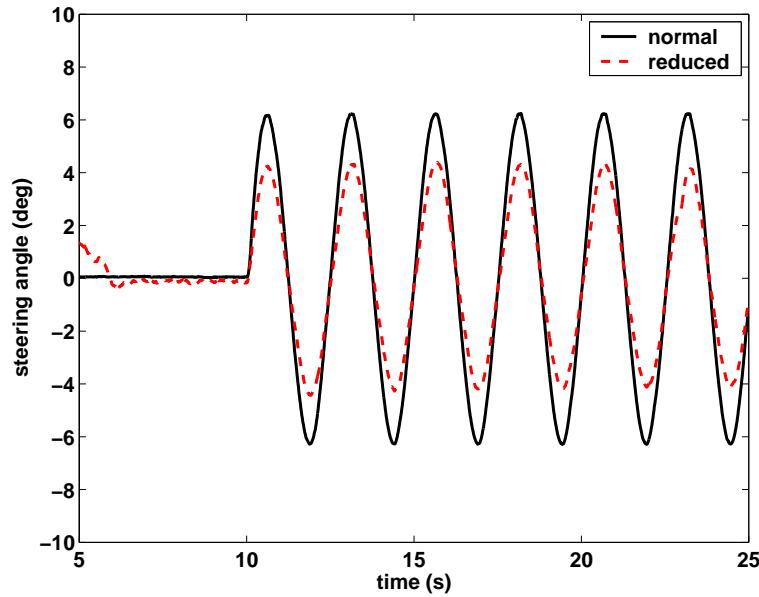


Figure 4.12: Difference in road wheel angle with effectively reduced front cornering stiffness.

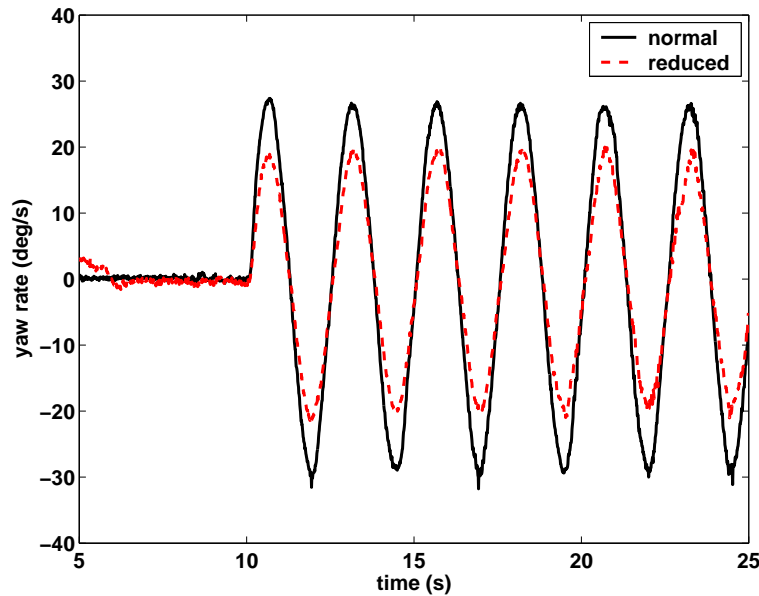


Figure 4.13: Comparison between yaw rate of normal and effectively reduced front cornering stiffness.

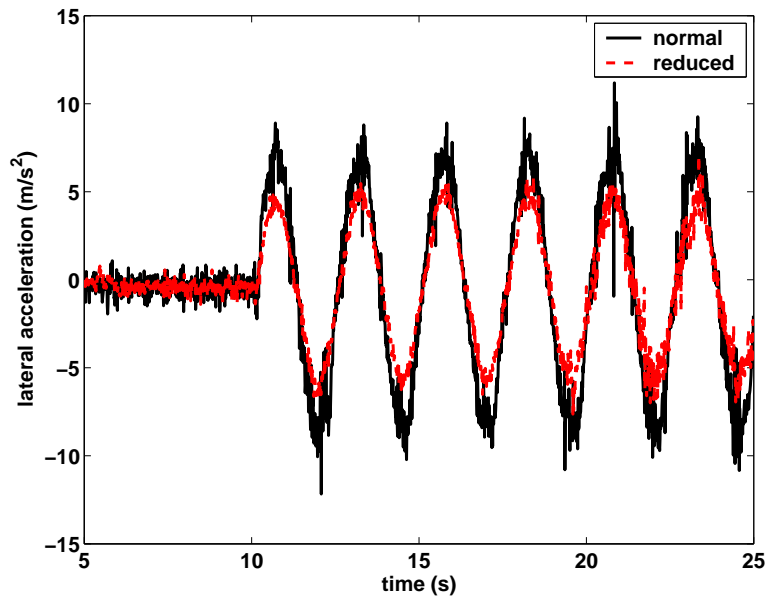


Figure 4.14: Comparison between lateral acceleration of normal and effectively reduced front cornering stiffness.

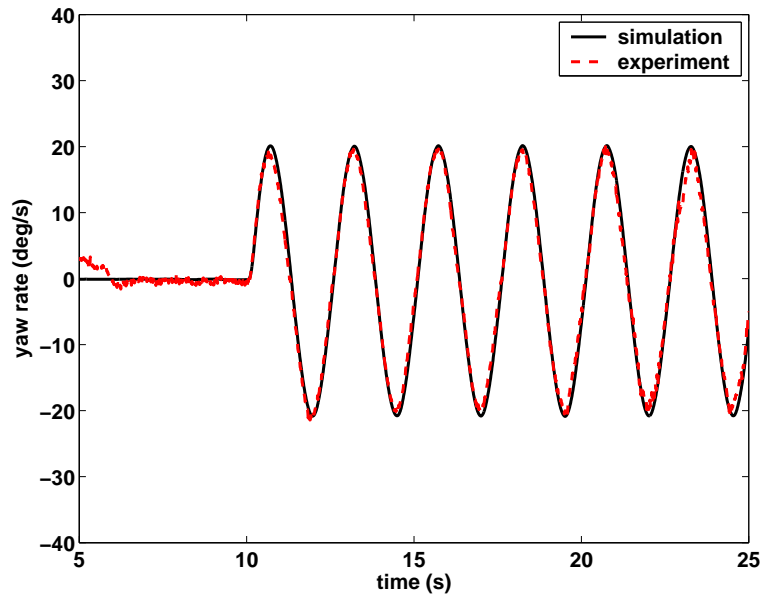


Figure 4.15: Comparison between yaw rate of bicycle model and experiment with reduced front cornering stiffness.

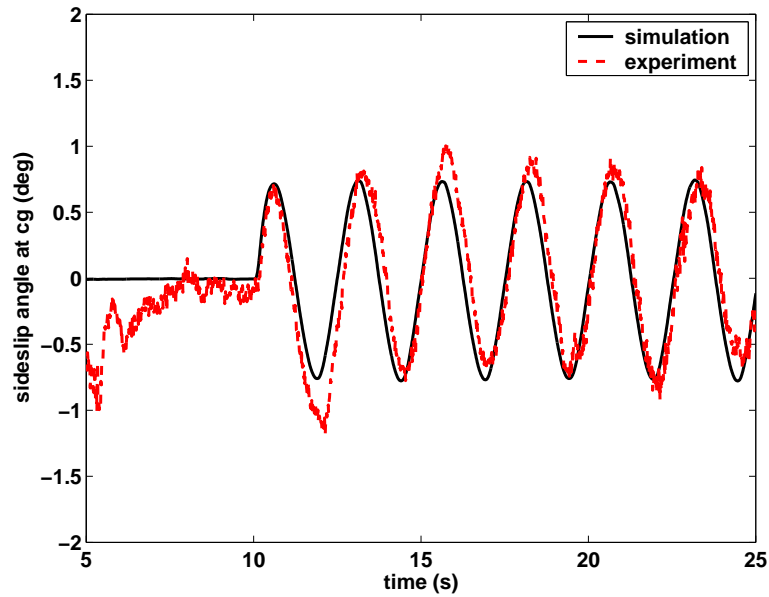


Figure 4.16: Comparison between sideslip angle of bicycle model and experiment with reduced front cornering stiffness.

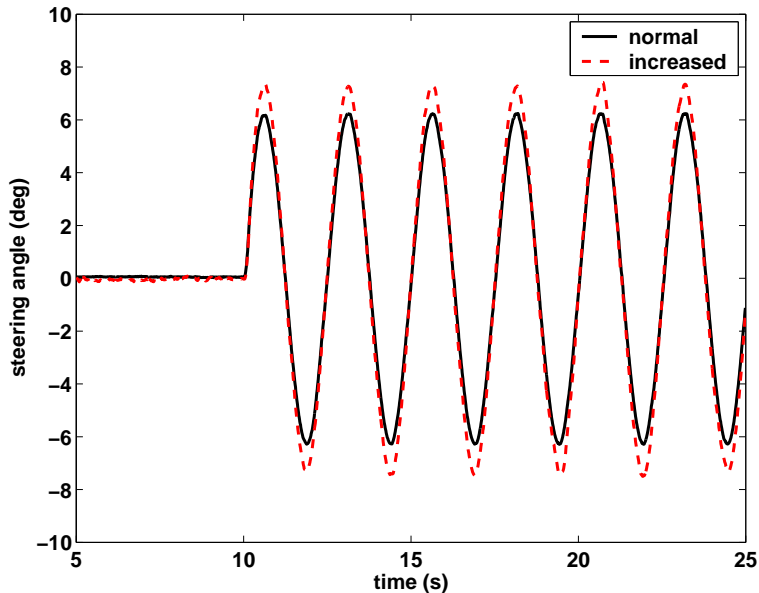


Figure 4.17: Difference in road wheel angle with effectively increased front cornering stiffness.

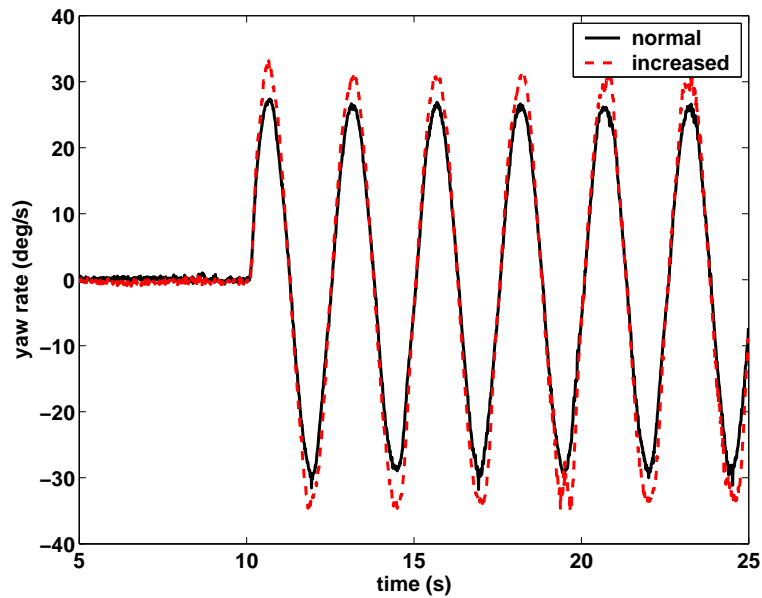


Figure 4.18: Comparison between yaw rate of normal and effectively increased front cornering stiffness.

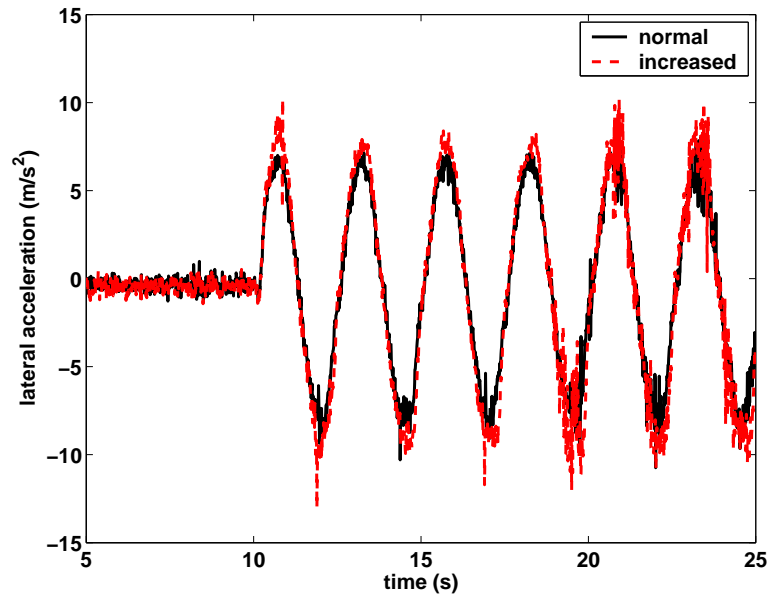


Figure 4.19: Comparison between lateral acceleration of normal and effectively increased front cornering stiffness.

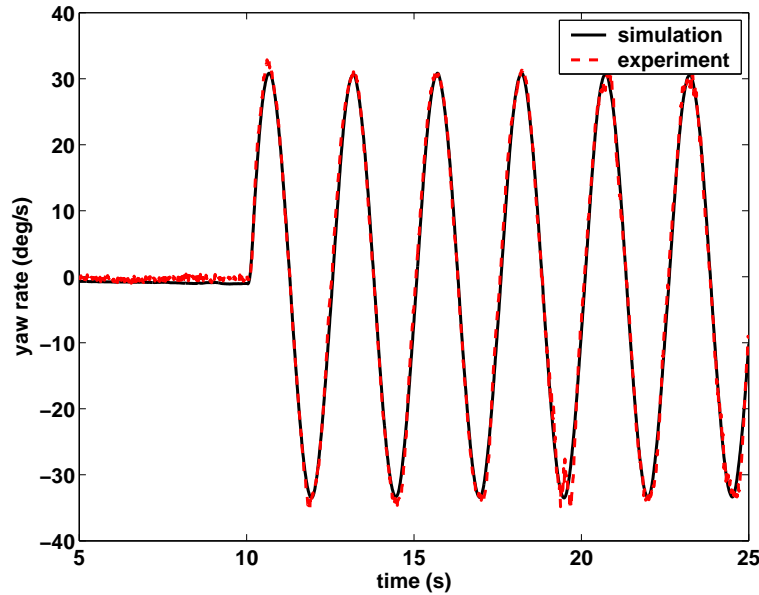


Figure 4.20: Comparison between yaw rate of bicycle model and experiment with increased front cornering stiffness.

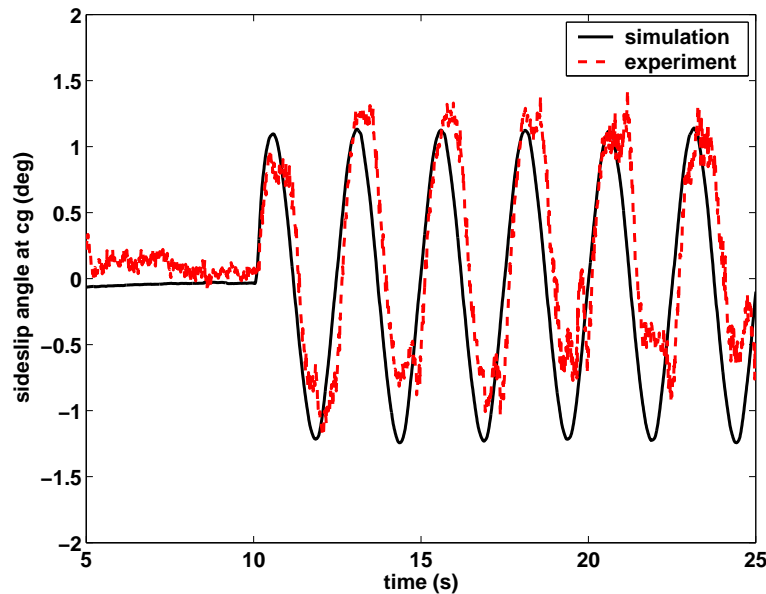


Figure 4.21: Comparison between sideslip angle of bicycle model and experiment with increased front cornering stiffness.

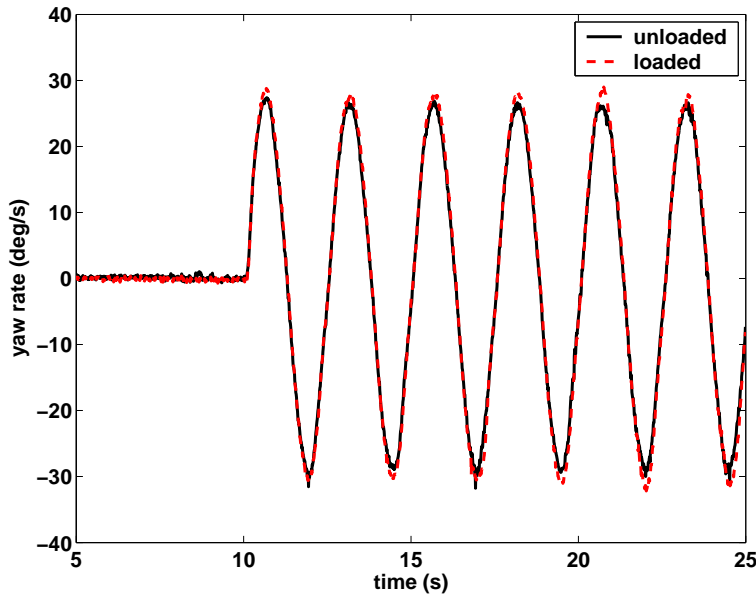


Figure 4.22: Comparison between yaw rate of unloaded and loaded vehicle.

vehicle so that 57% of the total vehicle weight lies over the rear axle with 43% over the front axle. The unloaded vehicle has a weight distribution balanced equally front to rear. As seen in Figure 4.22, the loaded vehicle exhibits slightly more oversteering behavior than the unloaded vehicle due to the rearward weight bias. However, with active handling modification, a 20% reduction in front cornering stiffness returns the controlled vehicle to the near neutral handling behavior of the unloaded vehicle (Figure 4.23). While the difference in handling behavior may seem small when viewed on a graph, the improvement is readily apparent to both driver and passenger.

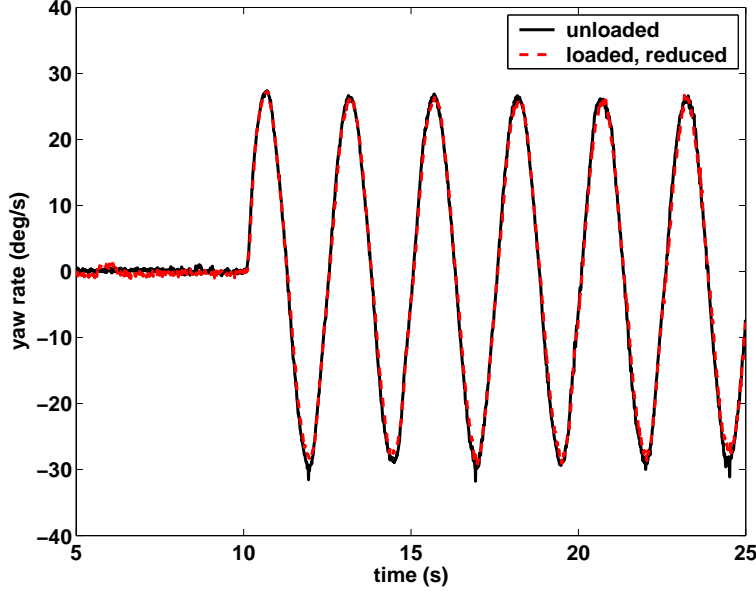


Figure 4.23: Comparison between yaw rate of unloaded vehicle and loaded vehicle with handling modification.

4.4 Limitations of front wheel active steering

To consider a more general case of full state feedback vehicle control, substituting Equation (4.16) into the bicycle model given by Equation (4.7) yields:

$$\begin{bmatrix} \dot{\beta}_{CG} \\ \dot{r} \end{bmatrix} = \begin{bmatrix} \frac{-C_{\alpha,f} - C_{\alpha,r} + C_{\alpha,f}K_\beta}{mV} & -1 + \frac{C_{\alpha,r}b - C_{\alpha,f}a + C_{\alpha,f}VK_r}{mV^2} \\ \frac{C_{\alpha,r}b - C_{\alpha,f}a + C_{\alpha,f}aK_\beta}{I_z} & \frac{-C_{\alpha,f}a^2 - C_{\alpha,r}b^2 + C_{\alpha,f}aVK_r}{I_zV} \end{bmatrix} \begin{bmatrix} \beta_{CG} \\ r \end{bmatrix} + \begin{bmatrix} \frac{C_{\alpha,f}K_\delta}{mV} \\ \frac{C_{\alpha,f}aK_\delta}{I_z} \end{bmatrix} \delta_d \quad (4.20)$$

Suppose the desired vehicle handling characteristics are given by:

$$\begin{bmatrix} \dot{\beta}_{CG} \\ \dot{r} \end{bmatrix} = \begin{bmatrix} \frac{-\hat{C}_{\alpha,f} - \hat{C}_{\alpha,r}}{\hat{m}\hat{V}} & -1 + \frac{\hat{C}_{\alpha,r}\hat{b} - \hat{C}_{\alpha,f}\hat{a}}{\hat{m}\hat{V}^2} \\ \frac{\hat{C}_{\alpha,r}\hat{b} - \hat{C}_{\alpha,f}\hat{a}}{\hat{I}_z} & \frac{-\hat{C}_{\alpha,f}\hat{a}^2 - \hat{C}_{\alpha,r}\hat{b}^2}{\hat{I}_z\hat{V}} \end{bmatrix} \begin{bmatrix} \beta_{CG} \\ r \end{bmatrix} + \begin{bmatrix} \frac{\hat{C}_{\alpha,f}}{\hat{m}\hat{V}} \\ \frac{\hat{C}_{\alpha,f}\hat{a}}{\hat{I}_z} \end{bmatrix} \delta_d \quad (4.21)$$

Rewriting as

$$\begin{bmatrix} \dot{\beta}_{CG} \\ \dot{r} \end{bmatrix} = \begin{bmatrix} \hat{a}_{1,1} & \hat{a}_{1,2} \\ \hat{a}_{2,1} & \hat{a}_{2,2} \end{bmatrix} \begin{bmatrix} \beta_{CG} \\ r \end{bmatrix} + \begin{bmatrix} \hat{b}_1 \\ \hat{b}_2 \end{bmatrix} \delta_d \quad (4.22)$$

and equating with Equation (4.20),

$$\frac{C_{\alpha,f}}{mV} K_\beta - \frac{C_{\alpha,f} + C_{\alpha,r}}{mV} = \hat{a}_{1,1} \quad (4.23)$$

$$\frac{C_{\alpha,f}}{mV} K_r + \frac{C_{\alpha,r} - C_{\alpha,f}}{mV^2} - 1 = \hat{a}_{1,2} \quad (4.24)$$

$$\frac{C_{\alpha,f}a}{I_z} K_\beta + \frac{C_{\alpha,r}b - C_{\alpha,f}a}{I_z} = \hat{a}_{2,1} \quad (4.25)$$

$$\frac{C_{\alpha,f}a}{I_z} K_r - \frac{C_{\alpha,f}a^2 + C_{\alpha,r}b^2}{I_z V} = \hat{a}_{2,2} \quad (4.26)$$

$$\frac{C_{\alpha,f}K_\delta}{mV} = \hat{b}_1 \quad (4.27)$$

$$\frac{C_{\alpha,f}aK_\delta}{I_z} = \hat{b}_2 \quad (4.28)$$

the full state feedback gains, K_β , K_r , and K_δ , can be expressed in terms of the desired parameters, $\hat{a}_{1,1}$, $\hat{a}_{1,2}$, $\hat{a}_{2,1}$, and $\hat{a}_{2,2}$:

$$K_\beta = \frac{mV}{C_{\alpha,f}} \hat{a}_{1,1} + \frac{C_{\alpha,f} + C_{\alpha,r}}{C_{\alpha,f}} \quad (4.29)$$

$$K_r = \frac{mV}{C_{\alpha,f}} \hat{a}_{1,2} + \frac{C_{\alpha,f} - C_{\alpha,r} + mV^2}{C_{\alpha,f}V} \quad (4.30)$$

$$K_\beta = \frac{I_z}{C_{\alpha,f}a} \hat{a}_{2,1} + \frac{C_{\alpha,f}a - C_{\alpha,r}b}{C_{\alpha,f}a} \quad (4.31)$$

$$K_r = \frac{I_z}{C_{\alpha,f}a} \hat{a}_{2,2} + \frac{C_{\alpha,f}a^2 + C_{\alpha,r}b^2}{C_{\alpha,f}Va} \quad (4.32)$$

$$K_\delta = \frac{mV}{C_{\alpha,f}} \hat{b}_1 \quad (4.33)$$

$$K_\delta = \frac{I_z}{C_{\alpha,f}a} \hat{b}_2 \quad (4.34)$$

However, since there are more equations than unknowns, the desired parameters cannot be chosen arbitrarily:

$$\hat{a}_{2,1} = \frac{mVa}{I_z} \hat{a}_{1,1} + \frac{C_{\alpha,r}(a+b)}{I_z} \quad (4.35)$$

$$\hat{a}_{2,2} = \frac{mVa}{I_z} \hat{a}_{1,2} + \frac{C_{\alpha,f}(1-a^2) - C_{\alpha,r}(1+b^2) + mV^2}{I_z V} \quad (4.36)$$

$$\hat{b}_2 = \frac{mVa}{I_z} \hat{b}_1 \quad (4.37)$$

The choice of modifying front tire cornering stiffness falls naturally from this derivation because of the way the cornering stiffness parameter interacts with both front steer angle and the vehicle dynamics. Other choices are possible, but they do not carry the physical meaning and significance of modifying a single physical parameter. Given four-wheel steering capability, however, the range of modifiable parameters expands to rear cornering stiffness, mass, and moment of inertia (see Appendix C).

While the idea of a variable dynamics vehicle has been considered before [42, 27], to the best of the author's knowledge this work represents the first successful implementation of true handling characteristic modification on an actual test vehicle. Two developments make it possible: precise active steering capability provided by the steer-by-wire system and accurate, smooth, and continuous state feedback from the GPS/INS system. The combination of these two systems allows a driver to transparently adjust the balance between handling responsiveness and safety by effectively changing the vehicle's physical characteristics and therefore its fundamental handling response. Handling modification is not, however, a guarantee of safety. Preventing complete loss of handling control requires knowledge of the tire forces at each corner and how close they are to reaching their limits. The next chapter applies an understanding of steering forces toward obtaining this critical piece of information and in turn developing an alternative method for sideslip estimation.

Chapter 5

A vehicle dynamics state observer

An interesting and very useful connection has emerged between the steering system dynamics and the vehicle dynamics as they are each transmitted through the tire forces. Chapter 3 described the tire aligning moment as a disturbance on the steering system—due to the lateral tire forces acting about the steering axis—that needs to be cancelled out by the steering controller. Chapter 4 discussed these same lateral tire forces as functions of the tire slip angles, which are directly related to the vehicle’s yaw and sideslip motion. If the steering controller is able to determine and cancel out the aligning moment, then it stands to reason that the same information can be used to help estimate the lateral tire forces and in turn the tire slip angles. In this role, not only does the steer-by-wire system serve a means of actuation to control the vehicle motion, but it also provides the measurements needed to estimate the vehicle states. As a matter of convenience and cost, steer-by-wire single-handedly addresses the problems of both vehicle dynamics control and state estimation.

This chapter develops two observer structures based on linear models of the vehicle and tire behavior to estimate the vehicle states from measurements of steering angle and yaw rate. Steering angle and yaw rate sensors are both inexpensive and common to vehicles already equipped with stability control systems. Steering torque sensors are intrinsic components of electric power steering systems [40]. Furthermore, as steer-by-wire technology approaches reality, complete knowledge of steering torque can be determined from the current applied to the electric steering actuator [30]. The

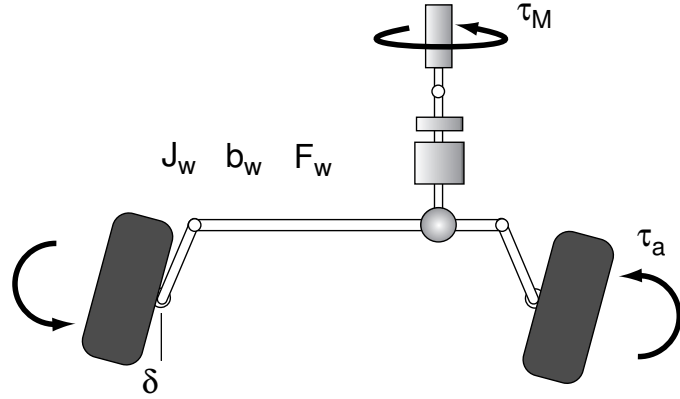


Figure 5.1: Steering system dynamics.

first of the two observers combines the vehicle and steering system models into a single observer structure to estimate four states at once: sideslip angle, yaw rate, steering angle, and steering rate. The second observer incorporates an intermediate step. A disturbance observer based on the steering system model estimates the tire aligning moment; this estimate becomes the measurement part of a vehicle state observer for sideslip and yaw rate. The performance of the observers is verified on the steer-by-wire test vehicle. The latter part of the chapter applies this state estimation scheme to the full state feedback control approach developed in Chapter 4.

5.1 Steering system model

The steering system shown in Figure 5.1 is described by the following differential equation:

$$J_w \ddot{\delta} + b_w \dot{\delta} + \tau_f + \tau_a = r_s r_p \tau_M \quad (5.1)$$

where J_w and b_w are the moment of inertia and damping of the steering system at the road wheels and τ_f represents Coulomb friction. Furthermore, r_s is the steering ratio, and r_p is the torque magnification factor of the power steering system, here approximated by a constant. τ_M is the steering actuator torque, which can be written in terms of motor constant, k_M , motor current, i_M , motor efficiency, η , and gearhead

ratio, r_g :

$$\tau_M = k_M i_M r_g \eta \quad (5.2)$$

The tire self-aligning moment, τ_a , described earlier in Chapter 3, is given by:

$$\tau_a = (t_p + t_m) F_{y,f} \quad (5.3)$$

where t_p and t_m are approximately known. Rewriting Equation (5.1) in state space form yields:

$$\dot{x}_1 = A_1 x_1 + B_{1,1} u_1 + B_{1,2} \tau_a \quad (5.4)$$

where

$$\begin{aligned} x_1 &= \begin{bmatrix} \delta & \dot{\delta} \end{bmatrix}^T \\ A_1 &= \begin{bmatrix} 0 & 1 \\ 0 & -\frac{b_w}{J_w} \end{bmatrix} \\ B_{1,1} &= \begin{bmatrix} 0 & 0 \\ \frac{r_s r_p}{J_w} & -\frac{1}{J_w} \end{bmatrix} \\ u_1 &= \begin{bmatrix} \tau_M & \tau_f \end{bmatrix}^T \\ B_{1,2} &= \begin{bmatrix} 0 \\ -\frac{1}{J_w} \end{bmatrix} \end{aligned}$$

and the aligning moment, τ_a , is treated as an external input to the steering system. The resisting torque, τ_f , due to friction is treated as an input:

$$\tau_f = F_w \operatorname{sgn}(\dot{\delta}) \quad (5.5)$$

where the Coulomb friction constant, F_w , has been identified along with the inertia and damping constants.

5.2 Linear vehicle model

The vehicle representation for estimation is identical to the bicycle model introduced in Chapter 4. Here, Equation (4.7) is rewritten as:

$$\dot{x}_2 = A_2 x_2 + B_2 \delta \quad (5.6)$$

where

$$\begin{aligned} x_2 &= \begin{bmatrix} \beta & r \end{bmatrix}^T \\ A_2 &= \begin{bmatrix} -\frac{C_{\alpha,0}}{mV} & -1 + \frac{C_{\alpha,1}}{mV^2} \\ \frac{C_{\alpha,1}}{I_z} & -\frac{C_{\alpha,2}}{I_z V} \end{bmatrix} \\ B_2 &= \begin{bmatrix} \frac{C_{\alpha,f}}{mV} \\ \frac{C_{\alpha,fa}}{I_z} \end{bmatrix} \end{aligned}$$

and to consolidate notation,

$$\begin{aligned} C_{\alpha,0} &= C_{\alpha,f} + C_{\alpha,r} \\ C_{\alpha,1} &= C_{\alpha,r}b - C_{\alpha,f}a \\ C_{\alpha,2} &= C_{\alpha,f}a^2 + C_{\alpha,r}b^2 \end{aligned}$$

Again, recall that when operating in the linear tire region, the lateral force is related to tire slip angle by the cornering stiffness:

$$\begin{aligned} F_{y,f} &= -C_{\alpha,f}\alpha_f \\ F_{y,r} &= -C_{\alpha,r}\alpha_r \end{aligned} \quad (5.7)$$

and taking small angle approximations, the front and rear slip angles can be written in terms of β and r :

$$\alpha_f = \beta + \frac{ar}{V} - \delta \quad (5.8)$$

$$\alpha_r = \beta - \frac{br}{V}$$

As before, longitudinal velocity, V , is assumed to be constant.

5.2.1 Observability

When looking at the two state linear vehicle model described above, one might consider designing a simple state observer based on measurement of yaw rate alone. Unfortunately, there is one instance in which the sideslip angle is unobservable through yaw rate: the neutral steering case ($C_{\alpha,r}b - C_{\alpha,f}a = 0$). The bicycle model representation of a neutral steering vehicle is given by:

$$\dot{x}_2 = A_{2,N}x_2 + B_2\delta \quad (5.9)$$

where

$$A_{2,N} = \begin{bmatrix} -\frac{C_{\alpha,0}}{mV} & -1 \\ 0 & -\frac{C_{\alpha,2}}{I_z V} \end{bmatrix}$$

If yaw rate is the only measured state, then

$$y_2 = C_2x_2 \quad (5.10)$$

where

$$C_2 = \begin{bmatrix} 1 & 0 \end{bmatrix} \quad (5.11)$$

The observability matrix is given by:

$$O_2 = \begin{bmatrix} C_2 \\ C_2 A_{2,N} \end{bmatrix} = \begin{bmatrix} 0 & 1 \\ 0 & -\frac{C_{\alpha,2}}{I_z V} \end{bmatrix} \quad (5.12)$$

Since the observability matrix has less than full rank, the system is unobservable in yaw rate. Therefore, an observer based on yaw rate alone is impractical as the vehicle handling characteristics approach the neutral steering configuration.

5.3 Vehicle state estimation using steering torque

5.3.1 Conventional observer

One way to estimate sideslip in this situation is to combine the linear vehicle model with the steering system model. The aligning moment term in the steering system equation can be expressed as a function of the vehicle states and steering angle by substituting Equations (5.8) and (5.9) into Equation (5.3):

$$\tau_a = -C_{\alpha,f}(t_p + t_m)(\beta + \frac{a}{V}r - \delta) \quad (5.13)$$

Now combining Equations (5.4) and (5.6) yields the following state space model:

$$\dot{x}_3 = A_3 x_3 + B_3 u_3 \quad (5.14)$$

where

$$\begin{aligned} x_3 &= \begin{bmatrix} \beta & r & \delta & \dot{\delta} \end{bmatrix}^T \\ A_3 &= \begin{bmatrix} -\frac{C_{\alpha,0}}{mV} & -1 + \frac{C_{\alpha,1}}{mV^2} & \frac{C_{\alpha,f}}{mV} & 0 \\ \frac{C_{\alpha,1}}{I_z} & -\frac{C_{\alpha,2}}{I_z V} & \frac{aC_{\alpha,f}}{I_z} & 0 \\ 0 & 0 & 0 & 1 \\ \frac{C_{\alpha,3}}{J_w} & \frac{aC_{\alpha,3}}{J_w V} & -\frac{C_{\alpha,3}}{J_w} & -\frac{b_w}{J_w} \end{bmatrix} \\ B_3 &= \begin{bmatrix} 0 & 0 \\ 0 & 0 \\ 0 & 0 \\ \frac{r_s r_p k_M r_g \eta}{J_w} & -\frac{1}{J_w} \end{bmatrix} \\ u_3 &= \begin{bmatrix} i_M & \tau_f \end{bmatrix}^T \end{aligned}$$

and

$$C_{\alpha,3} = (t_p + t_m)C_{\alpha,f}$$

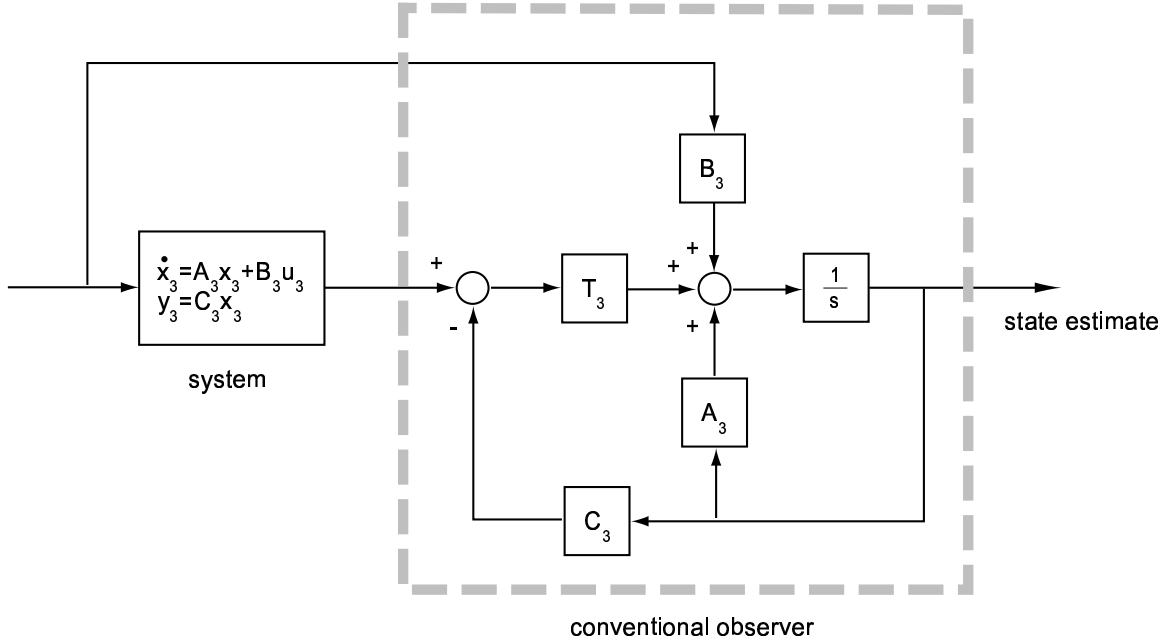


Figure 5.2: Conventional observer block diagram.

with states of vehicle sideslip angle, β , yaw rate, r , steering angle, δ , and steering rate, $\dot{\delta}$. The standard observer structure is shown in Figure 5.2 and is given by:

$$\dot{\hat{x}}_3 = A_3 \hat{x}_3 + B_3 u_3 + T_3(y_3 - C_3 \hat{x}_3) \quad (5.15)$$

The vector, \hat{x}_3 , contains the estimated states and y_3 is the vector of measurements—yaw rate and steering angle—directly available from vehicle sensors:

$$y_3 = \begin{bmatrix} r & \delta \end{bmatrix}^T = C_3 x_3 \quad (5.16)$$

where

$$C_3 = \begin{bmatrix} 0 & 1 & 0 & 0 \\ 0 & 0 & 1 & 0 \end{bmatrix}$$

Note that this system is now observable in the neutral steering case. The observability matrix is given by:

$$O_3 = \begin{bmatrix} C_3 \\ C_3 A_3 \\ C_3 A_3^2 \\ C_3 A_3^3 \end{bmatrix} \quad (5.17)$$

where

$$A_{3,N} = \begin{bmatrix} -\frac{C_{\alpha,0}}{mV} & -1 & \frac{C_{\alpha,f}}{mV} & 0 \\ 0 & -\frac{C_{\alpha,2}}{I_z V} & \frac{aC_{\alpha,f}}{I_z} & 0 \\ 0 & 0 & 0 & 1 \\ \frac{C_{\alpha,3}}{J_w} & \frac{aC_{\alpha,3}}{J_w V} & -\frac{C_{\alpha,3}}{J_w} & -\frac{b_w}{J_w} \end{bmatrix} \quad (5.18)$$

for the neutral steering vehicle. By looking at only the first six rows of the observability matrix,

$$\begin{bmatrix} C_3 \\ C_3 A_{3,N} \\ C_3 A_{3,N}^2 \end{bmatrix} = \begin{bmatrix} 0 & 1 & 0 & 0 \\ 0 & 0 & 1 & 0 \\ 0 & -\frac{C_{\alpha,2}}{IV} & \frac{aC_{\alpha,f}}{I} & 0 \\ 0 & 0 & 0 & 1 \\ 0 & \frac{C_{\alpha,2}^2}{I^2 V^2} & -\frac{aC_{\alpha,f} C_{\alpha,2}}{I^2 V} & \frac{aC_{\alpha,f}}{I} \\ \frac{C_{\alpha,3}}{J_w} & \frac{aC_{\alpha,3}}{J_w V} & -\frac{C_{\alpha,3}}{J_w} & -\frac{b_w}{J_w} \end{bmatrix} \quad (5.19)$$

one can already see that it has full rank and the system is therefore observable in yaw rate and steering angle.

The observer in Equation (5.15) can be rewritten as:

$$\dot{\hat{x}}_3 = (A_3 - T_3 C_3) \hat{x}_3 + B_3 u_3 + T_3 y_3 \quad (5.20)$$

As a general rule of thumb, the estimator gain matrix, T_3 , is chosen so that the matrix $A_3 - T_3 C_3$ has eigenvalues located at least ten times farther to the left than the system eigenvalues in the complex frequency plane. The sampling rate of the measurements is typically yet another order of magnitude faster than the estimation error dynamics,

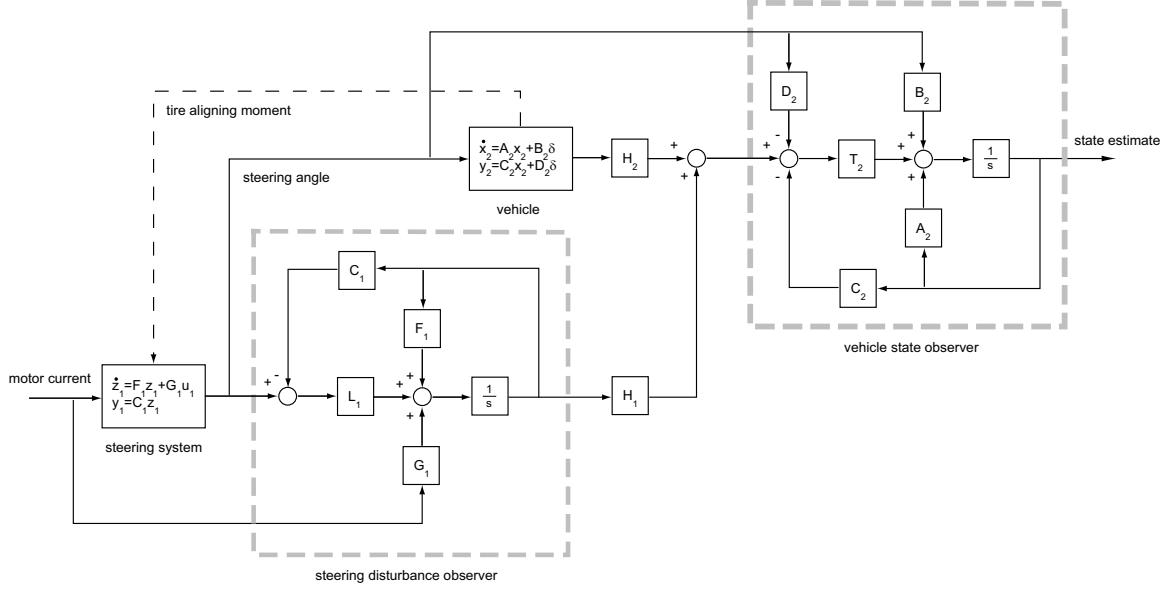


Figure 5.3: Cascaded observer block diagram.

which are given by:

$$\dot{\tilde{x}}_3 = (A_3 - T_3 C_3) \tilde{x}_3 \quad (5.21)$$

where the estimation errors are:

$$\tilde{x}_3 = x_3 - \hat{x}_3$$

When T_3 is selected so that $A_3 - T_3 C_3$ has stable eigenvalues, the error dynamics approach zero exponentially.

5.3.2 Disturbance observer

As an alternative, one can first estimate the aligning moment by applying a disturbance observer to the steering system model described by Equation (5.4). The aligning moment estimate then becomes a measurement for the state estimator based on the vehicle model given by Equation (5.6). This cascaded observer structure is illustrated in Figure 5.3. The state space equation for the disturbance observer is simply constructed by appending the disturbance, τ_a , to the state vector, x_1 , and

augmenting the corresponding rows in the state matrices with zeroes:

$$\dot{z}_1 = F_1 z_1 + G_1 u_1 + J_1 \dot{\tau}_a \quad (5.22)$$

where

$$\begin{aligned} z_1 &= \begin{bmatrix} \delta & \dot{\delta} & \tau_a \end{bmatrix}^T \\ F_1 &= \begin{bmatrix} A_1 & B_{1,2} \\ 0 & 0 \end{bmatrix} \\ G_1 &= \begin{bmatrix} B_{1,1} \\ 0 \end{bmatrix} \\ J_1 &= \begin{bmatrix} 0 & 0 & 1 \end{bmatrix}^T \end{aligned}$$

The available measurement, y_1 , is the steering angle, δ :

$$y_1 = \delta = C_1 z_1 \quad (5.23)$$

where

$$C_1 = \begin{bmatrix} 1 & 0 & 0 \end{bmatrix}$$

The disturbance observer is given by:

$$\dot{\hat{z}}_1 = F_1 \hat{z}_1 + G_1 u_1 + L_1 (y_1 - C_1 \hat{z}_1) \quad (5.24)$$

and the corresponding error dynamics are:

$$\dot{\tilde{z}}_1 = (F_1 - L_1 C_1) \tilde{z}_1 + J_1 \dot{\tau}_a \quad (5.25)$$

where the estimation errors are:

$$\tilde{z}_1 = z_1 - \hat{z}_1$$

As can be seen from Equation (5.25), the estimation errors do not necessarily approach zero due to the term containing the derivative of disturbance torque. However, this term is small if the disturbance is varying slowly. Making the assumption that $\dot{\tau}_a$ equals zero is similar to the approach taken in [57] and results in a close approximation of the disturbance torque from the observer.

5.3.3 Vehicle state observer

Now the standard observer structure is applied to Equation (5.6) only:

$$\dot{\hat{x}}_2 = A_2 \hat{x}_2 + B_2 \delta + T_2(y_2 - \hat{y}_2) \quad (5.26)$$

This can be rewritten as:

$$\dot{\hat{x}}_2 = A_{2,1} \hat{z}_1 + A_{2,2} \hat{x}_2 + T_2(y_2 - C_2 \hat{x}_2 - D_2 C_1 \hat{z}_1) \quad (5.27)$$

where

$$\begin{aligned} A_{2,1} &= \begin{bmatrix} B_2 & 0 & 0 \end{bmatrix} \\ A_{2,2} &= A_2 \end{aligned}$$

The vector, \hat{x}_2 , contains the vehicle states to be estimated and y_2 is the vector of “measurements”—in this case, yaw rate and the aligning moment estimate obtained from the disturbance observer:

$$y_2 = H_2 x_2 + H_1 \hat{z}_1 \quad (5.28)$$

where

$$\begin{aligned} H_1 &= \begin{bmatrix} 0 & 0 & 0 \\ 0 & 0 & 1 \end{bmatrix} \\ H_2 &= \begin{bmatrix} 0 & 1 \\ 0 & 0 \end{bmatrix} \end{aligned}$$

Recall that substituting Equations (5.8), (5.9) and (5.2) into Equation (5.1) expresses the aligning moment, τ_a , in terms of the vehicle states, β and r , so that the measurement vector can also be written as:

$$y_2 = \begin{bmatrix} r & \tau_a \end{bmatrix}^T = C_2 x_2 + D_2 \delta \quad (5.29)$$

where

$$\begin{aligned} C_2 &= \begin{bmatrix} 0 & 1 \\ -C_{\alpha,3} & -\frac{aC_{\alpha,3}}{V} \end{bmatrix} \\ D_2 &= \begin{bmatrix} 0 \\ C_{\alpha,3} \end{bmatrix} \end{aligned}$$

While Equation (5.6) is unobservable in the neutral steering case when yaw rate, r , is the sole measurement, the addition of aligning moment, τ_a , to the measurement vector means that the system given by Equations (5.6) and (5.29) will always be observable. Due to the cascaded structure of the observer, the error dynamics here depend on both the disturbance estimation errors and the vehicle state estimation errors:

$$\dot{\tilde{x}}_2 = (A_{2,1} - T_2 D_2 C_1) \tilde{z}_1 + (A_{2,2} - T_2 C_2) \tilde{x}_2 \quad (5.30)$$

where the estimation errors are:

$$\tilde{z}_1 = z_1 - \hat{z}_1$$

$$\tilde{x}_2 = x_2 - \hat{x}_2$$

5.3.4 Alternate formulation

As mentioned in the previous section, a more technically accurate formulation of the disturbance observer should include the derivative of the disturbance as a function of the steering rate as well as the dynamics of the vehicle:

$$\dot{\tau}_a = -C_{\alpha,f}(t_p + t_m)(\dot{\beta} + \frac{a}{V}\dot{r} - \dot{\delta}) \quad (5.31)$$

Now $\dot{\beta}$ and \dot{r} can be replaced by the results from the vehicle state observer of Equation (5.27):

$$\begin{aligned}\dot{\beta} &= -\frac{C_{\alpha,0}}{mV}\hat{\beta} + \left(-1 + \frac{C_{\alpha,1}}{mV^2}\right)\hat{r} + \frac{C_{\alpha,f}}{mV}\delta \\ \dot{r} &= -\frac{C_{\alpha,1}}{I_z}\hat{\beta} - \frac{C_{\alpha,2}}{I_zV}\hat{r} + \frac{aC_{\alpha,f}}{I_z}\delta\end{aligned}\quad (5.32)$$

The state space equations for the disturbance observer are alternatively written as:

$$\dot{z}_1 = F_{2,1}z_1 + F_{2,2}x_2 + G_1u_1 \quad (5.33)$$

where

$$\begin{aligned}F_{2,1} &= \begin{bmatrix} 0 & 1 & 0 \\ 0 & -\frac{b_w}{J_w} & -\frac{1}{J_w} \\ -C_{\alpha,3}\left(\frac{C_{\alpha,f}}{mV} + \frac{a^2C_{\alpha,f}}{I_zV}\right) & C_{\alpha,3} & 0 \end{bmatrix} \\ F_{2,2} &= \begin{bmatrix} 0 & 0 \\ 0 & 0 \\ C_{\alpha,3}\left(\frac{C_{\alpha,0}}{mV} + \frac{C_{\alpha,1}}{I_z}\right) & C_{\alpha,3}\left(1 - \frac{C_{\alpha,1}}{mV} + \frac{aC_{\alpha,2}}{I_zV^2}\right) \end{bmatrix}\end{aligned}$$

The available measurement, y_1 , is the same as before. The disturbance observer for the alternate formulation is given by:

$$\dot{\tilde{z}}_1 = F_{2,1}\tilde{z}_1 + F_{2,2}\hat{x}_2 + G_1u_1 + L_2(y_1 - C_1\hat{z}_1) \quad (5.34)$$

and the corresponding error dynamics are:

$$\dot{\tilde{z}}_1 = (F_{2,1} - L_2C_1)\tilde{z}_1 + F_{2,2}\tilde{x}_2 \quad (5.35)$$

Combining the error dynamics of the disturbance observer with those of the vehicle state observer, Equation (5.30), yields the overall error dynamics for the complete

cascaded observer structure:

$$\begin{bmatrix} \dot{\tilde{z}}_1 \\ \dot{\tilde{x}}_2 \end{bmatrix} = \begin{bmatrix} F_{2,1} - L_2 C_1 & F_{2,2} \\ A_{2,1} - T_2 D_2 C_1 & A_{2,2} - T_2 C_2 \end{bmatrix} \begin{bmatrix} \tilde{z}_1 \\ \tilde{x}_2 \end{bmatrix} \quad (5.36)$$

As before, the appropriate choice of observer gain matrices, L_2 and T_2 , will ensure that the estimation errors, \tilde{z}_1 and \tilde{x}_2 , approach zero exponentially.

While the cascaded observer has many similarities to the conventional observer described by Equation (5.15), the error dynamics clearly illustrate a fundamental difference between the two approaches. In the formulation of the conventional observer, the existence of aligning moment is implied through the merging of the steering system and vehicle into a single entity. In the cascaded observer, the separation of the steering system dynamics and vehicle dynamics is more distinct. By explicitly bringing out the aligning moment as a state to be observed, the cascaded structure emphasizes the intermediary role aligning moment plays in going from steering torque measurement to vehicle state estimates. Although both observer types are designed to estimate the vehicle states, the structural differences suggest that they will not perform in exactly the same way.

5.3.5 Observer performance

Both the conventional observer and the cascaded observer structure with the simplified disturbance observer have been implemented in real-time on the steer-by-wire test vehicle. The state estimates from the observers are simultaneously compared to results from the GPS/INS based sideslip estimation method described in Chapter 4. As a reference, vehicle states calculated from the linear vehicle model—with parameters matched to the test vehicle—are also included in the comparison. The following figures correspond to the same test cycle during which the vehicle accelerates from a standing stop to a steady speed of 6.7 m/s (15 mi/hr) at which time the steering maneuver is initiated.

Figures 5.4, 5.5, 5.6, and 5.7 show the state estimates from the four-state observer. As expected, since steering angle and yaw rate are measurements, the estimates of

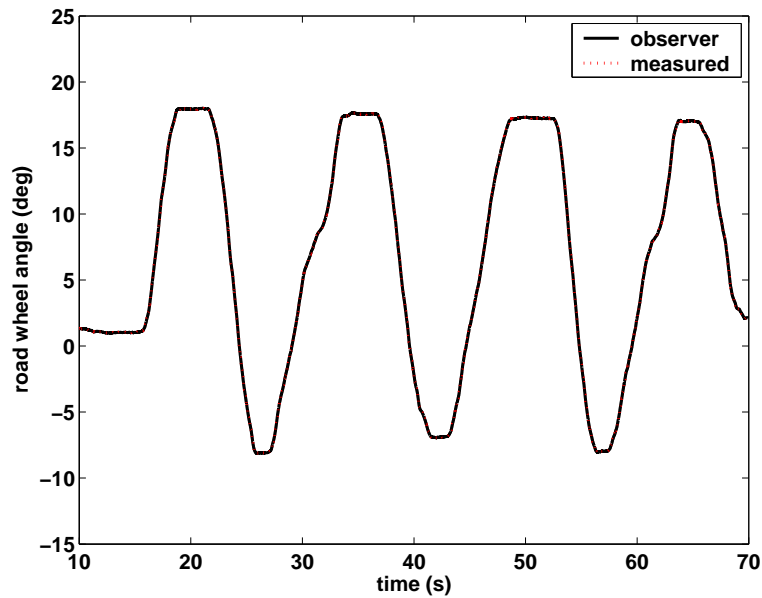


Figure 5.4: Estimated steer angle from conventional observer.

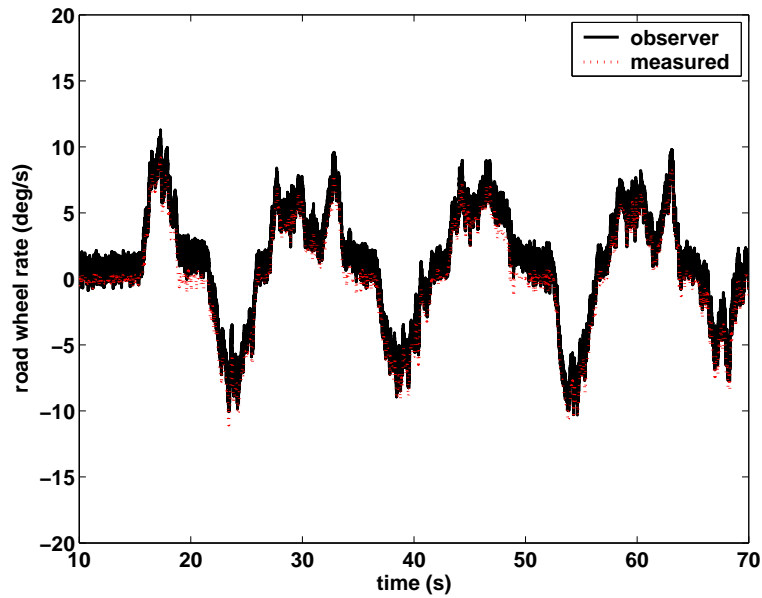


Figure 5.5: Estimated steer rate from conventional observer.

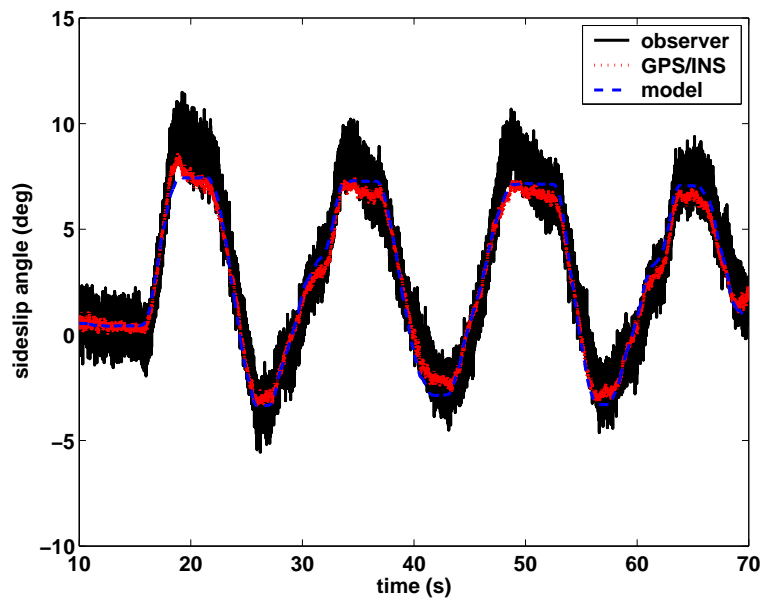


Figure 5.6: Estimated sideslip from conventional observer.

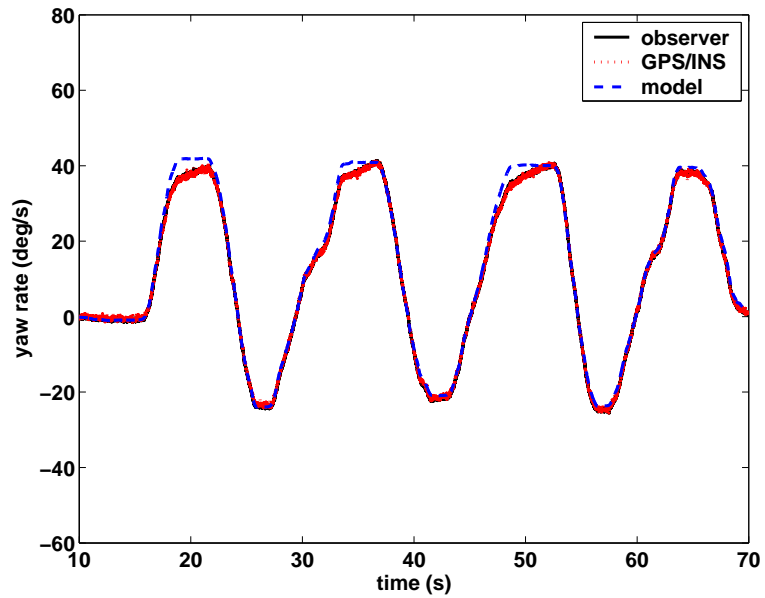


Figure 5.7: Estimated yaw rate from conventional observer.

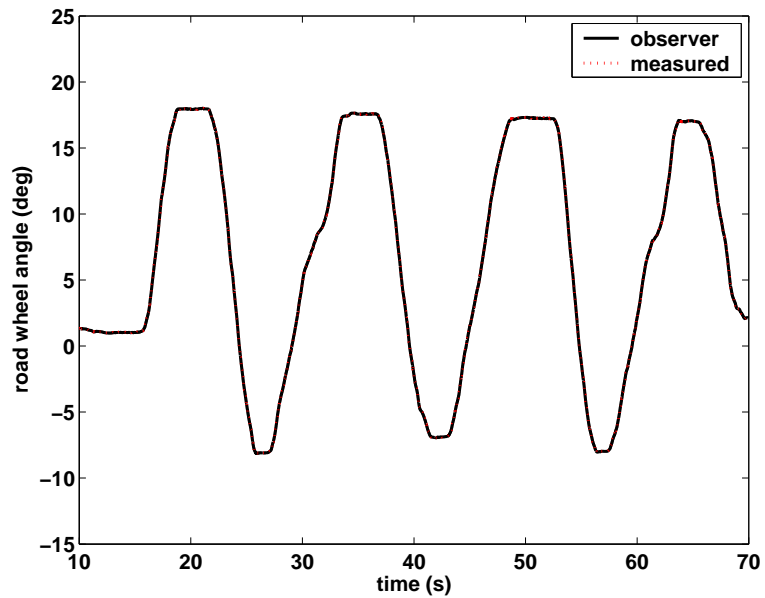


Figure 5.8: Estimated steer angle from disturbance observer.

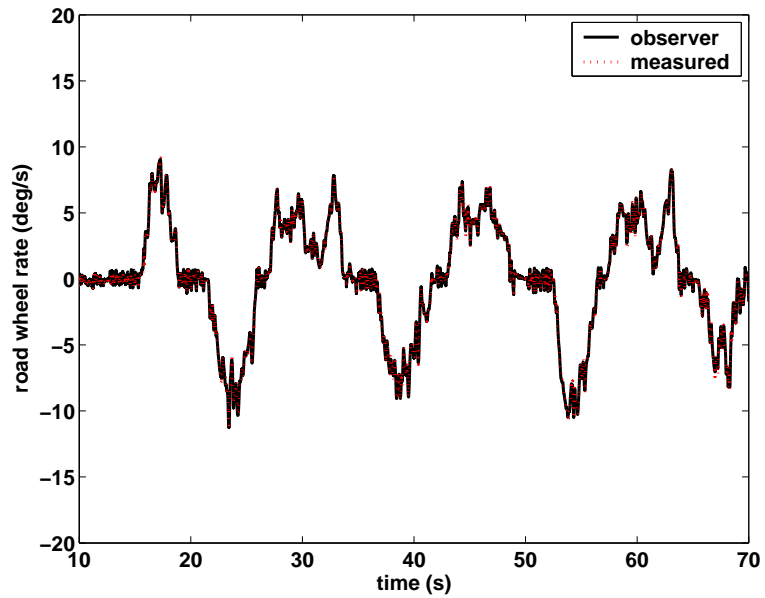


Figure 5.9: Estimated steer rate from disturbance observer.

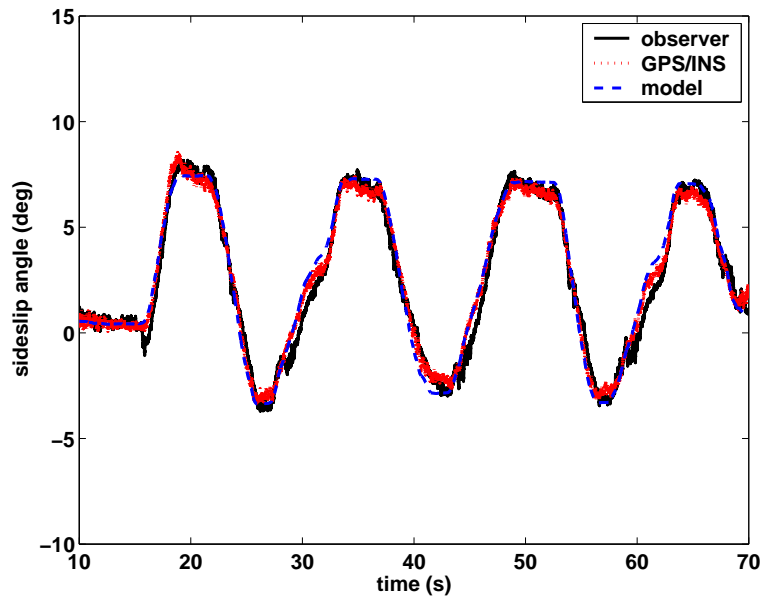


Figure 5.10: Estimated sideslip from disturbance observer.

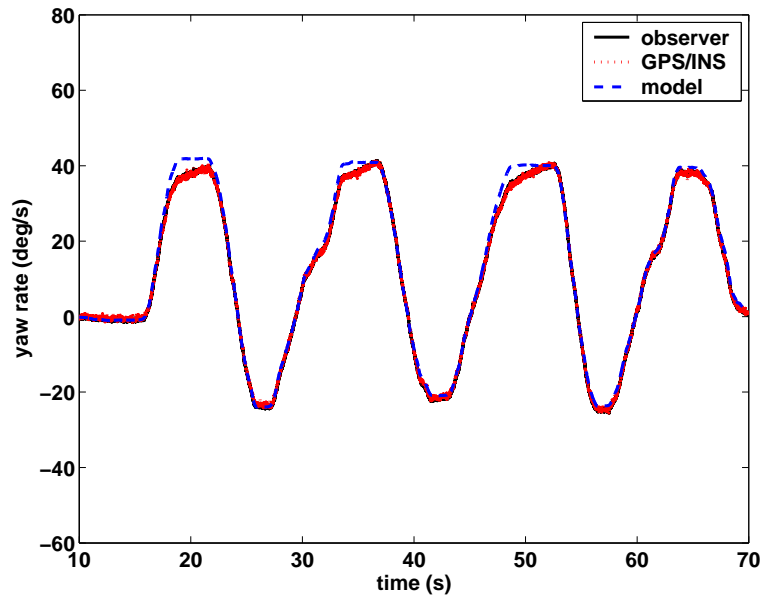


Figure 5.11: Estimated yaw rate from disturbance observer.

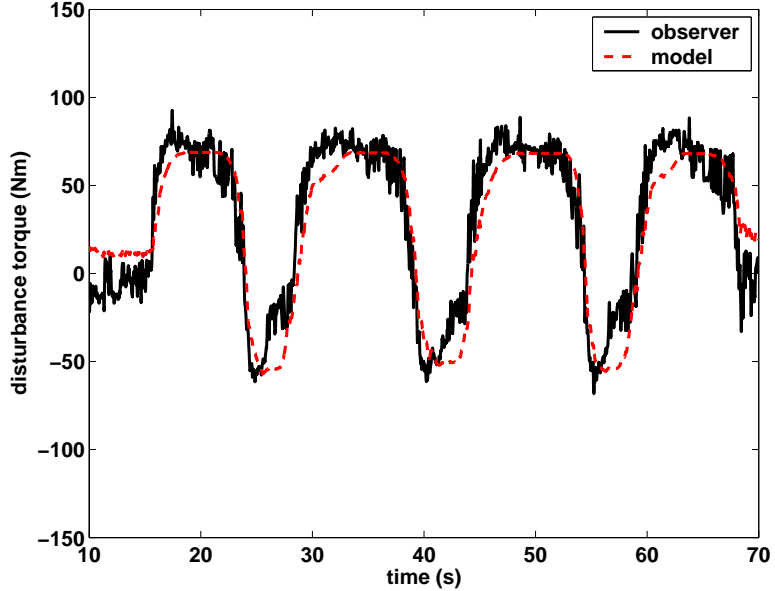


Figure 5.12: Estimated disturbance torque.

steering angle and yaw rate tend to match the measured values almost exactly. The observed state of primary interest, sideslip angle, correlates well with the GPS/INS sideslip estimate, but the choice of observer gains found to produce a good steering rate estimate fails to filter noise in the sideslip estimate (Figure 5.6). This problem illustrates the drawback of the four-state observer: the difficulty in choosing a single observer gain matrix often compromises estimation performance due to the fact that the steering system dynamics are significantly faster than the vehicle dynamics.

By separating the state estimation into a disturbance observer for the steering system and a two-state observer for the vehicle states, the cascaded observer structure facilitates the selection of observer gains appropriate to either set of dynamics. The improvement is clear in the steering rate estimate of Figure 5.9 and the sideslip estimate of Figure 5.10. Since the vehicle is operated well within the linear region of its dynamic behavior in these tests, the yaw rate (Figure 5.11) and sideslip predicted by the linear vehicle model follow the estimated values closely.

The estimated disturbance torque shown in Figure 5.12, however, is not as well

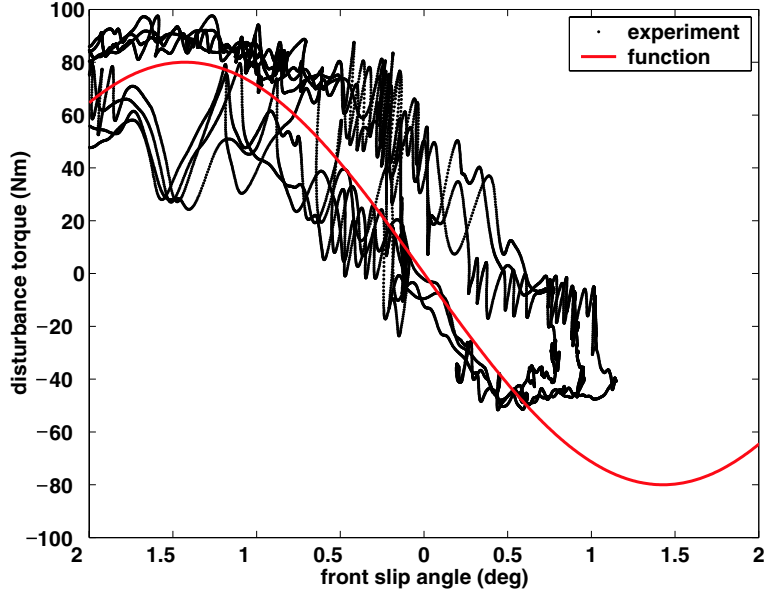


Figure 5.13: Estimated disturbance torque versus slip angle.

predicted by the aligning moment calculated from (5.3). In modelling the steering system of the test vehicle, several sources of uncertainty exist to cause such discrepancy, among them variations in mechanical trail due to steering and suspension motions and nonlinear hydraulic power steering characteristics (see Appendix B). For example, hysteresis in the power steering system clearly appears in the plot of aligning moment versus slip angle (Figure 5.13). While these effects are less evident in steering control, which benefits from feedback, the nonlinearities become apparent when dealing directly with steering forces.

It is important to observe that although the imperfect disturbance torque estimate is used as a measurement in the vehicle state observer, the estimates of the vehicle states do not suffer in the same way from these uncertainties. This results from the fact that in the vehicle state observer yaw rate feedback is weighted heavily. Therefore the two-tiered state estimation scheme can be made to be fairly robust to parameter uncertainty in the steering system model as long as there is a reliable vehicle model with accurate yaw rate measurement.

5.4 Closed loop vehicle control

5.4.1 Handling modification

The same closed loop handling modification technique introduced in Chapter 4 is now repeated with state estimates obtained from the disturbance observer method instead of the GPS/INS system. These tests determine whether the observer-based state estimation is suitable for use as feedback in a closed loop vehicle control system. The full state feedback control law for an active steering vehicle is given again by:

$$\delta = K_r r + K_\beta \beta + K_d \delta_d \quad (5.37)$$

where δ_d is the driver commanded steer angle and δ is the augmented angle. Now β comes from the observer of Equation (5.27). The modified front cornering stiffness is again defined by:

$$\hat{C}_{\alpha,f} = C_{\alpha,f}(1 + \eta) \quad (5.38)$$

and the state feedback gains as:

$$K_\beta = -\eta \quad K_r = -\frac{a}{V}\eta \quad K_d = (1 + \eta) \quad (5.39)$$

Substituting the feedback law, Equation (5.37), into Equation (5.6) yields a state space equation of the same form as Equation (5.6) but with the new cornering stiffness $\hat{C}_{\alpha,f}$:

$$\dot{x}_2 = \hat{A}_2 x_2 + \hat{B}_2 \delta \quad (5.40)$$

where

$$\begin{aligned} x_2 &= \begin{bmatrix} \beta & r \end{bmatrix}^T \\ \hat{A}_2 &= \begin{bmatrix} -\frac{\hat{C}_{\alpha,0}}{mV} & -1 + \frac{\hat{C}_{\alpha,1}}{mV^2} \\ \frac{\hat{C}_{\alpha,1}}{I_z} & -\frac{\hat{C}_{\alpha,2}}{I_z V} \end{bmatrix} \\ \hat{B}_2 &= \begin{bmatrix} \frac{\hat{C}_{\alpha,f}}{mV} \\ \frac{\hat{C}_{\alpha,f} a}{I_z} \end{bmatrix} \end{aligned}$$

and to consolidate notation,

$$\begin{aligned}\hat{C}_{\alpha,0} &= \hat{C}_{\alpha,f} + C_{\alpha,r} \\ \hat{C}_{\alpha,1} &= C_{\alpha,r}b - \hat{C}_{\alpha,f}a \\ \hat{C}_{\alpha,2} &= \hat{C}_{\alpha,f}a^2 + C_{\alpha,r}b^2\end{aligned}$$

5.4.2 Experimental results

As developed thus far in this chapter, all of the components necessary for physical implementation of closed loop vehicle dynamics control are now in place: 1) accurate state estimates are available from the disturbance observer described in the previous section, 2) a means of precise vehicle control is provided by the steer-by-wire system in the test vehicle, and 3) a full state feedback control law has been devised to fundamentally alter a vehicle's handling characteristics. The experimental results presented below are based on the same test procedure described in Chapter 4. From the first test run, with the vehicle driven in the unmodified mode (no state feedback), Figures 5.14 and 5.15) show the plots of yaw rate and sideslip angle. The estimated values from the disturbance observer are compared with both GPS/INS measurement and bicycle model simulation. Yaw rate estimated from the disturbance observer matches the GPS/INS numbers almost exactly since it is the "measured" state by which the observer determines the unmeasurable state of sideslip angle. More importantly, sideslip angle estimated from the disturbance observer also closely follows GPS measurement and model prediction.

Next, the same test is repeated with the effective front cornering stiffness reduced by 50%. Figure 5.16 shows how steering angle has been changed by the state feedback so as to exactly replicate the dynamic effect of reduced front cornering stiffness. The resulting difference in handling behavior is evident when comparing lateral acceleration (Figure 5.17) to the nominal case. As expected, the modified handling exhibits lower peak lateral acceleration values since the effect of reduced front cornering stiffness is more pronounced understeering behavior. Figures 5.18 and 5.19 confirm that results for the reduced case match simulation of the bicycle model with

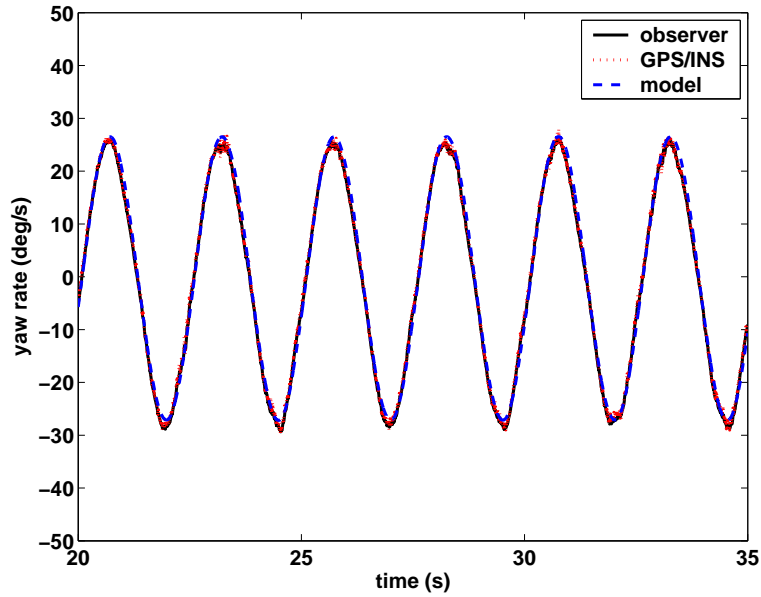


Figure 5.14: Comparison between estimated yaw rate, INS measurement, and bicycle model simulation with normal cornering stiffness.

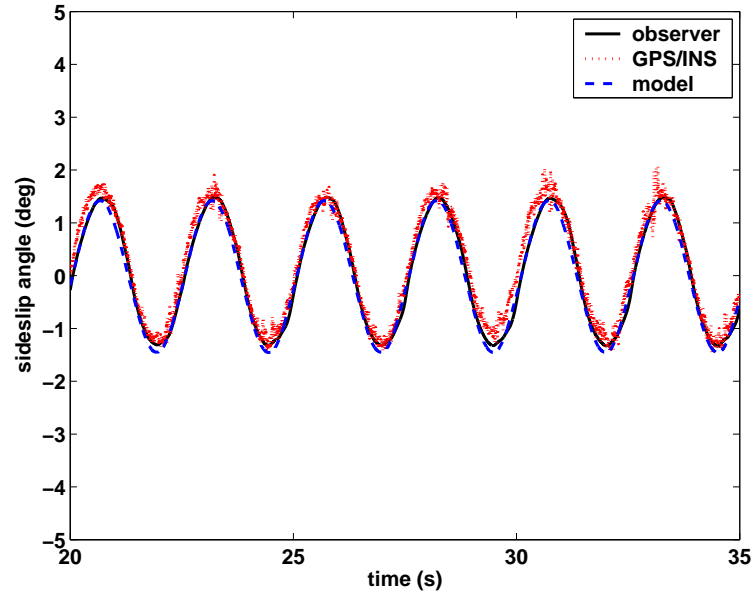


Figure 5.15: Comparison between estimated sideslip angle, GPS measurement, and bicycle model simulation with normal cornering stiffness.

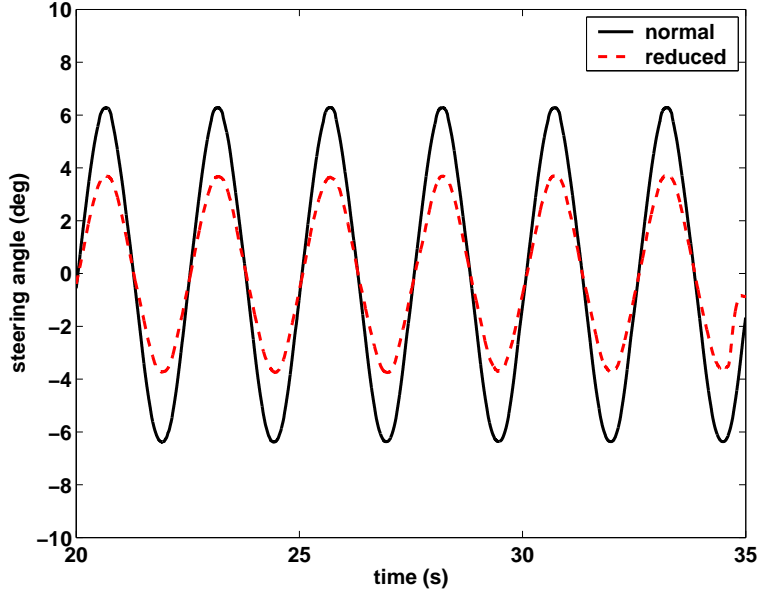


Figure 5.16: Difference in road wheel angle with effectively reduced front cornering stiffness.

an equivalent reduction in front cornering stiffness. Figure 5.19 also verifies that the observer-based sideslip estimate, which is applied to the state feedback, corresponds to sideslip estimated by the GPS/INS system.

Similar conclusions can be drawn from the experimental results in the oversteering case (Figure 5.20). As in Chapter 4, the vehicle approaches the nonlinear handling region (Figure 5.21), but state feedback still produces reasonable and predictable handling characteristics (Figures 5.22 and 5.23). More importantly, Figure 5.23 illustrates that the linear sideslip observer will generate an accurate state estimate up to the initial stages of nonlinear handling behavior. The ability of the observer to predict vehicle motion beyond the linear range of handling can be enabled by continuously adapting tire cornering stiffness to the current driving situation [16].

As steering torque information becomes more common in automotive steering systems—in the form of either electric power steering or steer-by-wire—a useful connection can be drawn between forces and vehicle motion: the knowledge of forces acting on the steering system through the tires in turn provides information on the

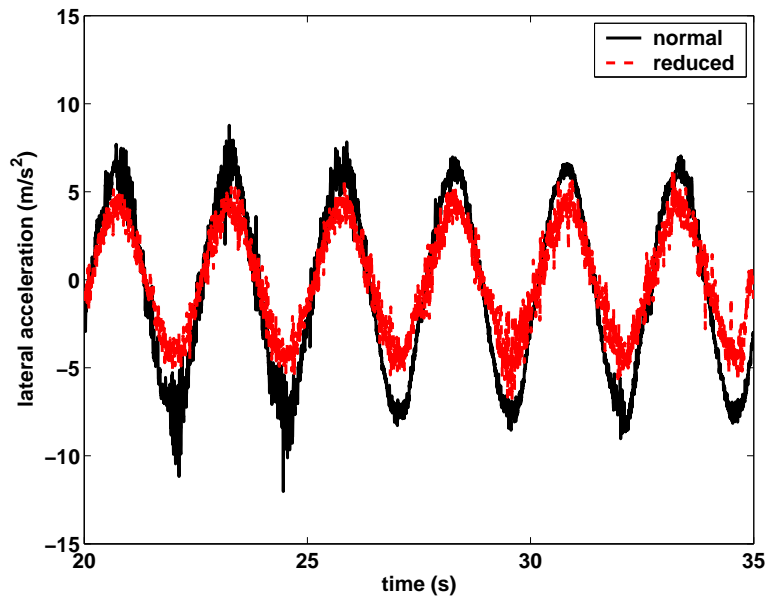


Figure 5.17: Comparison between lateral acceleration with normal and effectively reduced front cornering stiffness.

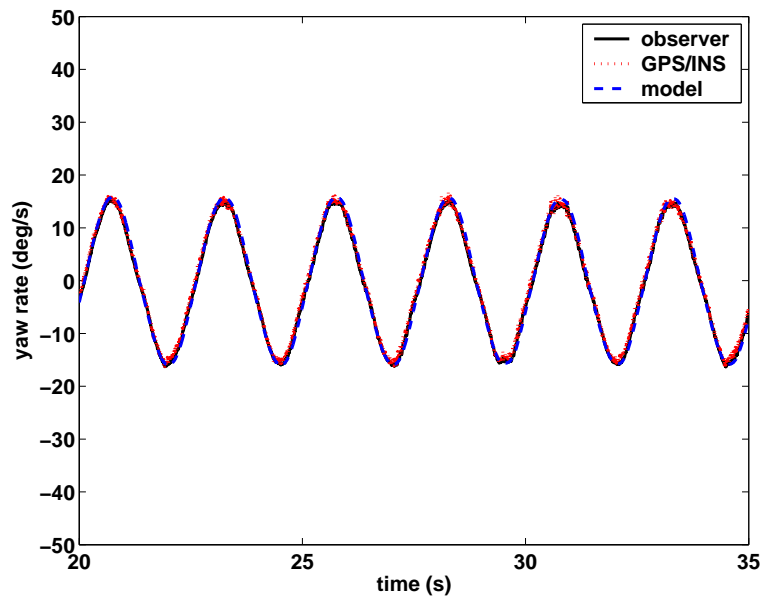


Figure 5.18: Comparison between estimated yaw rate, INS measurement, and bicycle model simulation with reduced front cornering stiffness.

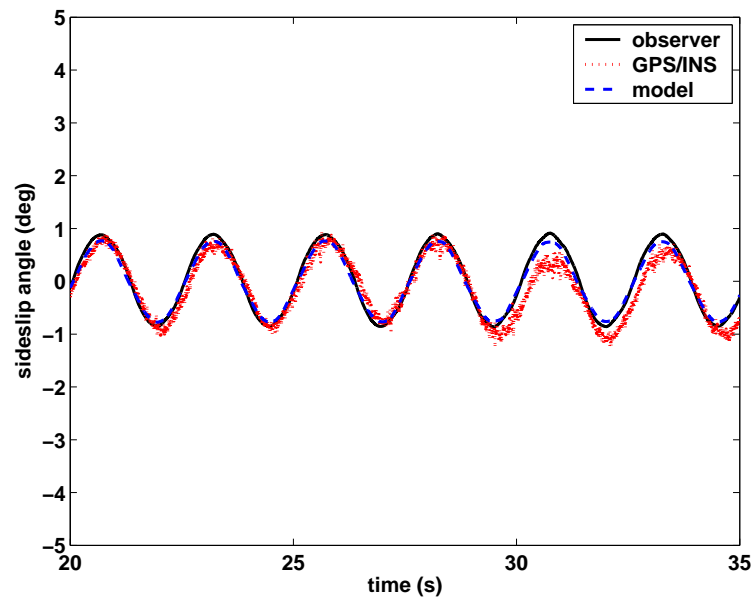


Figure 5.19: Comparison between estimated sideslip angle, GPS measurement, and bicycle model simulation with reduced front cornering stiffness.

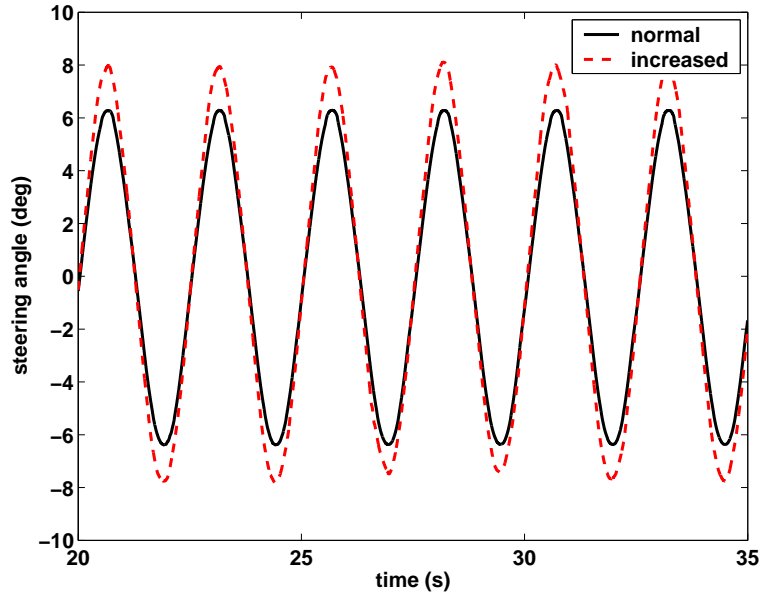


Figure 5.20: Difference in road wheel angle with effectively increased front cornering stiffness.

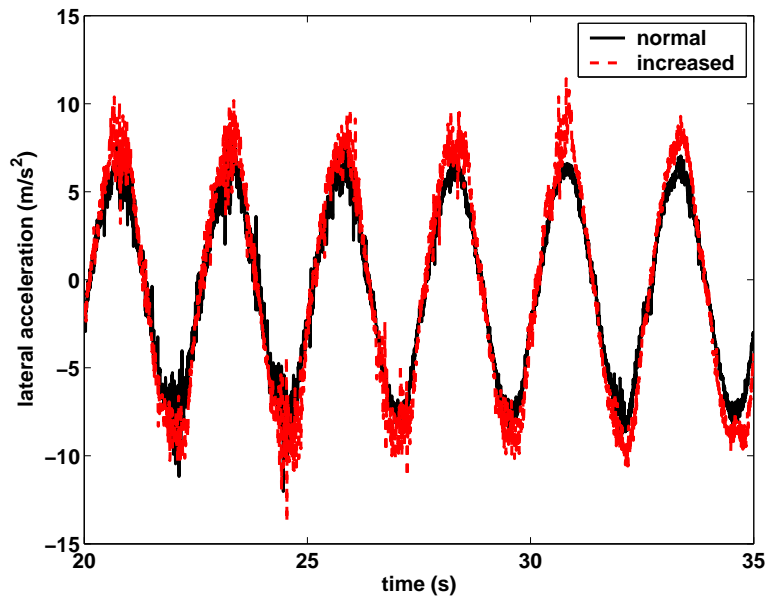


Figure 5.21: Comparison between lateral acceleration with normal and effectively increased front cornering stiffness.

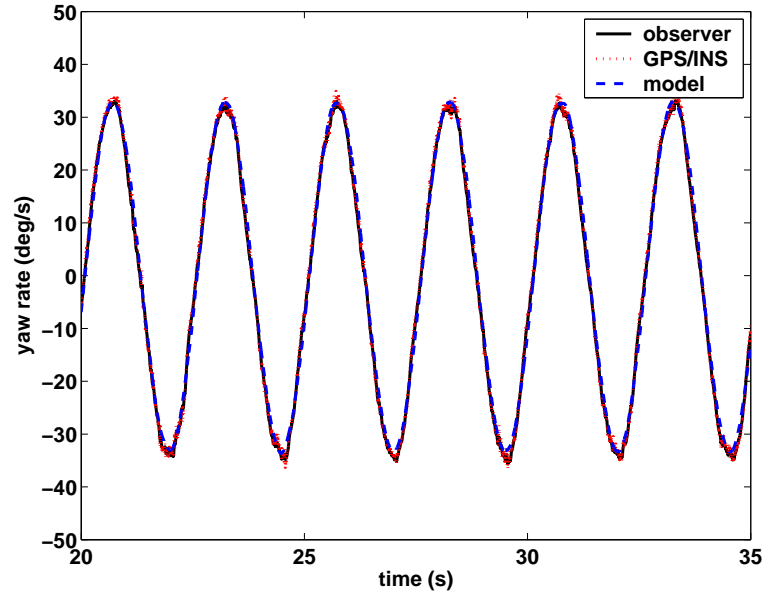


Figure 5.22: Comparison between estimated yaw rate, INS measurement, and bicycle model simulation with increased front cornering stiffness.

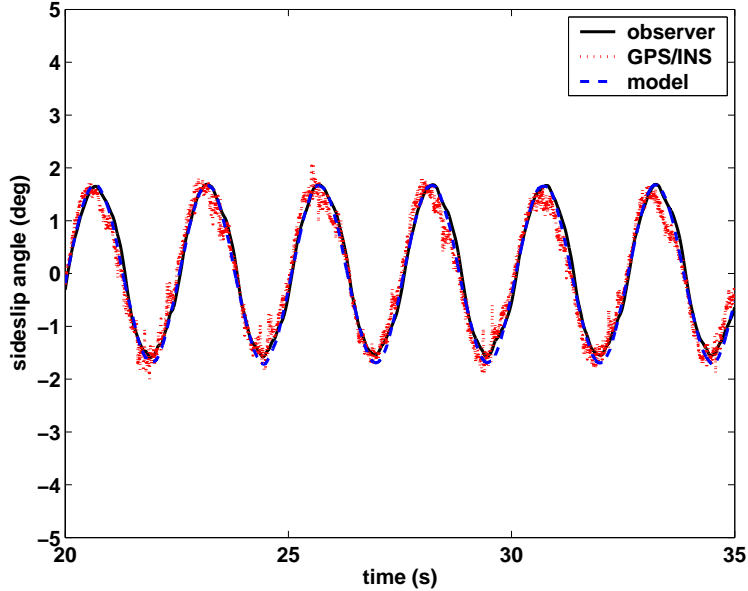


Figure 5.23: Comparison between estimated sideslip angle, GPS measurement, and bicycle model simulation with increased front cornering stiffness.

motion of the vehicle itself. Like GPS-based estimation, vehicle state estimation using steering torque is not subject to the problems of error accumulation from inertial sensor integration. Unlike GPS, however, the signal is never lost, and no extra and expensive equipment is necessary if a vehicle is equipped with electric power steering or, in the near future, steer-by-wire technology.

While the observer-based vehicle state estimation scheme was successfully implemented with handling modification, the inaccuracy of the aligning moment estimate from the disturbance observer illuminates a distinct drawback of the experimental steer-by-wire system used for these tests. Since the initial goal for developing this system encompassed less stringent functional requirements, the nonlinearities inherent in the stock hydraulic power assist system were not of primary concern. However, as the scope of research broadened to include the work discussed in this chapter, particularly estimation of steering forces, the inability to determine exactly how much torque was being contributed by the assist system became a hinderance. Although

it is possible to model the power steering system, doing so involves multiple complications such as obtaining boost curve data and representing both mechanical and hydraulic hysteresis. A more practical and realistic solution is to eliminate the hydraulic assist unit altogether in order to simplify the steering system dynamics. Plans are underway to modify the current system with this end in mind.

Chapter 6

Conclusion and Future Work

6.1 Conclusion

Given that commercial steer-by-wire systems are many years in the future and there are still a number of problems that need to be solved, the implementation of by-wire technology seems like an ideal area for academic research. Since steering is the primary means by which a driver controls a vehicle's motion, steer-by-wire opens many possibilities for investigating advanced steering control algorithms. The flexibility of steer-by-wire serves an entire range of research purposes, from replicating the driving dynamics of a conventional vehicle [27] to lane-keeping assistance [15] to fully automated operation [47]. This thesis strives to answer three primary questions on steer-by-wire: 1) what are the requirements for precise control of a steer-by-wire system? 2) how can steer-by-wire be used to influence a vehicle's dynamic characteristics? and 3) what does steer-by-wire reveal about a vehicle's dynamic behavior?

In developing an experimental steer-by-wire system, two requirements stand out: the need to understand the dynamics of the system being controlled and the need to account for the forces acting on the system during the normal course of operation. Beginning with a physically-based model, the steering system parameters are obtained via experimental identification techniques. Feedforward control is used to cancel out the system dynamics as well as the disturbance forces attributed to tire aligning moment. On top of that, feedback control is added to minimize the steering angle error

due to modelling uncertainties and real nonlinearities. These control techniques form a general guideline for the design of an accurate and precise steer-by-wire controller.

A vehicle's handling characteristics are decided by its physical parameters—weight distribution, tire cornering stiffness, and suspension roll stiffness, to name a few. Normally, the only way to make a vehicle handle differently is to change one of these parameters. With active steering capability and vehicle state information, however, a vehicle's handling characteristics can indeed be altered even though the vehicle remains physically unmodified. Experimental results show that a vehicle can be made more oversteering or understeering by artificially adjusting the front tire cornering stiffness via a combination of precisely controlled steering inputs and full state feedback. This represents one of the many safety and performance enhancements possible with steer-by-wire and also emphasizes the overall need for improved vehicle sensing and state estimation. To produce good handling responsiveness requires not only precise steering control but also smooth feedback signals.

One of the most important results involves the unlikely synergy between steering torque information and sideslip angle estimation. The relation between aligning moment and lateral tire force allows the combination of the steering system dynamics and vehicle dynamics into a unified observer structure. Consider that only three types of sensors—steering torque (or steering actuator current), steering angle, and yaw rate—are needed to generate sideslip angle estimates that can be compared to estimates obtained from highly accurate measurements by a sophisticated GPS/INS system. This approach has many practical implications for the next generation of fully integrated automotive stability control systems with or without steer-by-wire, since all of the measurement devices necessary for precise vehicle control already exist and have been inexpensively implemented on production cars.

The research presented in this thesis has answered some fundamental questions regarding the design of steer-by-wire systems as well as explored the interaction between steering and vehicle dynamics. By physically separating the act of steering a vehicle from the vehicle itself, steer-by-wire actually merges the two closer together in the way they are naturally linked. If there is one lesson to be learned here, it is this: the more we rely on electronics rather than mechanics, the more we must understand

the underlying mechanical principles at work in the system. The transition to by-wire technology does not simply eliminate the need for mechanical components. We must instead fill in the missing pieces with knowledge of how the system really functions.

6.2 Future work

The most important question of all is, does steer-by-wire make the car steer better and more safely? The answer is clearly affirmative, but much remains to be done toward this regard.

6.2.1 Handling at the limits

Most of the work presented thus far has been based on a linear vehicle model. However, the most safety critical situations occur near the limits of handling, just before the tires lose their grip on the road. In a carefully designed steering system, the aligning moment disturbance effectively communicates the tire forces acting on the vehicle—regardless of whether it is being operated in the linear or nonlinear handling region—and thus addresses the limitations of using a linear model-based observer structure as in Chapter 5. Until now, most approaches to analyzing vehicle dynamics have focused on measuring vehicle motion—longitudinal speed, yaw rate, lateral acceleration, sideslip angle, and roll angle. Here we have introduced a different way of thinking about vehicle dynamics that is actually quite basic: forces acting on a rigid body. If we can measure or estimate all of the forces acting on the vehicle, then we can completely predict its motion. If we can measure both force and motion, then we have a way of estimating parameters such as cornering stiffness, particularly in the nonlinear region of the tire force curve as shown in Figure 6.1 [19].

6.2.2 Steering wheel force feedback

Since a driver gains critical information about the vehicle from feedback through the steering wheel, steering feel will play a pivotal role in consumer acceptance of steer-by-wire systems. The desirable sensation of “connectedness” between the steering

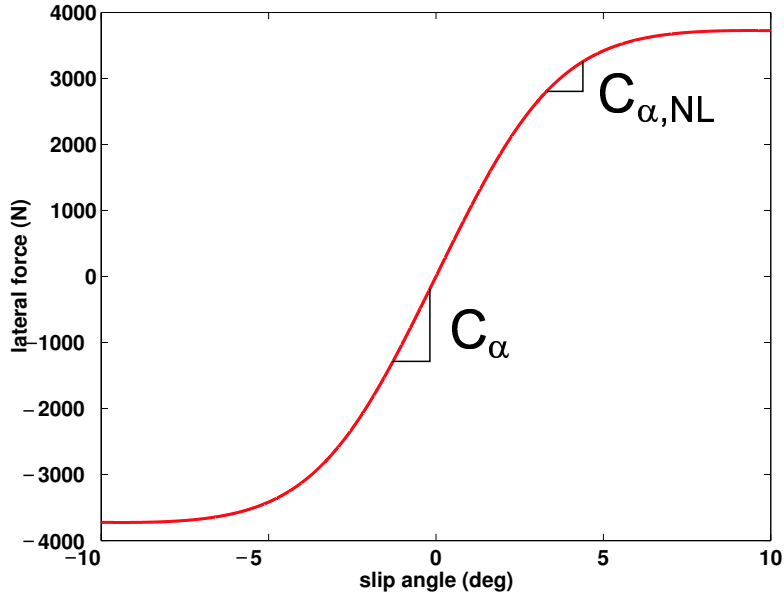


Figure 6.1: Tire cornering stiffness in the nonlinear region represented by $C_{\alpha,NL}$.

wheel and the road is subject to great scrutiny in the design conventional steering systems. Devices like hydraulic power assist tend to isolate the driver from forces at the road. With steer-by-wire, producing the feeling of “connectedness” will be an even greater challenge, because the steering wheel is completely removed from the mechanics of the steering system. While a prototype force feedback system has been developed for the experimental vehicle discussed in this thesis, many considerations still need to be addressed regarding the choice of actuator, drive system, and control laws in order to develop the right kind of steering feel.

As shown in Chapter 4, steer-by-wire gives the driver a near infinite ability to customize handling characteristics. The same flexibility exists for customizing steering wheel feedback. In fact, the scope of feedback goes beyond duplicating conventional steering forces; there is now the question of how best to communicate the combination of road friction, tire forces, and any other information that is pertinent to the safe handling of the vehicle. Such information might even include cues from the driving environment like lane position and road curvature [51].

6.2.3 Diagnostics

In removing the mechanical link between the steering wheel and the front wheels, steer-by-wire must rely solely on electronics to guarantee safe operation. To be acceptable for the mass market, steer-by-wire has to be at least as safe, if not safer, than a conventional steering system. This means that occurrence of faults in any part of the system should be exceedingly rare, and a fault should never be allowed to turn into a catastrophic failure (i.e. loss of steering control). Any by-wire application must therefore incorporate a diagnostic system that can quickly and accurately recognize a fault and take corrective action. The response to a fault might include transferring key functions to a redundant component or switching to a modified control law.

These strategies are similar to those used in fly-by-wire diagnostic systems. Unlike aircraft, however, ground vehicles are subject to much different operating conditions and constraints. Commercial aircraft typically operate with inter-aircraft spacing of five miles or more, which allows plenty of time for corrective action in case of a malfunction. In contrast, a typical roadway traffic lane is less than eight feet wide, so that should a fault occur, it would only take a fraction of a second for a vehicle to deviate from the lane and risk collision with other vehicles or fixed objects along the side of the road. Also, triply redundant sensors, actuators, and controllers, while common in aircraft, would be prohibitively expensive for passenger vehicles.

One solution currently under study is to use simple physically based models of the steering system and vehicle dynamics to compare multiple sensor outputs [14]. When appropriately filtered, the output residuals will indicate a fault by exceeding a predetermined threshold value. An experimental drive-by-wire platform has been developed to validate this diagnostic method (Figure 6.2). The vehicle features throttle-by-wire with independent rear electric drive motors and steer-by-wire with direct independent front steering. Many of the lessons learned from the steer-by-wire Corvette have been applied to the drive-by-wire test bed. Because it is a complete clean sheet design, the test bed will also provide the opportunity to develop steering geometries specifically adapted to steer-by-wire [26].



Figure 6.2: Next generation experimental drive-by-wire vehicle.

Appendix A

The Pacejka Tire Model

Tires are perhaps the most important, but difficult to model, component of an automobile. In addition to supporting the vehicle and damping out road irregularities, the tires provide the longitudinal and lateral forces necessary to change the speed and direction of the vehicle. These forces are produced by the deformation of the tire where it contacts the road during acceleration, braking, and cornering.

In the absence of side forces, a rolling tire travels straight ahead along the wheel plane. During a cornering maneuver, however, the tire contact patch “slips” laterally while rolling such that its motion is no longer in the direction of the wheel plane (Figure A.1). The angle between its direction of motion and the wheel plane is referred to as the slip angle, α . This lateral “slip” generates a lateral force, F_y , at the

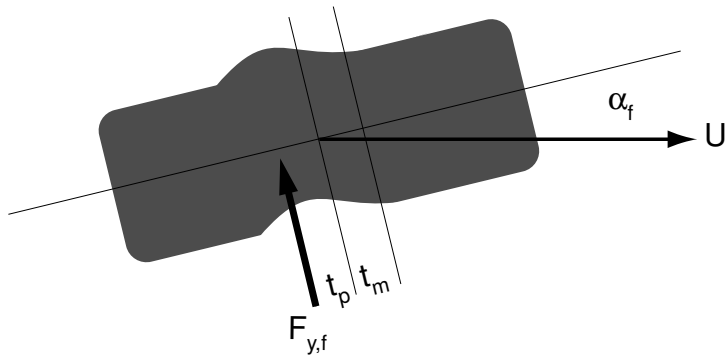


Figure A.1: Tire operating at a slip angle.

	a_1	a_2	a_3	a_4	a_5	a_6	a_7	a_8
F_y	-22.1	1011	1078	1.82	0.208	0.000	-0.354	0.707
M_z	-2.72	.2.28	-1.86	-2.73	0.110	-0.070	0.643	-4.04

Table A.1: Tire formulae coefficients for typical passenger car tire with load influence.

tire-ground interface. Because the resultant force acts slightly behind the center of the wheel, it produces a torque, M_z , which tends to realign the wheel in the direction of rolling.

Normal cornering maneuvers result in small slip angles, low lateral force, and minimal sliding of the tire. At larger slip angles lateral force increases and reaches a maximum as the tire begins to slide. Beyond this point, lateral force is reduced but maintains a relatively constant level. For small values of α —say, less than four degrees—the relationship is nearly linear. The initial slope of the curve is known as the cornering stiffness, C_α , described in units of force per degree. As slip angle increases, the peak aligning torque generally precedes the peak lateral force. Unlike lateral force, however, aligning torque rapidly declines past its peak. This is mainly due to the fact that the pneumatic trail, t_p , decreases with increasing slip angle and $M_z = F_y t_p$. The change in aligning torque near the limits of adhesion is transmitted through the steering system; drivers frequently rely on this phenomenon to gauge how close they are to the vehicle’s handling limits.

There exist a number of tire models that describe the full range of tire behavior beyond the linear region. One model commonly used in vehicle dynamics studies was developed by H. Pacejka of the Delft University of Technology [37]. The Pacejka tire formulae are special functions derived to fit experimentally measured tire data. The functions calculate lateral force and aligning torque based on slip angle and longitudinal force based on percent longitudinal slip. The basic formulae for lateral force and aligning torque are given here. Each formula contains four parameters known as the stiffness, shape, peak, and curvature factors, which in turn are functions of tire normal force, F_z (given in kN), and eight coefficients, a_1 through a_8 , whose values depend on tire type and characteristics. Table A.1 lists one set of load dependent coefficients for lateral force and aligning torque for a typical passenger car tire.

A.1 Lateral force (F_y)

For the lateral force formula, the stiffness, shape, peak, and curvature factors— C , D , B , and E , respectively—are calculated as follows.

$$\begin{aligned} C &= 1.30 \\ D &= a_1 F_z^2 + a_2 F_z \\ B &= \frac{a_3 \sin(a_4 \tan^{-1}(a_5 F_z))}{CD} \\ E &= a_6 F_z^2 + a_7 F_z + a_8 \end{aligned} \tag{A.1}$$

The lateral force, F_y , for each tire is a function of these factors and the tire slip angle.

$$\begin{aligned} F_y &= D \sin(C \tan^{-1}(B\phi)) \\ \phi &= (1 - E)\alpha + \frac{E}{B} \tan^{-1}(B\alpha) \end{aligned} \tag{A.2}$$

Note that to conform to the ISO standard sign conventions, the sign of the lateral force calculated from this equation must be reversed when applied to the vehicle model. Figure A.2 illustrates the tire lateral force as derived from Equation (A.3).

A.2 Aligning torque (M_z)

The factors for aligning torque are given by the following equations.

$$\begin{aligned} C &= 2.40 \\ D &= a_1 F_z^2 + a_2 F_z \\ B &= \frac{a_3 F_z^2 + a_4 F_z}{e^{a_5 F_z} CD} \\ E &= a_6 F_z^2 + a_7 F_z + a_8 \end{aligned} \tag{A.3}$$

Aligning torque, M_z , is a function of these factors and tire slip angle.

$$M_z = D \sin(\tan^{-1}(B\phi)) \tag{A.4}$$

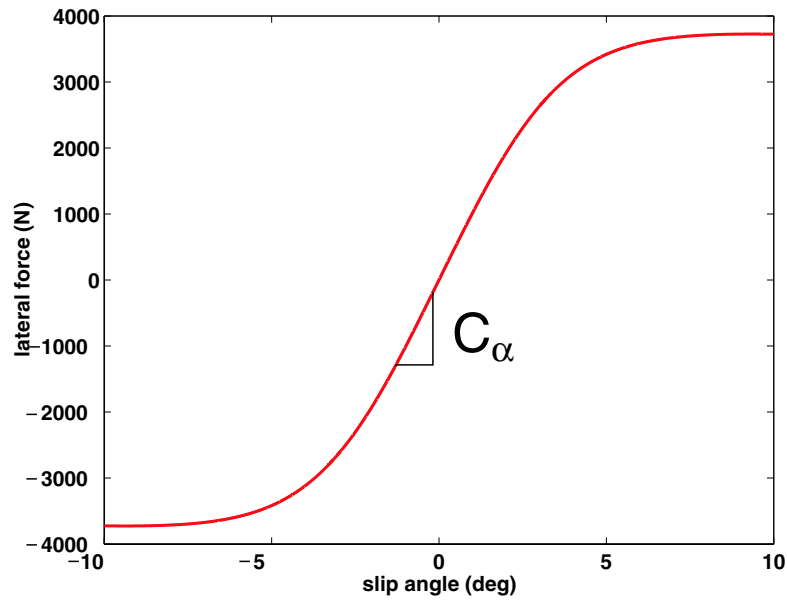


Figure A.2: Tire lateral force versus slip angle.

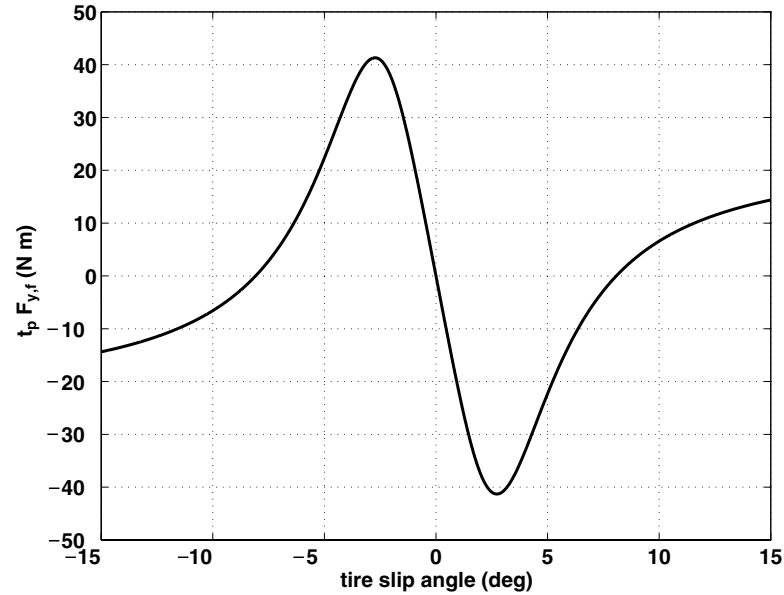


Figure A.3: Slip angle versus component of aligning moment due to pneumatic trail.

$$\phi = (1 - E)\alpha + \frac{E}{B} \tan^{-1}(B\alpha)$$

As mentioned in Chapter 3, only a portion of the total self-aligning moment is described by Equation (A.5); the remainder of the aligning moment is attributed to steering geometry effects that move the axis of steering rotation forward of the tire center and create a mechanical trail, t_m . However, the portion of the aligning moment due solely to pneumatic trail (Figure A.3) is extremely important because of the way it communicates critical changes in lateral force through the vehicle's steering system.

Appendix B

Hydraulic Power Assisted Steering

B.1 Power steering components

The key components of the hydraulic power assist system are the hydraulic pump, the rotary spool valve, and the rack piston (Figure B.1). The rotary spool valve consists of the torsion bar, inner spool, and outer sleeve. When the driver applies a torque to the steering wheel, the torsion bar twists, and the inner spool rotates with respect to the outer sleeve. This rotation of the valve opens metering orifices that increase the flow of hydraulic fluid to one side of the rack piston while restricting flow to the other side of the piston. The resulting differential pressure inside the cylinder pushes the piston to one side or the other depending on the direction of steering. The piston is connected to the steering rack, so hydraulic pressure directly translates to steering effort.

B.2 Hydraulic model

Volumetric flow rate, Q , through an orifice is described by the following equation:

$$Q = AC_d \sqrt{\frac{2\Delta P}{\rho}} \quad (\text{B.1})$$

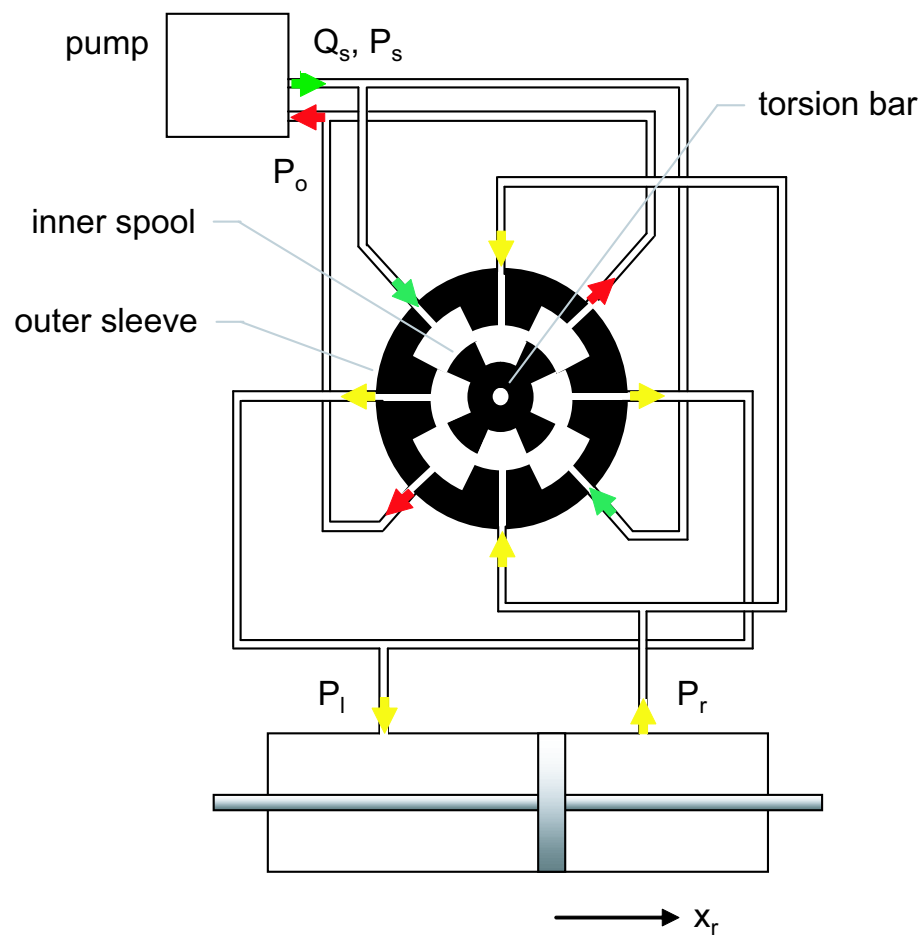


Figure B.1: Hydraulic power assist schematic.

where A is the cross-sectional area of the orifice, C_d is the flow coefficient, ρ is the fluid density, and ΔP is the differential pressure across the orifice. By applying this equation to each of the metering orifices of the rotary spool valve and taking the sum of the flows, the total flow rate into and out of the left and right chambers of the cylinder can be determined. In [41], Proca and Keyhani apply the orifice flow equation with principle of mass conservation to the entire hydraulic system to derive the following system equations:

$$\begin{aligned} Q_s - A_1 C_d \sqrt{\frac{2}{\rho}} \sqrt{|P_s - P_r|} - A_2 C_d \sqrt{\frac{2}{\rho}} \sqrt{|P_s - P_l|} &= \frac{V_s}{\beta} \dot{P}_s \\ A_1 C_d \sqrt{\frac{2}{\rho}} \sqrt{|P_s - P_r|} - A_2 C_d \sqrt{\frac{2}{\rho}} \sqrt{|P_s - P_o|} - A_p \dot{x}_r &= \frac{A_p (\frac{L}{2} + x_r)}{\beta} \dot{P}_r \\ A_2 C_d \sqrt{\frac{2}{\rho}} \sqrt{|P_s - P_l|} - A_1 C_d \sqrt{\frac{2}{\rho}} \sqrt{|P_l - P_o|} + A_p \dot{x}_r &= \frac{A_p (\frac{L}{2} - x_r)}{\beta} \dot{P}_l \end{aligned} \quad (\text{B.2})$$

A_p is the piston surface area, while A_1 and A_2 are the total orifice areas leading to the left and right cylinder chambers, respectively, and are functions of the torsion bar rotation angle. In [9], Claeys et al. derive a slightly modified version of the hydraulic system equations to include fluid leakage past the piston. Note that rack displacement, x_r , is steering angle at the front wheels, δ_w , multiplied by the steering arm length, l .

$$x_r = l \delta_w \quad (\text{B.3})$$

Thus, assist torque at the front wheels is net force on the piston due to hydraulic pressure multiplied the steering arm length.

$$\tau_{ps} = l A_p (P_l - P_r) \quad (\text{B.4})$$

B.3 Mechanical model

The presence of the torsion bar introduces an additional degree of freedom between the steering wheel and the road wheels and therefore creates additional dynamics

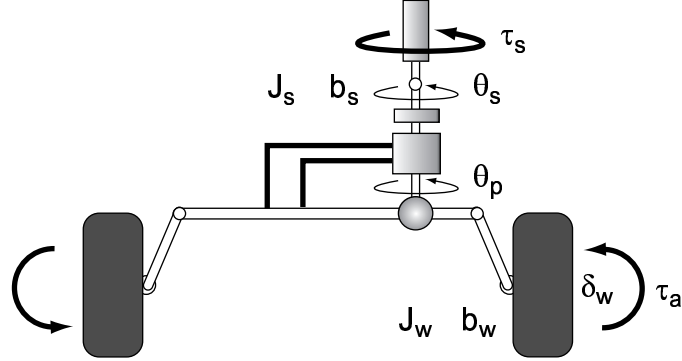


Figure B.2: Mechanical representation of steering system with hydraulic power assist.

in the system. Depending on the stiffness of the torsion bar, some lag in vehicle response and oscillation in feedback torque may be noticeable to the driver [33]. If these motions are substantial enough to be of concern, the steering system may instead be represented as two separate inertias connected via the torsion bar (Figure B.2). The portion of the system above the torsion bar is described by the following differential equation:

$$J_s \ddot{\theta}_s = -b_s \dot{\theta}_s + \tau_s - \tau_k \quad (\text{B.5})$$

where J_s is the overall moment of inertia, b_s is composite damping, τ_s is the steering motor torque, and τ_k is the torsion bar torque. The lower part of the system includes the pinion, rack, and wheels:

$$J_w \ddot{\delta}_w = -b_w \dot{\delta}_w + \tau_k r_s + \tau_{ps} - \tau_a \quad (\text{B.6})$$

where J_w is the overall moment of inertia with respect to road wheel angle, b_w is composite damping, r_s is the steering ratio, τ_{ps} is the power steering assist torque, and τ_a is the tire aligning moment. The torsion bar torque is given by:

$$\tau_k = k_t(\theta_s - \theta_p) \quad (\text{B.7})$$

where k_t is the torsion bar stiffness. Note that pinion angle is related to road wheel angle by the steering ratio:

$$\theta_p = r_s \theta_w \quad (\text{B.8})$$

B.4 Power steering nonlinearities

In studying power steering valve designs, Birsching [8] found that total orifice area is typically a linear function of the valve rotation angle with a discontinuity occurring when the metering orifices between the inner and outer spools close off (Figure B.3). Even when an orifice is closed, there is still some fluid flow through gaps in the valve. The differential pressure between the left and right chambers of the cylinder are shown to be nonlinearly related to the input steering torque (Figure B.4). The relationship between input and output torque is usually determined experimentally and can vary depending on the valve design and operating conditions. For a typical power assisted steering system, about 80% of the average steering effort comes from the hydraulic assist while the other 20% comes from the driver [56].

Another type of nonlinearity is hysteresis in both the power steering system and the steering rack [58]. Spool valve hysteresis, along with torsion bar displacement, is largely responsible for the lag in steering response associated with hydraulic power steering [39]. Since rack and pinion systems have an automatic clearance adjustment mechanism, most of the rack hysteresis comes from stick-slip friction between the gear teeth rather than free play in the gears [55].

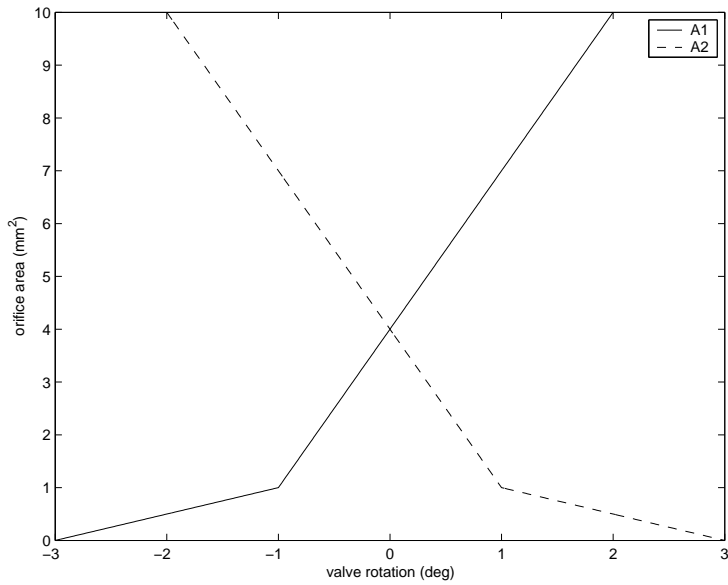


Figure B.3: Orifice area versus valve angle.

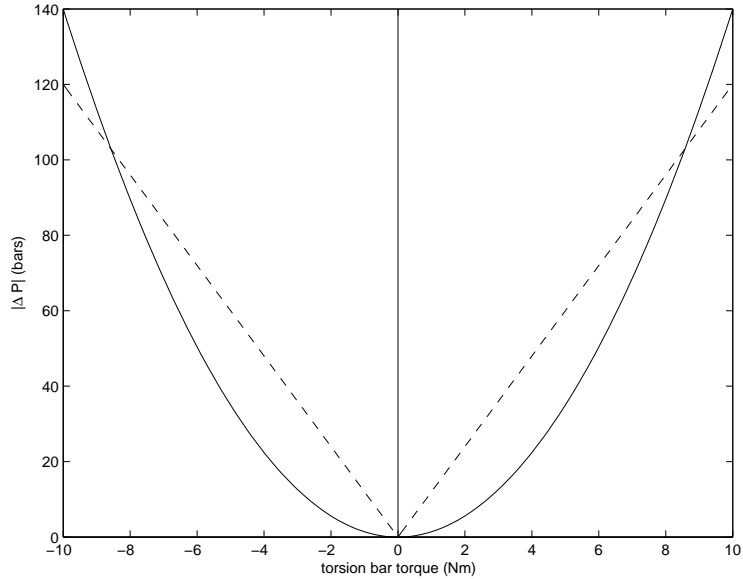


Figure B.4: Typical power steering boost curve: assist pressure versus input torque with linear approximation.

Appendix C

Extension to Four-Wheel Steering Vehicles

Four-wheel steering has often been proposed as a way to improve maneuverability, stability, and controllability of all types of vehicles. It is a natural extension of the modularity of the steer-by-wire concept.

C.1 Linear vehicle model with four-wheel steering

The bicycle model representation of a four-wheel steering vehicle (Figure C.1) adds rear steering angle, δ_r . The state equations of motion for the bicycle model with front and rear steering are given by:

$$\begin{bmatrix} \dot{\beta}_{CG} \\ \dot{r} \end{bmatrix} = \begin{bmatrix} \frac{-C_{\alpha,f} - C_{\alpha,r}}{mV} & -1 + \frac{C_{\alpha,r}b - C_{\alpha,f}a}{mV^2} \\ \frac{C_{\alpha,r}b - C_{\alpha,f}a}{I_z} & \frac{-C_{\alpha,f}a^2 - C_{\alpha,r}b^2}{I_z V} \end{bmatrix} \begin{bmatrix} \beta_{CG} \\ r \end{bmatrix} + \begin{bmatrix} \frac{C_{\alpha,f}}{mV} \\ \frac{C_{\alpha,f}a}{I_z} \end{bmatrix} \delta_f + \begin{bmatrix} \frac{C_{\alpha,r}}{mV} \\ -\frac{C_{\alpha,r}b}{I_z} \end{bmatrix} \delta_r \quad (\text{C.1})$$

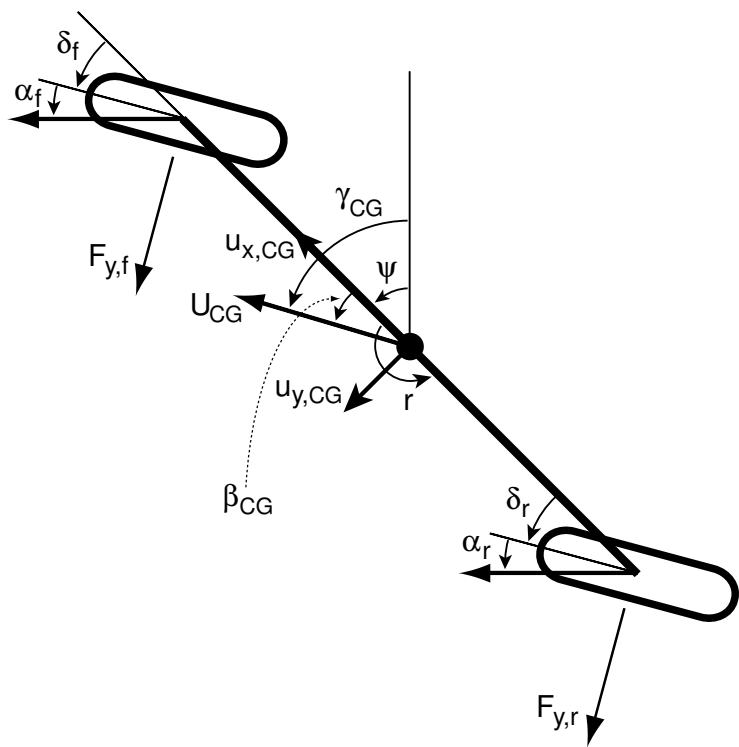


Figure C.1: Bicycle model with front and rear steering.

C.2 Full state feedback vehicle control

A full state feedback control law for an active four-wheel steering vehicle is given by

$$\delta_f = K_{r,f}r + K_{\beta,f}\beta + K_{\delta,f}\delta_{f,d} \quad (\text{C.2})$$

$$\delta_r = K_{r,r}r + K_{\beta,r}\beta \quad (\text{C.3})$$

where $\delta_{f,d}$ is the driver commanded steer angle, δ_f is the augmented front steer angle, and δ_r is the rear steer angle. Substituting the control law into Equation (C.1) yields:

$$\begin{bmatrix} \dot{\beta}_{CG} \\ \dot{r} \end{bmatrix} = \begin{bmatrix} \frac{-C_{\alpha,f} - C_{\alpha,r} + C_{\alpha,f}K_{\beta,f} + C_{\alpha,r}K_{\beta,r}}{mV} & -1 + \frac{C_{\alpha,r}b - C_{\alpha,f}a + C_{\alpha,f}VK_{r,f} + C_{\alpha,r}VK_{r,r}}{mV^2} \\ \frac{C_{\alpha,r}b - C_{\alpha,f}a + C_{\alpha,f}aK_{\beta,f} - C_{\alpha,r}bK_{\beta,r}}{I_z} & \frac{-C_{\alpha,f}a^2 - C_{\alpha,r}b^2 + C_{\alpha,f}aVK_{r,f} - C_{\alpha,r}bVK_{r,r}}{I_zV} \end{bmatrix} \begin{bmatrix} \beta_{CG} \\ r \end{bmatrix} + \begin{bmatrix} \frac{C_{\alpha,f}K_{\delta,f}}{mV} \\ \frac{C_{\alpha,f}aK_{\delta,f}}{I_z} \end{bmatrix} \delta_{f,d} \quad (\text{C.4})$$

Now, instead of targeting a new front cornering stiffness as in the active front steering case, we aim to fractionally adjust the mass and moment of inertia of the four-wheel steering vehicle:

$$\hat{I}_z = I_z(1 + \eta) \quad (\text{C.5})$$

$$\hat{m} = m(1 + \eta) \quad (\text{C.6})$$

This can be accomplished by choosing the state feedback gains as:

$$K_{\beta,f} = \frac{\eta}{1 + \eta} \quad K_{r,f} = \frac{a}{V} \frac{\eta}{1 + \eta} \quad K_{d,f} = \frac{1}{1 + \eta} \quad (\text{C.7})$$

$$K_{\beta,r} = -\frac{\eta}{1 + \eta} \quad K_{r,r} = -\frac{b}{V} \frac{\eta}{1 + \eta} \quad K_{d,r} = \frac{1}{1 + \eta} \quad (\text{C.8})$$

Substituting these feedback gains into the four-wheel steer model (Equation (C.4)) yields a state space model of the exact same form as the front wheel steer model

(Equation (4.7)) but with the new mass, \hat{m} , and moment of inertia, \hat{I}_z :

$$\begin{bmatrix} \dot{\beta}_{CG} \\ \dot{r} \end{bmatrix} = \begin{bmatrix} \frac{-C_{\alpha,f} - C_{\alpha,r}}{\hat{m}V} & -1 + \frac{C_{\alpha,r}b - C_{\alpha,f}a}{\hat{m}V^2} \\ \frac{C_{\alpha,r}b - C_{\alpha,f}a}{\hat{I}_z} & \frac{-C_{\alpha,f}a^2 - C_{\alpha,r}b^2}{\hat{I}_zV} \end{bmatrix} \begin{bmatrix} \beta_{CG} \\ r \end{bmatrix} + \begin{bmatrix} \frac{C_{\alpha,f}}{\hat{m}V} \\ \frac{C_{\alpha,f}a}{\hat{I}_z} \end{bmatrix} \delta \quad (\text{C.9})$$

C.3 Limitations of four-wheel active steering

Again, suppose the desired vehicle handling characteristics are given by:

$$\begin{bmatrix} \dot{\beta}_{CG} \\ \dot{r} \end{bmatrix} = \begin{bmatrix} \frac{-\hat{C}_{\alpha,f} - \hat{C}_{\alpha,r}}{\hat{m}\hat{V}} & -1 + \frac{\hat{C}_{\alpha,r}\hat{b} - \hat{C}_{\alpha,f}\hat{a}}{\hat{m}\hat{V}^2} \\ \frac{\hat{C}_{\alpha,r}\hat{b} - \hat{C}_{\alpha,f}\hat{a}}{\hat{I}_z} & \frac{-\hat{C}_{\alpha,f}\hat{a}^2 - \hat{C}_{\alpha,r}\hat{b}^2}{\hat{I}_z\hat{V}} \end{bmatrix} \begin{bmatrix} \beta_{CG} \\ r \end{bmatrix} + \begin{bmatrix} \frac{\hat{C}_{\alpha,f}}{\hat{m}\hat{V}} \\ \frac{\hat{C}_{\alpha,f}\hat{a}}{\hat{I}_z} \end{bmatrix} \delta_{f,d} \quad (\text{C.10})$$

Rewrite as

$$\begin{bmatrix} \dot{\beta}_{CG} \\ \dot{r} \end{bmatrix} = \begin{bmatrix} \hat{a}_{1,1} & \hat{a}_{1,2} \\ \hat{a}_{2,1} & \hat{a}_{2,2} \end{bmatrix} \begin{bmatrix} \beta_{CG} \\ r \end{bmatrix} + \begin{bmatrix} \hat{b}_1 \\ \hat{b}_2 \end{bmatrix} \delta_{f,d} \quad (\text{C.11})$$

and equate with Equation C.4:

$$\frac{-C_{\alpha,f} - C_{\alpha,r} + C_{\alpha,f}K_{\beta,f} + C_{\alpha,r}K_{\beta,r}}{mV} = \hat{a}_{1,1} \quad (\text{C.12})$$

$$-1 + \frac{C_{\alpha,r}b - C_{\alpha,f}a + C_{\alpha,f}VK_{r,f} + C_{\alpha,r}VK_{r,r}}{mV^2} = \hat{a}_{1,2} \quad (\text{C.13})$$

$$\frac{C_{\alpha,r}b - C_{\alpha,f}a + C_{\alpha,f}aK_{\beta,f} - C_{\alpha,r}bK_{\beta,r}}{I_z} = \hat{a}_{2,1} \quad (\text{C.14})$$

$$\frac{-C_{\alpha,f}a^2 - C_{\alpha,r}b^2 + C_{\alpha,f}aVK_{r,f} - C_{\alpha,r}bVK_{r,r}}{I_zV} = \hat{a}_{2,2} \quad (\text{C.15})$$

$$\frac{C_{\alpha,f}K_{\delta,f}}{mV} = \hat{b}_1 \quad (\text{C.16})$$

$$\frac{C_{\alpha,f}aK_{\delta,f}}{I_z} = \hat{b}_2 \quad (\text{C.17})$$

In contrast to the front-wheel steering case, the full state feedback gains, $K_{\beta,f}$, $K_{\beta,r}$, $K_{r,f}$, and $K_{r,r}$, can be expressed explicitly in terms of the desired vehicle parameters,

$\hat{a}_{1,1}$, $\hat{a}_{1,2}$, $\hat{a}_{2,1}$, and $\hat{a}_{2,2}$:

$$K_{\beta,f} = \frac{mV}{C_{\alpha,f}} \left(1 + \frac{a}{a+b} \right) \hat{a}_{1,1} + \frac{I_z}{C_{\alpha,f}(a+b)} \hat{a}_{2,1} + \frac{C_{\alpha,f}(2a+b-1) + C_{\alpha,r}(a-1)}{C_{\alpha,f}(a+b)} \quad (\text{C.18})$$

$$K_{\beta,r} = \frac{mVa}{C_{\alpha,r}(a+b)} \hat{a}_{1,1} - \frac{I_z}{C_{\alpha,r}(a+b)} \hat{a}_{2,1} + 1 \quad (\text{C.19})$$

$$K_{r,f} = \frac{mV}{C_{\alpha,f}(a+b)} \hat{a}_{1,2} + \frac{I_z - I_z C_{\alpha,r}^2(a+b)b}{C_{\alpha,f}a} \hat{a}_{2,2} + \frac{C_{\alpha,f}a^3 + C_{\alpha,r}ab^2}{C_{\alpha,f}Va(a+b)} \quad (\text{C.20})$$

$$K_{r,r} = \frac{mVa}{C_{\alpha,r}(a+b)} \hat{a}_{1,2} - I_z C_{\alpha,r} \hat{a}_{2,2} + \frac{mV^2a + C_{\alpha,r}(b^2+ab)}{C_{\alpha,r}V(a+b)} \quad (\text{C.21})$$

However,

$$K_{\delta,f} = \frac{mV}{C_{\alpha,f}} \hat{b}_1 \quad (\text{C.22})$$

$$K_{\delta,r} = \frac{I_z}{C_{\alpha,f}a} \hat{b}_2 \quad (\text{C.23})$$

which requires

$$\hat{b}_2 = \frac{mVa}{I_z} \hat{b}_1 \quad (\text{C.24})$$

such that not all of the desired parameters can be chosen independently. Still, the restriction is far less rigorous than for the front-wheel steering vehicle. For a four-wheel steering vehicle, one may use full state feedback to alter the rear tire cornering stiffness independent of and in addition to the front cornering stiffness, vehicle mass, and moment of inertia.

Bibliography

- [1] M. Abe, Y. Kano, K. Suzuki, Y. Shibahata, and Y. Furukawa. An experimental validation of side-slip control to compensate vehicle lateral dynamics for a loss of stability due to nonlinear tire characteristics. In *Proceedings of the International Symposium on Advanced Vehicle Control (AVEC), Ann Arbor, MI*, pages 36–41, 2000.
- [2] T. Acarman, K. A. Redmill, and Ü. Özgüner. A robust controller design for drive by wire hydraulic power steering system. In *Proceedings of the 2002 American Control Conference, Anchorage, AK*, pages 2522–2527, 2002.
- [3] J. Ackermann. Yaw disturbance attenuation by robust decoupling of car steering. In *Proceedings of the IFAC World Congress, San Francisco, CA*, pages 1–6, 1996.
- [4] M. Aga and A. Okada. Analysis of vehicle stability control (VSC)’s effectiveness from accident data. In *Proceedings of the 18th International Technical Conference on the Enhanced Safety of Vehicles, Nagoya, Japan*, 2003.
- [5] S. Amberkar, M. Kushion, K. Eschtruth, and F. Bolourchi. Diagnostic development for an electric power steering system. *SAE Technical Paper Series 2000-01-0819*, 2000.
- [6] A. Badawy, J. Zuraski, F. Bolourchi, and A. Chandy. Modeling and analysis of an electric power steering system. *SAE Technical Paper Series 1999-01-0399*, 1999.
- [7] E. J. Bedner and H. H. Chen. A supervisory control to manage brakes and four-wheel-steer systems. *SAE Technical Paper Series 2004-01-1059*, 2004.

- [8] J. E. Birsching. Two dimesional modeling ofa rotary power steering valve. *SAE Technical Paper Series 1999-01-0396*, 1999.
- [9] X. Claeys, C. Canudas de Wit, and H. Bechart. Modeling and control of steering actuator for heavy duty vehicles. In *Proceedings of the 1999 European Control Conference, Karlsruhe, Germany*, 1999.
- [10] J. N. Dang. Preliminary results analyzing the effectiveness of electronic stability (ESC) systems. *NHTSA Evaluation Note DOT HS 809 790*, 2004.
- [11] J. C. Dixon. *Tires, Suspension and Handling*. Society of Automotive Engineers, Warrendale, PA, 1996.
- [12] C. M. Farmer. Effecto of electronic stability control on automobile crash risk. *Traffic Injury Prevention*, 5:317–325, 2004.
- [13] Y. Fukada. Slip-angle estimation for vehicle stability control. *Vehicle System Dynamics*, 32:375–388, 2000.
- [14] C. D. Gadda, P. Yih, and J. C. Gerdes. Incorporating a model of vehicle dynamics in a diagnostic system for steer-by-wire vehicles. In *Proceedings of the International Symposium on Advanced Vehicle Control (AVEC), Arnheim, The Netherlands*, pages 779–784, 2004.
- [15] J. C. Gerdes and E. Rossetter. A unified approach to driver assistance systems based on artifical potential fields. *ASME Journal of Dynamic Systems, Measurement, and Control*, 123:431–438, 2001.
- [16] M. Hiemer, U. Kiencke, T. Matsunaga, and K. Shirasawa. Cornering stiffness adaptation for improved side slip angle observation. In *Proceedings of the IFAC Symposium on Advances in Automotive Control, Salerno, Italy*, pages 685–690, 2004.
- [17] A. Higuchi and Y. Saito. Optimal control of four wheel steering vehicle. In *Proceedings of the International Symposium on Advanced Vehicle Control (AVEC), Yokohama, Japan*, pages 233–238, 1992.

- [18] S. Horiuchi and N. Yuhara. An analytical approach to the prediction of handling qualities of vehicles with advanced steering control system using multi-input driver model. *ASME Journal of Dynamic Systems, Measurement, and Control*, 122:490–497, 2000.
- [19] Y. J. Hsu and J. C. Gerdes. Stabilization of a steer-by-wire vehicle at the limits of handling using feedback linearization. *Submitted to the 2005 American Control Conference, Portland, OR*, 2005.
- [20] K. Huh and J. Kim. Active steering control based on the estimated tire forces. *ASME Journal of Dynamic Systems, Measurement, and Control*, 123:505–511, 2001.
- [21] H. Inagaki, K. Akuzawa, and M. Sato. Yaw rate feedback braking force distribution control with control-by-wire braking system. In *Proceedings of the International Symposium on Advanced Vehicle Control (AVEC), Yokohama, Japan*, 1992.
- [22] Y. Jeong, D. Kim, K. Kim, D. Hwang, K. Oh, and T. Koh. Development of a steering sensor for vehicle control systems. In *Proceedings of the International Symposium on Advanced Vehicle Control (AVEC), Nagoya, Japan*, pages 213–217, 1998.
- [23] J. Kasselmann and T. Keranen. Adaptive steering. *Bendix Technical Journal*, 2:26–35, 1969.
- [24] W. M. Kauffman, C. J. Liddell, A. Smith, and R. D. VanDyke. An apparatus for varying effective dihedral in flight with application to a study of tolerable dihedral on a conventional fighter airplane. *National Advisory Committee for Aeronautics Report 948*, 1949.
- [25] K. Langwieder, J. Gwehenberger, T. Hummel, and J. Bende. Benefit potential of ESP in real accident situations involving cars and trucks. In *Proceedings of the 18th International Technical Conference on the Enhanced Safety of Vehicles, Nagoya, Japan*, 2003.

- [26] S. Laws, S. Kohn, C. D. Gadda, P. Yih, J. C. Gerdes, and J. C. Milroy. Steer-by-wire suspension design for controllability. *Submitted to the 16th IFAC World Congress, Prague, Czech Republic*, 2005.
- [27] A. Y. Lee. Matching vehicle responses using the model-following control method. *SAE Technical Paper Series 970561*, 1997.
- [28] A. Lie, C. Tingvall, M. Krafft, and A. Kullgren. The effectiveness of ESP (electronic stability program) in reducing real life accidents. *Traffic Injury Prevention*, 5:37–41, 2004.
- [29] A. Liu and S. Chang. Force feedback in a stationary driving simulator. In *Proceedings of the IEEE International Conference on Systems, Man, and Cybernetics*, volume 2, pages 1711–1716, 1995.
- [30] H. Lupker, J. Zuurbier, R. Verschuren, S. Jansen, and D. Willemsen. Steer-by-wire innovations and demonstrator. In *Proceedings of the International Symposium on Advanced Vehicle Control (AVEC), Hiroshima, Japan*, pages 665–670, 2002.
- [31] S. Mammar and D. Koenig. Vehicle handling improvement by active steering. *Vehicle System Dynamics*, 38:211–242, 2002.
- [32] R. McCann. Variable effort steering for vehicle stability enhancement using an electric power steering system. *SAE Technical Paper Series 2000-01-0817*, 2000.
- [33] V. D. Mills and J. R. Wagner. Behavioural modelling and analysis of hybrid vehicle steering systems. *IMechE Journal of Automobile Engineering*, 217:349–361, 2003.
- [34] M. Nagai, S. Yamanaka, and Y. Hirano. Integrated control law of active rear wheel steering and direct yaw moment control. In *Proceedings of the International Symposium on Advanced Vehicle Control (AVEC), Aachen, Germany*, pages 451–470, 1996.

- [35] E. Ono, S. Hosoe, H. D. Tuan, and S. Doi. Bifurcation in vehicle dynamics and robust front wheel steering control. *IEEE Transactions on Control Systems Technology*, 6:412–420, 1998.
- [36] A. Y. Orbak, K. Youcef-Toumi, and M. Senga. Model reduction and design of a power steering system. In *Proceedings of the 1999 American Control Conference, San Diego, CA*, pages 4476–4481, 1999.
- [37] H. Pacejka, E. Bakker, and L. Nyborg. Tyre modelling for use in vehicle dynamic studies. *SAE Technical Paper Series 870421*, 1987.
- [38] Y. E. Papelis, T. Brown, G. Watson, D. Holtz, and W. Pan. Study of ESC assisted driver performance using a driving simulator. *National Advanced Driving Simulator Document ID N04-003-PR*, 2004.
- [39] J. P. Pauwelussen and J. J. A. Pauwelussen. Exploration of steering wheel angle based workload measures in relationship to steering feel evaluation. In *Proceedings of the International Symposium on Advanced Vehicle Control (AVEC), Arnheim, The Netherlands*, pages 427–432, 2004.
- [40] D. Peter and R. Gerhard. Electric power steering—the first step on the way to steer by wire. *SAE Technical Paper Series 1999-01-0401*, 1999.
- [41] A. B. Proca and A. Keyhani. Identification of power steering dynamic models. *Mechatronics*, 8:255–270, 1998.
- [42] H. S. Radt. *Variable Dynamic Testbed Vehicle: Analysis of Handling Performance With and Without Rear Steer*. Milliken Research Associates, Inc., Williamsville, NY, 1997.
- [43] E. J. Rossetter. *A Potential Field Framework for Active Vehicle Lanekeeping Assistance*. PhD thesis, Stanford University, December 2003.
- [44] J. Ryu and J. C. Gerdts. Integrating inertial sensors with global positioning system (GPS) for vehicle dynamics control. *ASME Journal of Dynamic Systems, Measurement, and Control*, 126:243–254, 2004.

- [45] J. Ryu, E. Rossetter, and J. C. Gerdes. Vehicle sideslip and roll parameter estimation using GPS. In *Proceedings of the International Symposium on Advanced Vehicle Control (AVEC), Hiroshima, Japan*, pages 373–380, 2002.
- [46] C. L. Seacord and D. K. Vaughn. Preliminary system design for a digital fly-by-wire flight control system for an F-8C aircraft. *NASA Center for Aerospace Information NASA-CR-2609*, 1976.
- [47] R. Sebastian, T. Kaufmann, F. Bolourchi, and H. S. Tan. Design of an automated highway systems steering actuator control system. In *Proceedings of the IEEE Conference on Intelligent Transportation Systems*, pages 254–259, 1997.
- [48] M. Segawa, K. Nishizaki, and S. Nakano. A study of vehicle stability control by steer by wire system. In *Proceedings of the International Symposium on Advanced Vehicle Control (AVEC), Ann Arbor, MI*, pages 7–12, 2000.
- [49] R. S. Sharp and R. Granger. On car steering torques at parking speeds. *IMechE Journal of Automobile Engineering*, 217:87–96, 2003.
- [50] R. Subramanian. Analysis of crashes involving 15-passenger vans. *NHTSA Technical Report DOT HS 809 735*, 2004.
- [51] J. P. Switkes, E. J. Rossetter, I. A. Coe, and J. C. Gerdes. Handwheel force feedback for lanekeeping assistance: Combined dynamics and stability. In *Proceedings of the International Symposium on Advanced Vehicle Control (AVEC), Arnheim, The Netherlands*, pages 47–52, 2004.
- [52] J. Tajima and N. Yuhara. Effects of steering system characteristics on control performance from the viewpoint of steer-by-wire system design. *SAE Technical Paper Series 1999-01-0821*, 1999.
- [53] A. Taneda and T. Yamanaka. Design of actuator for active-rear-steer system. *SAE Technical Paper Series 981114*, 1998.

- [54] A. van Zanten. Evolution of electronic control systems for improving the vehicle dynamic behavior. In *Proceedings of the International Symposium on Advanced Vehicle Control (AVEC), Hiroshima, Japan*, pages 7–15, 2002.
- [55] A. Wohnhaas and U. Essers. Nonlinear modeling and simulation of a rack and pinion steering. In *Proceedings of the International Symposium on Advanced Vehicle Control (AVEC), Yokohama, Japan*, pages 68–73, 1992.
- [56] T. Wong. Hydraulic power steering system design and optimization simulation. *SAE Technical Paper Series 2000-01-0479*, 2001.
- [57] Y. Yasui, W. Tanaka, E. Ono, Y. Muragishi, K. Asano, M. Momiyama, S. Ogawa, K. Asano, Y. Imoto, and H. Kato. Wheel grip factor estimation apparatus. *United States Patent Application Pub. No. US 2004/0019417 A1*, 2004.
- [58] J. Yu, J. Aston, C. Gilsinger, J. Shutway, and H. Tokunaga. Vehicle dynamic feeling study with a focus on the on-center steering feeling of north american highway driving. In *Proceedings of the International Symposium on Advanced Vehicle Control (AVEC), Arnheim, The Netherlands*, pages 415–420, 2004.
- [59] N. Yuhara and J. Tajima. Advanced steering system adaptable to lateral control task and driver’s intention. *Vehicle System Dynamics*, 36:119–158, 2000.
- [60] N. Yuhara, J. Tajima, S. Sano, and S. Takimoto. Steer-by-wire-oriented steering system design: Concept and examination. *Vehicle System Dynamics*, 33:692–703, 2000.